STUDY ON THE ACCURACY OF SQUEEZE FILM DAMPING CALCULATION WITH FINITE ELEMENT ANALYSIS

MUHAMMAD SYAKIR BIN HARUN

UNIVERSITI SAINS MALAYSIA

2013

STUDY ON THE ACCURACY OF SQUEEZE FILM DAMPING CALCULATION WITH FINITE ELEMENT ANALYSIS

by

MUHAMMAD SYAKIR BIN HARUN

Thesis submitted in fulfillment of the requirements
for the degree of
Master of Science

December 2013

ACKNOWLEDGEMENTS

First of all, praise to Allah for enabling me finishing my master project. I would like to thank Dr. -Ing Muhammad Razi Bin Abdul Rahman for his support and for the direction he provided for this thesis and for his patience and his constructive comments.

I would like to thank my parents for the support that they give me all along during my progressing of this project. I also want to thanks the others for their support and guidance in finishing my master project.

I am gratefully acknowledging the assistance of everybody who helped directly and indirectly in the execution of this project. Thank you so much.

Muhammad Syakir Bin Harun

December 2013

TABLE OF CONTENTS

CHAPTER FIVE - RESULTS AND DISCUSSIONS

CHAPTER SIX - CONCLUSIONS AND RECOMMENDATIONS

LIST OF TABLES

LIST OF FIGURES

NOMENCLATURE

Roman symbols

A	Cross-sectional area
a	Equivalent cell radius
b	Equivalent hole radius
D	Displacement
D_b	Elasticity tensor for bending
D_s	Elasticity tensor for shear
E	Young's modulus of material
h	Film thickness
I_0	Modified Bessel function of the first kind of order zero
I_1	Modified Bessel function of the first kind of order one
K_0	Macdonald's function of the second kind of order zero
K_1	Macdonald's function of the second kind of order one
Kn	Knudsen number
L	Plate length
L_b	Beam length
l	Lateral dimension
N	Number of holes
N_i	Shape functions
n	Number of nodes
P	Pressure
Q	Volume flow rate

q	Holes pitch
Re	Reynolds number
R_p	Total flow resistance
r_h	Hydraulic radius
r_i	Hole radius
r_o	Cell radius
S_0	Hole side
T_b	Beam thickness
T_p	Plate thickness
t	Time
v	Fluid velocity
W	Plate width
W_b	Beam width

Greek symbols

β	Ratio of the hole to cell radius
λ	Mean free path
μ	Viscosity
ν	Poisson's ratio
ρ	Density
ρ_o	Unpertubed air density
σ	Squeeze number
ω	Radial frequency

KAJIAN TERHADAP KETEPATAN PENGIRAAN REDAMAN FILEM MAMPAT MENGGUNAKAN ANALISIS UNSUR TERHINGGA

ABSTRAK

Redaman filem mampat yang terhasil daripada udara yang terperangkap di antara struktur membran yang berayun melintang dan substrat tetap merupakan pertimbangan yang penting di dalam reka bentuk peranti MEMS kerana ia mempengaruhi keupayaan dinamik sesuatu sistem. Oleh itu, pembangunan peranti MEMS sangat bergantung kepada kaedah pemodelan dan simulasi untuk mengoptimumkan dan menguji reka bentuk tersebut sebelum proses pengeluaran. Tesis ini mencadangkan kaedah untuk pemodelan redaman filem mampat menggunakan kaedah unsur terhingga untuk mencapai hasil ketepatan yang tinggi di dalam masa yang sama dapat mengurangkan darjah kebebasan, dan keberkesanannya dikaji dengan membandingkan dengan kaedah yang lain. Analisis berangka dilakukan menggunakan perisian komersial ANSYS untuk pengiraan pekali redaman. Struktur bagi model-model tersebut dibina menggunakan model tiga dimensi (3D) dan model dua dimensi (2D). Keputusan yang diperolehi dari model-model kaedah unsur terhingga ini dibandingkan dengan data eksperimen yang sedia ada dan juga penyelesaian analitik. Hasil keputusan mendapati bahawa dalam pengiraan pekali redaman, model dua dimensi menghasilkan ketepatan yang lebih kurang sama dengan model tiga dimensi apabila dibandingkan dengan data eksperimen bagi kes jumlah lubang yang sedikit. Sebaliknya, bagi kes jumlah lubang yang banyak, model dua dimensi

yang dibangunkan di dalam kerja ini menunjukkan ketepatan yang lebih tinggi. Keputusan yang diperolehi jelas mengesahkan bahawa model yang dicadangkan di dalam tesis ini dapat mencapai ketepatan yang baik untuk penyelesaian pekali redaman, dan juga ia hanya memerlukan masa penyelesaian dan memori komputer yang rendah.

STUDY ON THE ACCURACY OF SQUEEZE FILM DAMPING CALCULATION WITH FINITE ELEMENT ANALYSIS

ABSTRACT

Squeeze film damping due to the air trapped between oscillating membrane structure and a fixed substrate is a critical consideration in the design of MEMS devices because it can adversely affect the dynamic behaviour of the system. Therefore, the development of MEMS depends highly on the modelling and numerical simulation in order to optimize and verify their design before the batch production process. In this thesis, a method to model squeeze film damping with finite element approach to attain sufficiently high accuracy while considerably reducing the degrees of freedom is proposed, and its effectiveness is studied by comparing with other methods. The numerical analysis was performed using commercial ANSYS software. The structures were modelled using three-dimensional (3D) element and two-dimensional (2D) element. Results obtained by finite element models are compared with existing experimental measurements and analytical solutions. It was found that for the computation of damping coefficient, two-dimensional model yields slightly similar accuracy with three-dimensional model with respect to experimental data for low number of holes. In contrast, for highly perforated membranes, the proposed two-dimensional model is shown to be more accurate. The results clearly validate the proposed model to achieve good accuracy for damping coefficient solution while consuming considerably less computer time and memory.

CHAPTER ONE

INTRODUCTION

1.1 Background of Project

Micro-electro-mechanical systems (MEMS) is micron-sized integrated devices consisting of mechanical and electronic components fabricated on a typically silicon material through the microfabrication technology processes. Advanced progress in integrated circuit (IC) technology has allowed the fabrication of unique MEMS devices that have been gaining widespread applications in industrial and consumer products such as microaccelerometers, pressure sensors, microresonators, and micromirrors (Bryzek et al., 1994). These demands stem from the capability of MEMS that can reduce manufacturing costs, allowing for miniaturization in terms of both size and weight to improve the performance of conventional devices.

A typical MEMS device can be characterized by structures where two parallel plates a few microns in sizes are separated by micron-sized gaps. One of the plates moves in transverse direction and another plate is fixed. Most of this device operates in the ambient conditions of air, in some cases for cost reason, and in other cases to meet requirement of specific motion. The schematic diagram of the structures is shown in Figure 1.1. However, the presence of air has siginificant effect on the dynamics response of the devices. Due to the normal motion of moving plate to the fixed plate, a thin film of air is trapped in a narrow gap between these two plates. The

thin film generates the damping and spring forces to the vibrating structures. At low operating frequencies, damping effect dominates, whereas at high frequencies, spring effect dominates. Since most MEMS devices operate at low frequencies, many researchers concentrate on the study of the damping effect due to the normal motion between the two plates that also has been known as squeeze film damping.

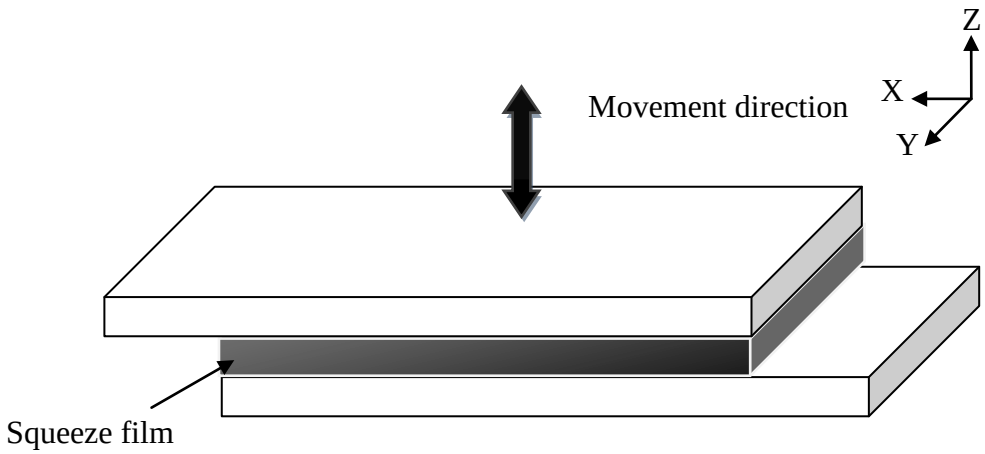

Figure 1.1: Schematic diagram of the MEMS structure.

One of the key requirements of such devices to meet is the low squeeze film damping on the structures. Perforation of the moving plate of the structures is a common solution for MEMS designers. Besides, perforated microstructure also has another function such as for efficient etching of sacrificial layers in the microfabrication process (Homentcovschi and Miles, 2005) and for controlling the stiffness of the structure (Clark *et al*., 2002). Alternatively, packaging these devices in a vacuum can help minimizing this damping, but it is not always desirable or even

practical to vacuum seal all such devices (Pandey and Pratap, 2007). The presence of holes makes the analysis of pressure distribution on the microstructure quite complicated since the flow of air surrounding the structure also needs to be considered in the analysis. A reasonably accurate determination of the fluid pressure distribution on the microstructures is a key to computing the squeeze film damping.

1.2 Squeeze Film in Macro- and Micro-Sized Domains

To design a system to meet its performance criteria, it is often necessary to model the system and then to analyze it in the context of those criteria. The type of model one uses may be a function of its size. The model will also be a function of its geometry, the way it is supported, and how it is constrained. The system's environment, in conjuction with its size, will determine which type of damping is important and if it must be taken into account.

Generally, MEMS devices range in size from micrometre to a milimetre. At these size scales, the standard cosntructs of classical physics are not always useful. As the size of devices becomes smaller, the surface to volume ratio increases, and the gas–surface interaction becomes important in microscale gas flows. Thus, surface effects such as electrostatics and wetting become more dominant than volume effects such as inertia or thermal mass in micro systems.

In micro devices, the effects of gas rarefaction including Knudsen number and surface accomodations effects, and surface roughness become important (Li, 2004) under the conditions of low ambient pressure or small gap. Three important parameters in micro devices are: the Knudsen number (K_n), the accomodation coefficients (AC_s), and the film thickness ratio.

1. The Knudsen number, K_n is defined as the ratio of the mean free path of gas to the characteristic length of the squeeze film.
2. The accomodation coefficients, AC_s (α_1, α_2) also called the tangential momentum accomodation coefficient, *TMAC* is an indicator of the average tangential momentum exchange of the collision between gas molecules and the solid boundary.
3. The film thickness ratio is defined as the ratio of the nominal film thickness to the standard deviation of composite roughness, which is an indicator of surface roughness.

Thus, with the introduction of more physical parameters to the model, the range of complexity in modelling approaches has been increased resulting in a more accurate calculation in the analysis of squeeze film damping.

1.3 Problem Statement

Research on squeeze film damping effect is of major interest since it critically influences the dynamic response of a MEMS device. Understanding the response are essential since many such devices have a wide range of industrial and consumer applications. The cost factor becomes a major issue with experimental works since fabrication of MEMS prototypes are in general very costly. Hence, the study of MEMS behaviour relies highly on modelling techniques. Generally, there are two different approaches of modelling the squeeze film behaviour: analytical model and numerical simulation using finite element analysis (FEA).

Typically, the analytical solution has limited application to simple geometrical structures of MEMS only. The real MEMS design consists of a complex and irregular geometry which is not adequate to solve with the analytical model. Instead, the numerical simulation approach is often used. However, numerical approach so far have centered on using three-dimensional (3D) model in structural domain that requires huge computational resource.

Due to most of MEMS devices having a thickness much smaller compared to lateral dimension, two-dimensional (2D) model of the membrane part should be always preferable in MEMS analysis. However the applicability of classical and modern plate theories for perforated, micron-sized plates remains on open question. The present research is motivated by the lack of studies in using two-dimensional model of perforated plates in modelling the structural part as this approach considerably reduces computational effort.

In addition, despite the many published analytical models in the literature, most of these papers lack extensive validations of the models with experimental data. This is understandable since measurements of test structures would require costly manufactured devices for test purposes. Another method to verify the models is with respect to the numerical modelling. Related analytical models will be used as another comparison with the proposed numerical models.

1.4 Objectives of Research

The objectives of this research are:

1. To construct a finite element model in two and three dimensions that accurately include established structural and fluidic theoretical frameworks in the dynamic analysis of MEMS perforated structures using the commercial finite element software package ANSYS.
2. To compare the model with established closed-form solutions and experimental data where applicable.
3. To validate the proposed model based on thin plate theories.
4. To assess the reduction in computational cost for the proposed model in terms of time and memory.

1.5 Thesis Outline

This thesis is organized into six chapters. An introduction of this work was presented in the first chapter which provides an overview of the MEMS and squeeze film damping, problem statement and the motivation of this work. In Chapter Two, the underlying theories that related to this work are discussed in detail. Literature review of the previous studies regarding to experimental, analytical, and numerical approach were also been presented. Next, the finite element formulation to develop the numerical model will be demonstrated in Chapter Three. Chapter Four describes the methodology of numerical scheme used to analyze the squeeze film damping. Chapter Five presents the comparison between analytical and numerical results to the existing experimental data. Discussion on the results are include in this chapter. Finally, Chapter Six outlines the conclusions of this work and recommendations for the future work.

CHAPTER TWO

LITERATURE REVIEW

This chapter provides an overview of the literature pertaining to squeeze film damping. In the first section, the fundamental of squeeze film will be reviewed. The second section describes the rarefaction, compressibility, and inertia effects in squeeze film behaviour. Third section focuses on a review of the modelling approaches of the squeeze film damping behaviour. This is divided into two subsections: analytical solutions and numerical approaches. The subsequent section presents a review of the plate theory. The next section provides a review of experimental studies of squeeze film damping behaviour where some results will be used to compare with the current work. The literature studies are critically summarized in the last section.

2.1 Squeeze Film Damping

There are numerous studies attempted to explain the different loss mechanism in MEMS devices (Zook *et al*. (1992); Mihailovich and MacDonald (1995); Cho *et al*. (1994); Lifshitz and Roukes (2000); Yasumura *et al*. (2000); Ye *et al*. (2003)). The most common mechanisms identified by Tilmans *et al*. (1992) include losses into surrounding fluid due to acoustic radiation and viscous damping, losses into support structure mount, and intrinsic damping caused by losses inside the material of mechanical structure. Among different sources of

energy dissipation, losses into surrounding caused by viscous damping have been shown to be a significant loss mechanism for devices operated near the atmospheric condition (Hosaka *et al*., 1995).

The behaviour of squeeze film between moving plate and fixed substrate was first discovered from the theory of fluid lubrication (Langlois, 1961). Generally, the characteristics of squeeze film are determined by both viscous and inertial effect of the fluid. Due to the very small sizes featured in MEMS devices, fluid inertia is often neglected in the squeeze film analysis (Bao and Yang, 2007). Therefore, the behaviour of fluid film is analyzed through the well-known Reynolds equation. The Reynolds equation is a nonlinear partial differential equation derived based on the classical Navier-Stokes equation under certain assumptions of the fluid flow behaviour (Pratap *et al*., 2007). A derivation of Reynolds equation can be referred in Bao (2005). Starr (1990) wrote the commonly used nonlinear Reynolds equation as:

$$\frac{\partial}{\partial x}\left(\frac{\rho h^3}{\mu}\frac{\partial P}{\partial x}\right)+\frac{\partial}{\partial y}\left(\frac{\rho h^3}{\mu}\frac{\partial P}{\partial y}\right)=12\frac{\partial(\rho h)}{\partial t} \tag{2.1}$$

where P is the film pressure, ρ is density, μ is viscosity, h is film thickness, and x and y are spatial coordinates.

The viscous flow effect arises when the fluid particles in the gap are moving in and out through the plate gap boundary regions. The force from this viscous flow is known as the damping force. On the other hand, if the fluid is not able to escape the gap region, it will be compressed due to normal movement of

the plate to the substrate. The spring force will generate due to the compression of the fluid.

The introduction of perforated holes to the microstructure causes the above conventional Reynolds equation to be no longer applicable since the mentioned equation only considers the fluid flow through the gap only (Feng *et al*., 2007). Since the perforated holes allow the air to flow across them, a new viscous force will be produced in the microstructure. Therefore, in the analysis of squeeze film for perforated microstructure, the Reynolds equation need to be modified by accounting the parameters related to the viscous flow through the holes (Bao *et al*., 2003).

These viscous and inertial forces are sometimes used as design parameters and desired in the MEMS devices. In other cases, these forces could decrease the device performance. For both reasons, prediction of these forces in MEMS device becomes very crucial.

2.2 Rarefaction, Compressibility, and Inertia Effects

In modelling the squeeze film effect in a perforated microstructure, it is important to understand the various phenomenons related to the gas flow and the geometry itself. The main effects that should be considered are gas rarefaction, compressibility, and inertial effects. These effects are characterized in term of non-dimensional numbers.

2.2.1 Rarefaction

The rarefaction effect becomes a more crucial consideration when a fluid flows in a micro-channel. In a perforated microstructure, air rarefaction effect in both flows in the air gap and through the holes must be recognized. Knudsen number is the indicator of characterizing the rarefaction effect. The Knudsen numbers for both flows in the air gap Kn_g and through the holes Kn_h are expressed in Eqs. (2.2) and (2.3). The value of Knudsen number will determine the regimes of flows taken in the microstructure as shown in Table 2.1 (Karniadakis *et al*., 2005). It is possible to have to different flow regimes in the air gap and the holes.

$$Kn_g = \frac{\lambda}{h} \tag{2.2}$$

$$Kn_h = \frac{\lambda}{r} \tag{2.3}$$

where r is the radius of the holes side and λ is the mean free path of particle.

Table 2.1: Flow regimes and their Knudsen number ranges.

Flow regimes	Knudsen number, Kn
Continuum flow	< 0.01
Slip flow	0.01 < Kn < 0.1
Transition flow	0.1 < Kn < 10
Molecular flow	> 10

The mean free path of particle is inversely proportional to the pressure. So, under very low pressure condition, the mean free path will be larger so that the Knudsen number also will be higher. The mean free path in micrometer can be expressed as:

$$\lambda = \frac{0.069}{P} \tag{2.4}$$

When the Knudsen number lies on the slip flow regime, the translational flow regime or the free molecular regime, the rarefied gas effect must be considered in the analysis. In the slip flow regime, a difference between surface velocity and average fluid velocity occur at the surface. This slip boundary condition can be treated using the 'effective' viscosity coefficient to replace the viscosity coefficient of fluid. An effective viscosity coefficient is a function of the Knudsen number. Veijola *et al*. (1995) has proposed a relationship that approximates the pressure and film thickness dependence of the viscosity as below:

$$\mu_{eff} = \frac{\mu}{1 + 9.638{K_n}^{1.159}} \tag{2.5}$$

However, when the pressure becomes much lower than an atmospheric pressure, the distance travelled by a gas particle between collisions becomes larger than the gap thickness. Hence, the collision among the particles will reduce such that the assumption of the gas as a viscous fluid is not applicable. This regime is known as the free molecular flow regime. There are some free molecular models had published by several authors to define this regime in the analysis (Christian (1966); Kádár *et al*. (1996); Li *et al*. (1999); Bao *et al*. (2002);

Hutcherson and Ye (2004)). The study of squeeze film damping in this regime also can be found in (Sumali, 2007).

For translational flow regime, the mean free path is neither very small nor very large to the characteristic dimension of the structure. The collision of the molecules with the surface of the body and intermolecular collisions are of more or less equal importance and consequently the analysis becomes very complicated (Pandey *et al*., 2008).

2.2.2 Compressibility

Compressibility effect is characterized with the squeeze number σ. If the squeeze number is less than 1, the compressibility effect is ignored and the flow can be treated as incompressible. For the higher value than 1, the compressibility effect becomes a significant to the analysis. Hence, the compressibility effect needs to be take consideration in the analysis. The squeeze number can be defined as (Pratap *et al*., 2007):

$$\sigma = \frac{12\mu l^2 \omega}{P_a h^2} \tag{2.6}$$

where l is the characteristic dimension related to the smallest dimension of the structure and ω is the radial frequency. Eq. (2.6) clearly shows that compressibility are proportional depending on the operating frequency and the ratio of characteristic dimension to the air gap height whereas it is inversely proportional to the pressure condition.

2.2.3 Inertia

The presence of inertial effect is defined in term of non-dimensional Reynolds number. The Reynolds number for both flows through the gap Re_g and the holes Re_h are given by Eqs. (2.7) and (2.8), respectively (Pratap *et al*., 2007).

$$Re_g = \frac{\rho \omega h^2}{\mu} \tag{2.7}$$

$$Re_h = \frac{\rho \omega r^2}{\mu} \tag{2.8}$$

Fluid inertial effect may be neglected when the Reynolds number is below than 1 (Re<1). Both equations suggest that the inertial effect is in dependence on the operating frequency, air gap height, and the radius of perforated holes. However, since most MEMS devices is fabricated in micron and nano scale sizes, operating frequency will be the major influence of the inertia effect.

2.3 Analytical and Computational Approaches

There are two different approaches used in modelling the squeeze film damping in microstructures. The first one is by analytical solution or compact modelling, and the second one is based on the numerical models. The major advantage of analytical approaches is their simplicity. However their applications are limited to simple geometry of the structure and certain regime conditions. The numerical modelling is a much more applicable to various geometries and the complete analysis of fluid flow is also possible. In modelling approaches, a major issue is to accurately estimate the pressure distribution in the microstructure

especially in the presence of the holes. The proper calculation of this pressure patterns is the goal of many studies.

2.3.1 Analytical Solutions

In an analytical model, all the relevant physical aspects of the system are described precise using the mathematical closed-form equations. During the past decades, a considerable amount of analytical models have been introduced to describe the behaviour of squeeze film effect in perforated microstructures. Basically, there are two common approaches were used to solve the modified Reynolds equation in the literatures. The main concept used in both approaches is representing the perforated plate as uniformly distributed cells with each cell having a single perforation. Table 2.2 gives an overview of the various squeeze film analytical models at a glance.

Figure 2.1(a) illustrates the schematic diagram of a vibrating perforated plate with circular holes considered as a set of uniformly distributed cells. r_o is the cell radius and r_i is the hole radius. The shape and size of these cells depends on the flow characteristics around the holes and the pitch of the hole distribution over the plate (Pandey and Pratap, 2008).

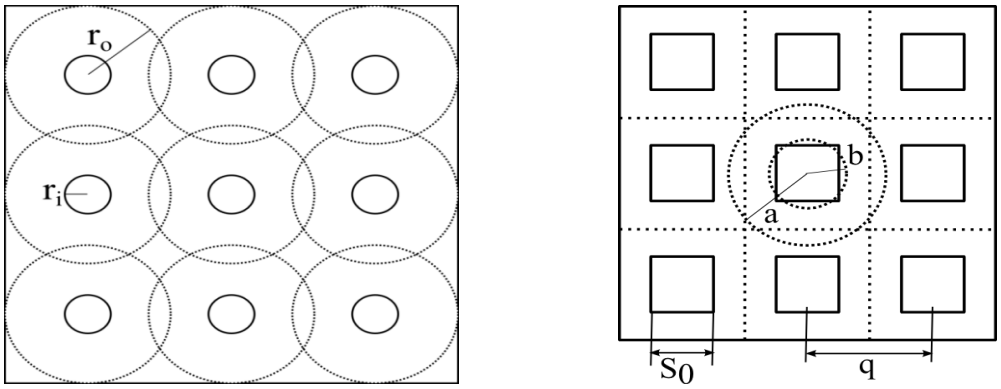

(a) (b)

Figure 2.1: Schematic diagram of the perforated plate with uniformly distributed cell of (a) circular holes and (b) square holes.

For a plate with uniformly distributed square section of the hole with size S_0 and pitch q as in Figure 2.1(b), the equivalent hole radius, b can be determined by comparing the resistance through a square channel and a circular pipe of the same length. The cell radius a is calculated by equating the areas of the square and circular shapes. The expression for the equivalent hole radius b and the cell radius a are (Veijola, 2006):

$$b = \frac{1.096 S_0}{2} \tag{2.9}$$

$$a = \frac{q}{\sqrt{\pi}} \tag{2.10}$$

In the first approach, the squeeze film damping within a single cell was obtained first by solving the related equation. Then, the overall damping is calculated by multiplying the damping of the single cell with the total number of cells. It has been applied in the studies done by the Mohite *et al*. (2005), Kwok *et al*. (2005) and Homentcovschi and Miles (2010).

Table 2.2: An overview of the different analytical models for perforated structures.

Damping coefficient	Authors	Equation	Important effects modelled
c_M	Mohite *et al*. (2005)	(2.11)	Rarefaction and compressibility
c_K	Kwok *et al*. (2005)	(2.12)	Rarefaction
c_H	Homentcovschi and Miles (2010)	(2.13)	Compressibility
c_B	Bao *et al*. (2003)	(2.14), (2.15)	-
c_P	Pandey and Pratap (2008)	(2.16), (2.17), (2.18)	Rarefaction and compressibility
c_V	Veijola (2006)	(2.19)	Rarefaction

In 2005, Mohite *et al*. proposed the closed-form solution for the damping and stiffness coefficients for perforated back plates of MEMS. They include the rarefaction and compressibility effect in their model. However, the model would appear to be inaccurate when they applied zero pressure condition at the inner cell while neglecting the flow rate across the holes for the boundary conditions. Neglecting flow across the holes is suitable for the cases where too small thickness of the holes is considered. According to this model, the damping coefficient is:

$$c_M = \frac{\pi P_a {r_o}^2}{h\omega} \times \left[Img \left[\frac{2R_i\left[I_1\left(\sqrt{\sigma j}R_0\right)K_1\left(\sqrt{\sigma j}R_i\right) - I_1\left(\sqrt{\sigma j}R_i\right)K_1\left(\sqrt{\sigma j}R_0\right)\right]}{\sqrt{\sigma j}\left[I_0\left(\sqrt{\sigma j}R_i\right)K_1\left(\sqrt{\sigma j}R_0\right) - K_0\left(\sqrt{\sigma j}R_i\right)I_1\left(\sqrt{\sigma j}R_0\right)\right]} \right] - \left({R_0}^2 - {R_i}^2\right) \right] \quad (2.11)$$

where $R_i = r_i/r_o$, $R_o = r_o/r_o = 1$, I_0 and I_1 are the modified Bessel functions of the first kind of order zero and one, respectively, K_0 and K_1 are the Macdonald's function of the second kind of order zero and one, respectively.

Then, Kwok *et al*. (2005) derived the formula of damping constant based on the solution of Reynolds equation by using non-zero pressure at the inner boundary and zero pressure at the outer boundary for the boundary conditions of the cell. They show that the pressure at the inner boundary can be represented by the product of the squeeze number, a geometry term, and a rarefaction term. The damping coefficient of Kwok's model is determined by:

$$c_K = \frac{3\mu_{eff} q^4 N}{8h^3} K(\beta) + 8\pi\mu_{eff} T_p N \frac{(q^2 - {s_0}^2)^2}{{s_0}^4} \quad (2.12)$$

where N is the number of holes, T_p is the plate thickness, $\beta = r_i/r_o$ is the ratio of the hole to cell radius, and $K(\beta) = 4\beta^2 - \beta^4 - 4In\beta - 3$. The damping constant expression in this case captures the loss due to flow in the gap under the cell on the first term of equation and the loss due to flow through the holes on the second term.

In another study, Homentcovschi and Miles (2010) developed the analytical solution for fluid damping based on the Navier-Stokes equation. This model is developed for cases when the Reynolds equation cannot be applied in which the air gap is the same order with the characteristic dimension of the plate. They characterize the fluid flow through the holes by using 2D axisymmetrical pattern problem. The damping coefficient in this case is given by:

$$c_H = \frac{i\omega\rho_o}{\beta}\frac{\pi {r_o}^2 \cos(kh)}{k\sin(kh)}\left[1 - \frac{{r_i}^2}{{r_o}^2 cos(kh)}W_o\right] \times N \qquad (2.13)$$

where ρ_o is the unpertubed air density, k, β and W_o are the constants as defined in (Homentcovschi and Miles, 2010).

In this approach, it seems the major sources of error comes from the assumption of each cell is identical to each other. This is because the cells located around the plate boundary and the cells in the interior are considerably having different pressure distribution. This error becomes more significant in the small perforation ratio plate and when the number of holes in the boundary is comparable to the number of holes in the interior.

In the second approach, the total squeeze film damping was determined by directly solving the modified Reynolds equation within the whole plate. Some examples of this approach were found in Bao *et al*. (2003), Pandey and Pratap (2008) and Veijola (2006).

Bao *et al*. (2003) have solved the modified Reynolds equation for uniformly perforated rectangular plate. Here, the incompressible gas is assumed. The authors validated their model by comparing with the experimental results done by Kim *et al*. (1999). The damping coefficient can be written as:

$$c_B = \gamma \frac{\mu L^3 W}{h^3} \tag{2.14}$$

Here, the expression of γ is obtained as:

$$\gamma = 3\alpha^2 - 6\alpha^3 \frac{\sinh^2 \frac{1}{\alpha}}{\sinh \frac{2}{\alpha}} - \frac{24\alpha^3 \chi}{\pi^2} \sum_{n=1,3,5\ldots}^{\infty} \frac{\tanh\left(\frac{\sqrt{1+(n\pi\alpha/2)^2}}{\alpha\chi}\right)}{n^2(1+(n\pi\alpha/2)^2)^{3/2}} \tag{2.15}$$

where $\chi = W/L$ is the plate aspect ratio, and $\alpha = 2l/W$, where l is the attenuation length in (Bao *et al*., 2003), depending on the air gap height, the effective hole thickness, the ratio between the hole and cell radius, and the hole radius.

Further work on Bao's model was performed by Pandey and Pratap (2008). They have included the compressibility and rarefaction effects in their model. They also introduced an important term which captures the perforation effect coupling with the compressibility and rarefaction effects. The term is defined by the ratio of the width of the plate to the characteristics length given in (Pandey and Pratap, 2008). In this case, the width is the smallest dimension

compare to the length of the plate. The final expression of damping coefficient is given by:

$$c_P = c_s + c_h \tag{2.16}$$

where

$$c_s = \frac{16\sigma}{\pi^6}\frac{P_a \chi L^2}{\omega h}\sum_{m,n=odd}\frac{\left(\frac{\Gamma^2}{\pi^2}+m^2\chi^2+n^2\right)\left[4-f_{perf}\right]}{(mn)^2\left[\left(\frac{\Gamma^2}{\pi^2}+m^2\chi^2+n^2\right)^2+\frac{\sigma^2}{\pi^4}\right]} \tag{2.17}$$

and

$$c_h = 8\pi\mu\left(\frac{T_p}{Q_{th}}+\Delta_E b\right)\times N \tag{2.18}$$

The Q_{th} is the flow rate factors which account rarefaction effect in the flow through the holes given in (Veijola, 2006), and Δ_E is the relative elongation of the hole side (Pandey and Pratap, 2008).

Veijola (2006) published a paper that presented a very complete model which derived by dividing the perforation cell into several regions: the squeezed film and intermediate region in the air gap, the capillary flow in the hole, and the outflow region above the hole. Each region is defined with their flow resistances. On solving a modified Reynolds equation which takes into accounts both compressibility and rarefaction effects, an expression of damping coefficient are obtained as:

$$c_V = \frac{768\mu LW}{h^3\pi^6 Q_{ch}}\sum_{m,n=odd}\frac{1}{(mn)^2\left[\frac{m^2}{L^2}+\frac{n^2}{W^2}+\frac{768\mu LW}{64\pi^2 h^3 Q_{ch} N R_p}\right]} \tag{2.19}$$

where R_p is the total flow resistance.

In order to improve the model, De Pasquale *et al*. (2010) have proposed the contribution of the gas damping due to the supporting springs should be included. The approximate equation in estimation the damping coefficient due to the springs with considering four springs, slips conditions, non-translational motion and border elongation is:

$$c_b = \frac{4}{2}\frac{L_b[(W_b + 1.3(1 + 3.3K_{ch})h)]^3\mu}{h^3(1 + 6K_{ch})} \tag{2.20}$$

Besides, they also mentioned the relatively large spacing between the outmost holes and the plate border, S_2 causes an increased pressure frame around the perforated region that contributed to the total damping on the structure. The expression of damping coefficient for the pressure frame is:

$$c_f = \frac{(2a + 2b - 4S_2){S_2}^3\mu}{h^3(1 + 6K_{ch})} \tag{2.21}$$

2.3.2 Numerical Approaches

Typically, analytical solutions are restricted to relatively simple structures of MEMS only. Often actual MEMS designs consist of a complex and irregular geometry structures with non uniform size and distribution of holes which is not adequate to solve with the analytical model. In addition, non-linear pressure response may also present. Numerical simulations using finite element method (FEM) approach is often used to evaluate the behaviour of MEMS at device design stage. Moreover, the numerical approach has been commonly used to assess the accuracy of the analytical model or the experimental test.

Recently, there is increasing capability of modelling squeeze film damping in commercial FEA package like ANSYS, and numerical results are often found in the literatures. Somà and De Pasquale (2007) and Somà and De Pasquale (2008) predicted the damping and stiffness coefficients numerically using two different techniques: constant imposed velocity method and a modal projection method. They concluded that the mesh density significantly influences the accuracy of results in the modal projection method while the effect is negligible for the first method.

From the literatures, the absence of 2D models for modelling the perforated plate vibration is rather glaring considering high aspect ratios of MEMS plates should lead one to model them in 2D. So far, most studies use the 3D solid modelling the structural part, but there are no attempts at that using 2D shell plates or model in evaluating the squeeze film damping behaviour. Such papers that using the 3D solid element are presented in Beltman *et al*. (1997), Pandey and Pratap (2007), Guo *et al*. (2007), and Chaterjee and Pohit (2010). In 2009, De Pasquale and Soma has suggested the application of 2D shell element structure model however it is limited to predict the resonance frequency of the MEMS structure only (De Pasquale and Somà, 2009).

Alternative approach to numerical solutions of Reynolds equation is also proposed in the literatures. A Perforation Profile Reynolds (PPR) method was presented by Veijola and Råback in solving the squeeze film damping problem (Veijola and Råback, 2007). This method is also based on the same Reynolds equation as Eq. (2.1) but the equation is improved with an additional term to

account the leakage flow resistance through the perforations. The same method was also utilized in De Pasquale and Veijola (2008) study. They found the damping force results from PPR method give a better agreement than the conventional method in 3D simulations.

A semi-analytical approach was presented by Nayfeh and Younis (2004) in modelling and simulation of flexible microstructures under the effect of squeeze-film damping by first using perturbation techniques to linearize the coupled equation of elasticity and the Reynolds equation to expressing the pressure distribution in terms of the structural mode shapes. The resulting governing equation is then solved using a FEM to extract natural frequencies, structural mode shapes, corresponding pressure distribution, and quality factor.

2.4 Plates Vibration Modelling

The vibration of plates is a special case of the more general problem of mechanical vibrations. The equations governing the vibration of plates are simpler than those for a general three-dimensional object due to one of the dimensions of a plate is much smaller than the other two. A plate theory takes advantage of this disparity in length scale to reduce the analysis of three-dimensional structures to a two-dimensional problem. This suggests that a two-dimensional plate theory will give an excellent approximation to the actual three-dimensional motion of a plate. The theory of plates is an approximation of the three-dimensional elasticity theory to two dimensions, which permits a description of the deformation of every point

in the plate in terms of only the deformation of the midplane of the plate (Rao, 2007).

There are several classical theories that have been developed to describe the motion of plates. The most commonly used are the Kirchhoff-Love theory and the Reissner-Mindlin theory. The Kirchoff-Love plate theory or classical plate theory is an extension of Euler-Bernoulli beam theory. The following assumptions are made (Rao, 2007):

1. The middle plane of the plate remains as the neutral plane after deformation.
2. The displacements of the midsurface of the plate are small compared to the thickness of the plate.
3. The influence of transverse shear deformation is neglected.

The Reissner-Mindlin theory of plates is an extension of Kirchoff-Love theory that takes into account shear deformations along the thickness of the plate. Another assumption is that the originally line normal to the middle surface remains straight, but it is not necessarily normal to middle surface (Bathe, 1996). It also often called the first-order shear deformation theory of plates.

Indeed, many different shell elements have already been proposed in the literature. Several studies on this shell element technology have been carried out on Schoop (1989), Wriggers *et al*. (1995), and Hauptmann and Schweizerhof (1998). However, these types of element are not available in commercial FEA software like ANSYS.

Fortunately, the analysis of solid plates is well established. However, for a plate having a holes, different theories have been introduced to solve such vibration of plate problem. By considering the hole as an extremely thin part of the plate, the vibration analysis of such plates with a hole can be transformed into an equivalent plate with non-uniform thickness (Huang and Sakiyama, 1999). Lee *et al*. (1990) pointed that the numerical methods for analysed the natural frequencies of perforated plate can be classified into three categories, namely the finite element and finite difference methods, the series-type analytical method, and the semi-analytical approach based on the Rayleigh-Ritz principle.

As in Leissa (1969), one of the major classical studies of this such problem was done by Takahashi (1958) who used the Rayleigh-Ritz method and deflection functions which are products of beam deflection functions to predict the fundamental frequency at the first mode of vibration. Elsewhere, Hegarty and Ariman (1975) has reported Takahashi's study where they found that the frequency increased constantly with increasing hole size.

2.5 Experimental Data

In order to validate the accuracy of the analytical and numerical modelling approaches which previously explained, we need the experimental data as the benchmark to evaluate the models effectiveness. However, the major drawback is the quite small amounts of experimental data were reported in the literatures.

Typically, the measured damping and stiffness values were only extracted at first mode resonance frequency.

The preliminary work on measured the damping coefficients in vibrating perforated microstructure was undertaken by Kim *et al*. (1999). They had done the experimental work on a set of nine polysilicon structures, having three different holes sizes with three different numbers of holes. The measured data has been validated with the theoretical values comes from finite element analysis. They have found bigger discrepancy from the theoretical value so that they conclude the major possibility error comes from the zero pressure boundary condition applied on the holes edges in the finite element analysis.

Pandey and Pratap (2008) performed an experiment on polysilicon square MEMS structure to validate their proposed analytical model. It also compared with the different analytical models that already exist in the literature. They show that their proposed model agrees within 5% to the experimental results while the other models lie far from the experimental value. They also measured the quality factor of the structure as the result validation.

Then, Soma *et al*. provide the measurement data of six different polysilicon structures which the first four specimens in the same size in plate dimensions but differ by holes cross section size while the other two structures are characterized by the same holes dimension but a different plate width. The plate structure is supported by four lateral clamped beams. The experimental measurements were conducted by the optical interferometric microscope where

the damping and stiffness extraction were done by the Frequency Shift technique (Somà and De Pasquale, 2008).

Later, Veijola *et al*. carried out experiment on six rectangular polysilicon perforated microstructures. The structure consists of various dimension sizes, number of holes and sizes of holes. They have compared their measured damping coefficients with the different compact models and the reasonable error of differences value was also been discussed (Veijola *et al*., 2009).

In this work, we considered the data provided by De Pasquale *et al*. (2009). The authors carried out experiment on six gold rectangular plates and twenty-eight gold square plates with variety of cases in term of the number of holes and the holes sizes. The plate side dimension is also variable. The experiments have been performed by the structures were electrostatically excited to vibrate at their fundamental mode. Then the vibration amplitudes were measured optically. The half-power method has been used to extract damping parameters of the vibrating system. The details dimension of this structure will be shown in the Chapter Four.

2.6 Summary

There are three main effects that need to be understood in modelling perforated MEMS structure behaviour. The compressibility and inertial effects are dominant only at higher operating frequencies. On the contrary, rarefaction effect can be apparent even at low frequencies.

To date, based on a review of literature presented, it is evident that modelling the perforated MEMS structure with two-dimensional model are scarce and most of the work previously focused on three-dimensional model. Based on literature on the plate theory, it suggested the capability to model the structural part using two-dimensional element. Experimental work done by De Pasquale *et al*. (2009) is used as case study. The relevant analytical has been selected for validation of accuracy of the proposed model.

CHAPTER THREE

FINITE ELEMENT METHOD FOR PLATES VIBRATION WITH SQUEEZE FILM DAMPING

This chapter presents the theoretical background to the Finite Element Method (FEM) used in the analysis of squeeze film damping. It illustrates how the FEM can be applied to solve for problems involving squeeze film. The theoretical overview of the plate theory and their finite element formulation was discussed first. Then, the finite element formulation for fluid domain was presented. Approach of Modal Projection Method is explained in the last section. By studying the relevant theoretical frameworks, a suitable approach to obtain optimal computations for the solutions is expected.

3.1 Structural Domain

A plate is a structure where its thickness is small compared with other characteristic dimensions, i.e., length and width. They are widely used in many engineering applications such as bridges, turbine disks, airplanes and ships. Plates used in such applications are normally subjected to lateral loads, causing bending of the plate. In general, plate can be classified into three major categories according to the ratio of the lateral dimension of a plate, l to the plate thickness, T_p. The various types of plate classification are given in Table 3.1 (Ventsel and Krauthammer, 2001).

Table 3.1: Classification of the different types of plate.

Plate types	Thick	Thin	Membrane
Lateral dimension/thickness	$\leq \{8 - 10\}$	$\{8 - 10\} \leq l/T_p \leq \{80 - 100\}$	$\geq \{80 - 100\}$
Equivalent theory	Elasticity theory	Classical plate theory	Nonlinear plate theory

For a plate with ratios $l/T_p \leq \{8 - 10\}$, the analysis of such a plate is based on general three-dimensional theory of elasticity. However, as the thickness becomes very small, several assumptions may be introduced to simplify the solution. The basic assumption is that the stress through the thickness (i.e., perpendicular to the mid-surface) of the plate is zero. Applying the above assumptions, a three-dimensional model of the plate may be reduced to a two-dimensional model.

The thin plate behaviour is studied first using the classical plate theory that is based on the Love-Kirchoff assumption. In the Love-Kirchoff theory, the shear deformations along the thickness of the plate are neglected and an imaginary straight line perpendicular to the midsurface remains straight line during deformation. Later, the development of Kirchoff-Love plate theory called Reissner-Mindlin plate theory was proposed which takes into account the shear deformation along the thickness of the plate. As the thickness becomes very small, i.e., the ratio l/T_p get extremely high, $l/T_p \geq \{80 - 100\}$, the plate will potentially undergo considerably large deflections, hence nonlinear plate theory is crucial for this case.

In this work, it is observed that, in general the plate vibration is modelled in three dimension which obviously requires more computational resource in finite element (FE) computations. Hence, the main focus is to validate the viability of reducing the problem into its two-dimensional equivalence. The accuracy between the three-dimensional and two-dimensional finite element model for structural domain in modelling the squeeze film analysis is on interest in this study. Here, we summarize the essential theory of plate with their finite element formulation related to two and three dimensions. General FE formulation for structural analysis can be found in Zienkiewicz and Taylor (2005) and Bathe (1996).

3.1.1 Three-Dimensional (3D) Model

In general, theory of elasticity is used to predict the behaviour of a three-dimensional structural plate. Consider a plate that is discretized using quadratic 20-nodes isoparametric hexahedral element. The standard element is as shown in Figure 3.1. The element has three degrees of freedom (DOF) on each node: displacements in the *x*, *y*, and *z* directions.

The nodal displacements are given by:

$$u = \{x_1\ y_1\ z_1\ x_2\ y_2\ z_2\ \dots\ x_n\ y_n\ z_n\}^T \tag{3.1}$$

where *n* is refer to the number of nodes of the element and *T* donates the matrix transpose.

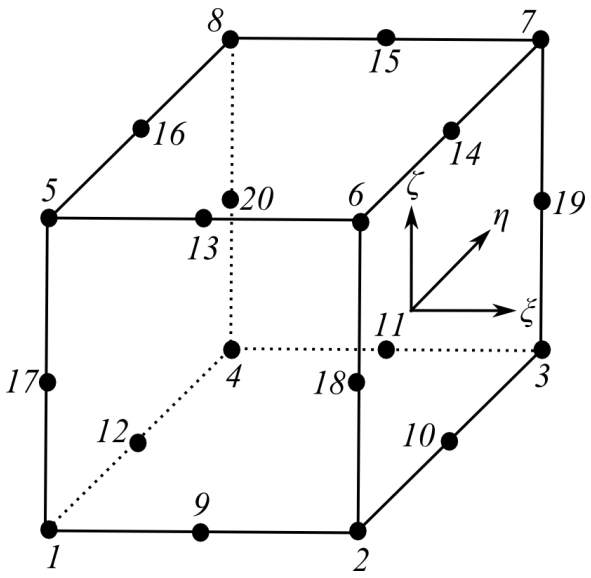

Figure 3.1: A 20-nodes hexahedral element.

The approximation values of displacement within an element can be determined with:

$$x = \sum_{i=1}^{n} N_i x_i\,, \quad y = \sum_{i=1}^{n} N_i y_i\,, \quad z = \sum_{i=1}^{n} N_i z_i \tag{3.2}$$

where x, y, and z are the local displacements at any point of the element and x_i, y_i, and z_i are the corresponding element displacements at ith node. The term of N_i represents the shape functions associated with ith node. The shape functions for the quadratic element with 20 nodes can be written as the following form:

$$N_i = \frac{1}{8}(1+\xi_0)(1+\eta_0)(1+\zeta_0)$$

$$(\xi_0 + \eta_0 + \zeta_0 - 2), \quad i = 1,2,\dots,8;$$

$$N_i = \frac{1}{4}(1-\xi^2)(1+\eta_0)(1+\zeta_0), \quad i = 9,11,13,15; \tag{3.3}$$

$$N_i = \frac{1}{4}(1-\eta^2)(1+\xi_0)(1+\zeta_0), \quad i = 10,12,14,16;$$

$$N_i = \frac{1}{4}(1-\zeta^2)(1+\xi_0)(1+\eta_0), \quad i = 17,18,19,20;$$

where $\xi_0 = \xi\xi_i$, $\eta_0 = \eta\eta_i$, and $\zeta_0 = \zeta\zeta_i$. The ξ_i, η_i, and ζ_i are values of local coordinates ξ, η, and ζ at nodes.

By using either the Lagrange dynamical equations or Hamilton's variational principle, the consistent element mass matrix for structure element can be written as (Bathe, 1996):

$$m_e = \int_{\Omega_s} \rho N^T N d\Omega_s \tag{3.4}$$

where ρ is the mass density of the material and Ω_s is the element's structure domain. The matrix of shape functions is:

$$N = \begin{bmatrix} N_1 & 0 & 0 & \dots & N_n & 0 & 0 \\ 0 & N_1 & 0 & \dots & 0 & N_n & 0 \\ 0 & 0 & N_1 & \dots & 0 & 0 & N_n \end{bmatrix} \tag{3.5}$$

Assuming a linear elastic body with the stress-strain relation $\sigma = D_b\epsilon$ and a strain-displacement relation $\epsilon = Bd$, the element stiffness matrix corresponding to general plane stress is given by the expression:

$$k_e = \int_{\Omega_s} B^T D_b B d\Omega_s \tag{3.6}$$

The elasticity tensor D_b for isotropic material reads as follows:

$$D_b = \frac{E}{1-v^2}\begin{bmatrix} 1 & v & v & 0 & 0 & 0 \\ v & 1 & v & 0 & 0 & 0 \\ v & v & 1 & 0 & 0 & 0 \\ 0 & 0 & 0 & \frac{1-v}{2} & 0 & 0 \\ 0 & 0 & 0 & 0 & \frac{1-v}{2} & 0 \\ 0 & 0 & 0 & 0 & 0 & \frac{1-v}{2} \end{bmatrix} \tag{3.7}$$

where E is Young's modulus and v is the Poisson's ratio.

The strain-displacement matrix B is described by:

$$B = \begin{bmatrix} \partial N_i/\partial x & 0 & 0 \\ 0 & \partial N_i/\partial y & 0 \\ 0 & 0 & \partial N_i/\partial z \\ \partial N_i/\partial y & \partial N_i/\partial x & 0 \\ 0 & \partial N_i/\partial z & \partial N_i/\partial y \\ \partial N_i/\partial z & 0 & \partial N_i/\partial x \end{bmatrix} \tag{3.8}$$

Integration of expressions for mass m_e and stiffness k_e matrices are usually evaluated numerically using Gauss-Legendre quadrature.

3.1.2 Two-Dimensional (2D) Model

In two dimensions, the structural domain is modelled using the Reissner-Mindlin plate theory which takes into account both bending and shear deformation through the thickness of the plate. Derivation of the element mass and stiffness matrices can be constructed from the principle of virtual work (Bathe, 1996). The expression for the principle of virtual work describes the energy U_e due to bending and shear forces are:

$$U_e = \int_{\Omega_s} \kappa^T D_b \kappa \, d\Omega_s + \int_{\Omega_s} \gamma^T D_s \gamma \, d\Omega_s \tag{3.9}$$

where the internal bending moments and shear forces are $D_b\kappa$ and $D_s\gamma$, respectively with

$$\kappa = \begin{bmatrix} \dfrac{\partial \theta_x}{\partial x} \\ \dfrac{\partial \theta_y}{\partial y} \\ \dfrac{\partial \theta_y}{\partial x} + \dfrac{\partial \theta_x}{\partial y} \end{bmatrix} \qquad \gamma = \begin{bmatrix} \dfrac{\partial u}{\partial x} - \theta_x \\ \dfrac{\partial u}{\partial y} - \theta_y \end{bmatrix} \tag{3.10}$$

The elasticity tensors for isotropic element in 2D for bending (D_b) and shear (D_s) are:

$$D_b = \frac{Eh^3}{12(1-v^2)} \begin{bmatrix} 1 & v & 0 \\ v & 1 & 0 \\ 0 & 0 & \dfrac{1-v}{2} \end{bmatrix} \qquad D_s = \frac{Ehk}{2(1+v)} \begin{bmatrix} 1 & 0 \\ 0 & 1 \end{bmatrix} \tag{3.11}$$

where u is the displacement of the plate, θ_x and θ_y are the rotations around x and y axis, respectively, and κ is the shear energy correction factor.

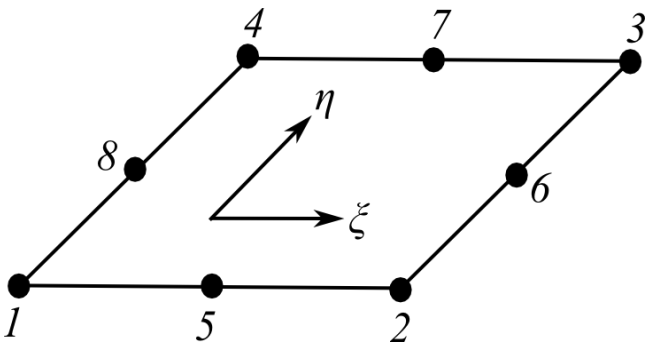

Figure 3.2: A 8-nodes quadrilateral element.

Using eight-nodes quadrilateral elements as shown in Figure 3.2, each node has three DOF: displacements in the *x*, *y*, and *z* axis. The nodal degrees of freedom and the approximation displacement within an element using their nodal values are same as given in Eqs. (3.1) and (3.2), respectively. Now, the shape functions for the 8-nodes quadrilateral two-dimensional elements are presented as below:

$$N_i = \frac{1}{4}(1+\xi\xi_i)(1+\eta\eta_i), \quad i = 1,2,3,4;$$

$$N_i = \frac{1}{2}(1-\xi^2)(1+\eta\eta_i), \quad i = 5,7; \tag{3.12}$$

$$N_i = \frac{1}{2}(1+\xi\xi_i)(1-\eta^2), \quad i = 6,8;$$

The consistent element mass matrix is equivalent to:

$$m_e = \int_{\Omega_s} \rho N^T \begin{bmatrix} h & 0 & 0 \\ 0 & h^3/12 & 0 \\ 0 & 0 & h^3/12 \end{bmatrix} N d\Omega_s \tag{3.13}$$

Then, the element stiffness matrix is:

$$k_e = \int_{\Omega_s} \frac{h^3}{12} B^T D_b B d\Omega_s + \int_{\Omega_s} \kappa h {B_s}^T D_s B_s d\Omega_s \tag{3.14}$$

where B and B_s denotes the derivatives of the shape function, N in accordance with Eq. (3.10).

Refer to Eq. (3.14), the thickness of the element is implicitly defined here. The numerical integration is also based on Gauss-Legendre quadrature.

3.2 Fluidic Domain

As described in the previous chapter, the flow of a fluid in a thin channel between two solids in relative motion is describes by the Reynolds equation. The most important assumption in the derivation of this Reynolds equation is that the film thickness is small compared to the other dimensions of the domain. It is further assumed that the viscosity and pressure are constant across the film, and that the flows are laminar and isothermal condition (Pratap *et al*., 2007). As a result the Reynolds equation represents the mass conservation of the fluid in terms of the pressure and film thickness as written in Eq. (2.1). However, this form of equation is not suitable for FEM discretization (Hannot and Rixen, 2009).

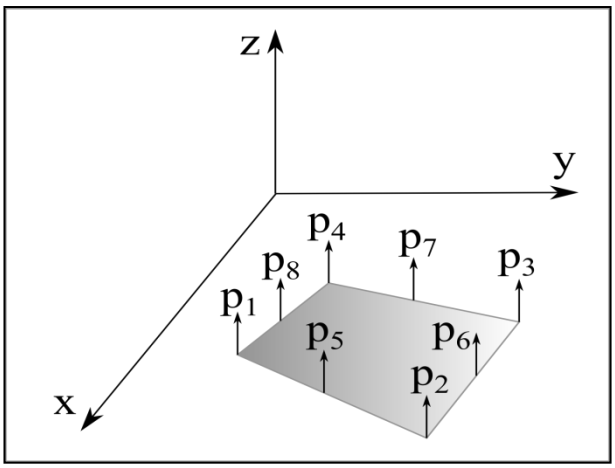

Figure 3.3: Fluid element geometry with pressure DOF.

In general case, the Reynolds equation is a two-dimensional equation that is based on the assumption that there is no variation of pressure across the fluid film. Consider the squeeze film to be discretized with 2D plain element with 8-

nodes quadrilateral elements that provide quadratic approximation of pressure as shown in Figure 3.3. The element consists of one pressure DOF at each node. The pressure within an element is approximated using the nodal values as given by:

$$P = \sum_{i=1}^{n} N_{fi} P_i \tag{3.15}$$

for n = 8 and N_{fi} represents the shape function of a fluid element associated with i node. The same shape functions for the structural domain are used for the fluid domain.

The element degrees of freedom are:

$$P_e = \{ P_1 \; P_2 \; \ldots P_n \}^T \tag{3.16}$$

By using the Einstein's summation convention, the Reynolds equation in Eq. (2.1) can be simplified in the following form:

$$\frac{\partial(\rho h)}{\partial t} = \frac{\partial}{\partial x_i}\left(\frac{\rho h^3}{12\mu}\frac{\partial P}{\partial x_i}\right) \tag{3.17}$$

where i runs from 1 to 2, i.e., x and y.

When it is assumed that the flow is to be isothermal, the density is proportional to the pressure:

$$h\frac{\partial P}{\partial t} + P\frac{\partial h}{\partial t} = \frac{\partial}{\partial x_i}\left(\frac{P h^3}{12\mu}\frac{\partial P}{\partial x_i}\right) \tag{3.18}$$

For the boundary conditions, it is assumed that the pressure on the open edges of the plate is equal to the ambient pressure and that zero pressure gradient at the closed edges of the plates:

$$\frac{\partial P}{\partial x_i} n_i = 0 \tag{3.19}$$

where the n_i is the component of the normal vector in the direction of x_i.

In order to discretized the Reynolds equation for finite element formulation, Eq. (3.18) is transformed into its weak form by multiplying with a test function v, and integrated over the fluid domain:

$$\int v \left[h \frac{\partial P}{\partial t} + P \frac{\partial h}{\partial t} - \frac{\partial}{\partial x_i} \left(\frac{P h^3}{12\mu} \frac{\partial P}{\partial x_i} \right) = 0 \right] d\Omega \tag{3.20}$$

The last term of the above equation can be rewritten as:

$$\begin{aligned} &\int v \frac{\partial}{\partial x_i} \left(\frac{P h^3}{12\mu} \frac{\partial P}{\partial x_i} \right) d\Omega \\ &\qquad = \int v \frac{P h^3}{12\mu} \frac{\partial P}{\partial x_i} n_i \, d\Gamma - \int \frac{\partial v}{\partial x_i} \frac{P h^3}{12\mu} \frac{\partial P}{\partial x_i} d\Omega \end{aligned} \tag{3.21}$$

where Γ is the boundary of the fluid domain. When the boundary condition of the Eq. (3.19) is substituted into Eq. (3.21), this leads to:

$$\int v \frac{\partial}{\partial x_i} \left(\frac{P h^3}{12\mu} \frac{\partial P}{\partial x_i} \right) d\Omega = - \int \frac{\partial v}{\partial x_i} \frac{P h^3}{12\mu} \frac{\partial P}{\partial x_i} d\Omega \tag{3.22}$$

Now the FEM discretization of pressure and fluid is defined with the:

$$P = {N_f}^T P, \qquad h = {N_f}^T h, \tag{3.23}$$

and with the Galerkin method, the shape functions are used as test functions:

$$v = N_f \tag{3.24}$$

Introducing of Eqs. (3.22), (3.23), and (3.24) into Eq. (3.20) gives:

$$\int N_f h {N_f}^T \, d\Omega \frac{\partial P}{\partial t} + \int \frac{\partial N_f}{\partial x_k} \frac{P h^3}{12\mu} \frac{\partial {N_f}^T}{\partial x_k} d\Omega P + \int N_f P {N_f}^T \, d\Omega \frac{\partial h}{\partial t} \tag{3.25}$$

Eq. (3.25) can be written in matrix vector form as:

$$M_f \dot{p} + K_f p + Q_f^T \dot{h} = 0 \tag{3.26}$$

where M_f and K_f are, respectively, the assembled global mass and stiffness matrices for the fluid. The global coupling matrix Q_f transfers the velocities of the structure to the fluid domain. A superposed dot represents the time derivative. The element-wise mass, stiffness and coupling matrix matrices can be defined with the following relations:

$$m_f = \frac{h}{P} \int N_f^T N_f \, d\Omega \tag{3.27}$$

$$k_f = \frac{h^3}{12\mu} \int \left(\frac{\partial N_f^T}{\partial x} \frac{\partial N_f}{\partial x} + \frac{\partial N_f^T}{\partial y} \frac{\partial N_f}{\partial y} \right) d\Omega \tag{3.28}$$

$$q_f = \int N_f^T N_f \, d\Omega \tag{3.29}$$

The numerical integration of Eqs. (3.27) and (3.28) is handled using 3×3 Gauss-Legendre quadrature.

For the element used to model the fluid flow through the perforation holes, there are some assumptions too: isothermal viscous flow at low Reynolds numbers, small channel length compared to the acoustic wave length, and a small pressure drop with respect to ambient pressure (ANSYS 12.0). As this element considers gas rarefaction, it also allowed channel lengths to be small compared to the mean free path.

Based on continuum flow theory, the volume flow rate Q of the square cross-sections channel is evaluated by the Hagen-Poiseuille equation:

$$Q = \frac{8{r_h}^2}{\mu\varphi}\frac{A}{l_c}\Delta_P \tag{3.30}$$

where r_h is the hydraulic radius, A is holes cross-sectional area, l_c is the hole length, φ is the friction factor, and Δ_P is the pressure gradient along the channel length. The hydraulic radius is defined as:

$$r_h = \frac{S_0}{2} \tag{3.31}$$

while the friction factor φ for square holes is approximated by:

$$\varphi = \frac{24}{0.422} \tag{3.32}$$

The mechanical resistance R_M of the holes can be estimated by:

$$R_M = \frac{F}{v} = \frac{\mu\varphi l_c A}{8{r_h}^2} \tag{3.33}$$

Note that $F = \Delta_P A$ and $v = Q/A$, where v is the fluid velocity at the cross-sections.

In summary, a linear elastic theory is used for three-dimensional model and the Reissner-Mindlin theory is used for two-dimensional model to analyze the displacement field, whereas the Reynolds equation is used for the air pressure field. The formulation is based on a finite element discretization of both the displacement and pressure fields.

3.3 Modal Projection Method

As the structure encounters the flexible oscillation dynamic motion, the modal projection method is used in ANSYS for the analysis of the squeeze film. Due to the displacement and the velocity varying along the flexible structure, the correlation between the deformed shapes to the fluid pressure acting on the structure need to be accurately determined. This technique analyzes the damping and stiffness coefficients of the squeeze film using the eigenvectors of the structure.

Due to the most dynamic MEMS devices employ microfabricated plate structures, the squeeze film analysis is generally performed using the 2D isothermal compressible Reynolds equation coupled with equations governing the plate deflection under the assumptions of small displacements and strains. Consider a microplate subjected to a net pressure force $p(x, y, t)$ per unit area due to the squeezing action of air underneath the plate due to its transverse motion pushing and pulling on the fluid film, we obtain the following equation governing the transverse motion of the plate:

$$D\left(\frac{\partial^4 w}{\partial x^4} + 2\frac{\partial^4 w}{\partial x^2 \partial y^2} + \frac{\partial^4 w}{\partial y^4}\right) + \rho T_p \frac{\partial^2 w}{\partial t^2} = -p(x, y, t) \qquad (3.34)$$

where $w(x, y, t)$ is the transverse deflection of a point (x, y) on the plate at time t, $D = \frac{E{T_p}^3}{12(1-v^2)}$ is the plate flexural rigidity, E is the Young modulus, and v is the Poisson's ratio.

The algorithm used to compute the damping and stiffness coefficients in this technique are expressed as follows (Mehner *et al.*, 2003):

1. First, the modal analysis of the elastic structure is carried out using FEM to extract the resonant frequencies and the eigenvectors of different modes by solving Eq. (3.34) without any forcing term. After finite element discretization, Eq. (3.34) can be written in the matrix form as:

$$[M]\{\ddot{w}\} + [K_s]\{w\} = \{F\} \tag{3.35}$$

where $[M]$ is the structural mass matrix, $[K_s]$ is the structural stiffness matrix, and $\{F\}$ is the nodal load vector. If the displacement $w(x, y, t)$ is written in terms of m eigenvectors $\emptyset_i(x, y)$ and a time-dependent modal coordinate $q_i(t)$ as:

$$w(x, y, t) = \sum_{i=1}^{m} \emptyset_i(x, y)\, q_i(t) \tag{3.36}$$

then the eigenvectors and the resonant frequencies can be calculated from the dynamic equilibrium equation:

$$[K_s]\{\emptyset_i\} = {\omega_i}^2[M]\{\emptyset_i\} \tag{3.37}$$

Based on the orthogonal properties of eigenvectors, we get the following expression for the resonance frequencies corresponding to different mode shapes:

$$\{\emptyset_i\}^T[K_s]\{\emptyset_i\} = {\omega_i}^2\{\emptyset_i\}^T[M]\{\emptyset_i\} \tag{3.38}$$

Letting,

$$\{\emptyset_i\}^T[M]\{\emptyset_i\} = M_i^* \text{ and } \{\emptyset_i\}^T[K_s]\{\emptyset_i\} = K_i^* \tag{3.39}$$

we get

$$\omega_i^2 = \frac{K_i^*}{M_i^*} \tag{3.40}$$

where M_i^* and K_i^* are the modal mass and stiffness of the structure corresponding to the *i*th eigenvector $\emptyset_i$ and the resonance frequency ω_i.

2. The squeeze film is excited with wall velocities that correspond to the values of the *i*th eigenvector of the structure.
3. A harmonic response analysis is performed to extract the pressure response within the desired frequency range.
4. The real and imaginary component of the element pressure is integrated for each frequency to compute the element nodal force vector:

$$\{F\} = \int_{area} N^T p(\emptyset_i, q_i) dA \tag{3.41}$$

where N^T is the finite element shape function, $\emptyset_i$ is the *i*th eigenvector, and q_i is the *i*th modal coordinate.

5. The nodal force vector is multiplied for each eigenvectors resulting the modal forces which indicate how much the pressure distribution acts on each mode shape (back projection):

$$\emptyset^T\{F\} = \emptyset^T \int_{area} N^T p(\emptyset_i, q_i) dA \tag{3.42}$$

6. The damping coefficient is extracted from the real component of modal force while the stiffness coefficient is extracted from the imaginary component as:

$$C_{ij} = \frac{\emptyset_i^T \int N^T Re\{p(\emptyset_j, q_j)\} dA}{\dot{q}}$$
$$K_{ij} = \frac{\emptyset_i^T \int N^T Im\{p(\emptyset_j, q_j)\} dA}{q} \quad (3.43)$$

The damping and spring coefficients of each mode due to the squeeze film are the main diagonal entries $C_{ii}$and K_{ii}. Off-diagonal terms $(i \neq j)$ represent the fluidic cross-talk among modes which occurs in the case of asymmetric air gap.

7. The procedure from step 2 is repeated for the next eigenmode.

CHAPTER FOUR

NUMERICAL IMPLEMENTATION

In this chapter, detail descriptions of the steps involved in performing the squeeze film analysis and the method for assessing the computational approach are discussed. All the computations are performed with the commercial FEA package ANSYS.

4.1 ANSYS Simulation Methodology

In this work, the analyses were conducted with the industrial-strength commercial finite element analysis software package ANSYS version 12.0. This version of ANSYS has all the features to successfully implement the squeeze film damping effect.

Generally, a typical analysis using ANSYS consist of three main phases: pre-processing, solution, and post-processing stages. In the pre-processing stage, the data such as the geometry, materials, and element types are provided to the program. The analysis type will be defined in the solution stage. The finite element solution will be initiated in this stage. The boundary conditions may be specified in either pre-processing or solution stages. In the post-processing stage, the results of the analysis can be reviewed through visualization and data listings.

The details flow of the steps involved in such typical analysis in ANSYS is illustrated in Figure 4.1.

ANSYS Parametric Design Language, APDL is powerful scripting language that allows a user to parameterize model and automate common tasks. The most benefit of this tool is it can save the set up time compared if an individual command were manually performed by a user. In this work, the analyses in ANSYS were performed using the APDL script.

4.2 Geometry Model

In this work, we considered two different sets of test structures based on the past researchers (De Pasquale *et al*., 2009). Both sets are required in validation the numerical models that will be discussed in the next chapter in terms of natural frequency and squeeze film damping coefficients, respectively. The first set of test structure is a gold rectangular shape plate whereas the second type is a gold square plate structure.

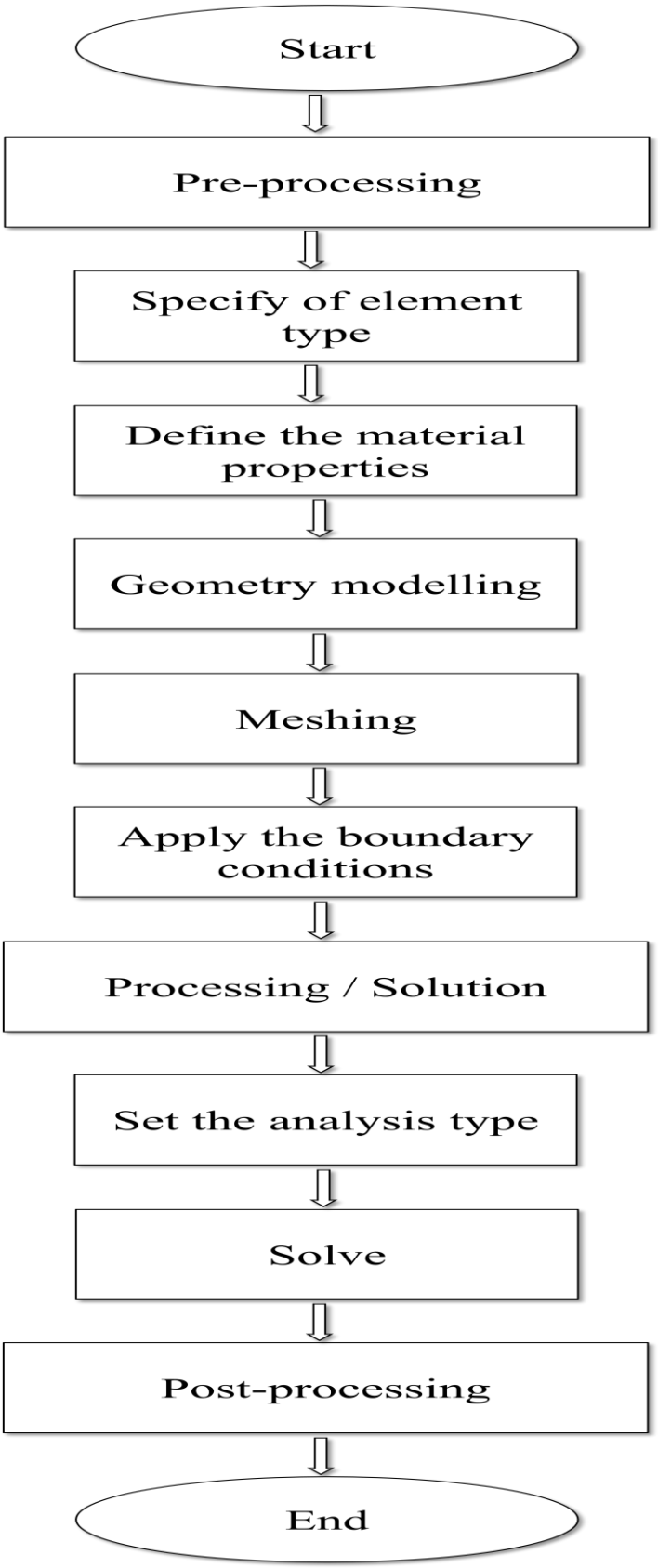

Figure 4.1: Flow of the steps involved in ANSYS simulation.

4.2.1 Perforated Rectangular Structures

In the study of natural frequency, the gold rectangular plate MEMS structures fabricated by De Pasquale *et al*. (2009) is used as the case study. The structures are characterized by different plate widths and holes sizes. The plate thickness T_p and the air gap height h are 6.3 μm and 3.0 μm, respectively. Table 4.1 lists the characteristic dimensions of the test structures. The dimensions of the supporting beams acting as suspensions at the both ends are presented in Table 4.2.

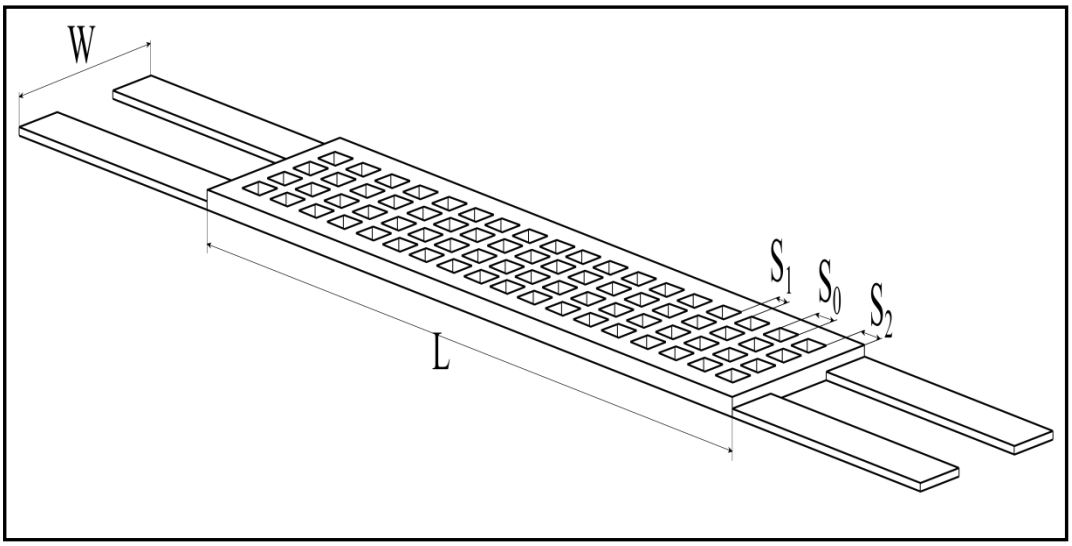

Figure 4.2: Rectangular plate with square holes structure.

Table 4.1: Plate dimensions of the rectangular plate structures with plate thickness, T_p = 6.3 μm.

Plate No.	Plate length, L (μm)	Plate width, W (μm)	Holes side, S_0 (μm)	No. of holes, $M \times N$
1	376	99	7.20	18 × 4
2			9.30	
3			10.70	
4			12.60	
5		158	7.20	18 × 7
6		277	7.20	18 × 13

Table 4.2: Suspension beams dimensions for rectangular structures.

Parameter	Symbol	Value (μm)
Length	L_b	96.08
Width	W_b	13.52
Thickness	T_b	2.620

The geometric parameters of S_1 and S_2 along the plate length L as depicted in Figure 4.2 can be calculated from the following relations:

$$S_1 = \frac{L}{M+1} - S_0 \tag{4.1}$$

$$S_2 = \frac{L}{M+1} - \frac{S_0}{2} \tag{4.2}$$

Along the plate width W, the values of S_1 and S_2 are:

$$S_1 = \frac{W}{N+1} - S_0 \tag{4.3}$$

$$S_2 = \frac{W}{N+1} - \frac{S_0}{2} \tag{4.4}$$

S_0, S_1, and S_2 provide unique dimensions of a perforated plate with specific size and arrangement of the holes.

4.2.2 Perforated Square Structures

In the analysis of squeeze film damping, the gold square plates of MEMS structures designed by De Pasquale *et al*. (2009) are considered as shown in Figure 4.3. The authors fabricated 28 gold square plates with variety of plate side dimensions, as the number of holes and the hole sizes. The plate thickness and the air gap height are the same as the gold rectangular plate structures. The geometrical parameters of the gold square structures are listed in Table 4.3 while Table 4.4 provides the dimensions of the supporting beams.

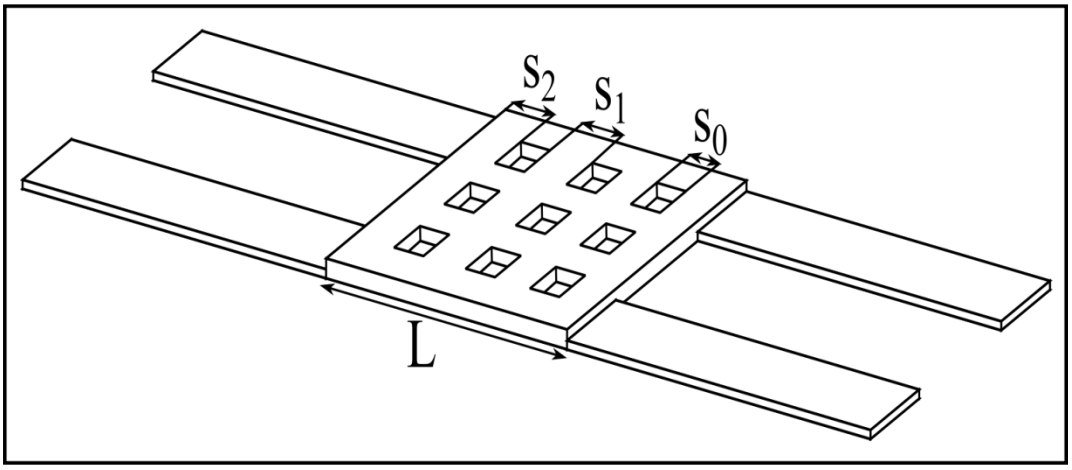

Figure 4.3: Square plate with square holes structure.

Table 4.3: Plate dimensions of the square plate structures with plate thickness, T_p = 6.3 μm.

Plate No.	Plate side, L (μm)	Holes side, S_0 (μm)	No of holes, $M \times M$
7	55	7.20	2 × 2
8		9.30	
9		10.70	
10		12.60	
11	76	7.20	3 × 3
12		9.30	
13		10.70	
14		12.60	
15	96	7.20	4 × 4
16		9.30	
17		10.70	
18		12.60	
19	115	7.20	5 × 5
20		9.30	
21		10.70	
22		12.60	
23	137	7.20	6 × 6
24		9.30	
25		10.70	
26		12.60	
27	157	7.20	7 × 7
28		9.30	
29		10.70	
30		12.60	
31	185	7.20	8 × 8
32		9.30	
33		10.70	
34		12.60	

Table 4.4: Suspension beams dimensions for square structures.

Parameter	Symbol	Value (μm)
Length	L_b	96.66
Width	W_b	12.88
Thickness	T_b	2.606

The values of S_1 and S_2 as indicated in Figure 4.3 can be calculated with the same expressions as Eqs. (4.1) and (4.2).

4.3 Boundary Conditions

For our analysis, two types of degrees of freedom are involved: the pressure magnitude and the displacement vectors. Firstly, the pressure at nodes along the plate edges is set to be zero as this will sets the pressure as atmospheric pressure. Secondly, the displacement vectors at the end of the each supporting beams are set to zero in all directions. Figure 4.4 shows the boundary conditions applied on a typical finite element model.

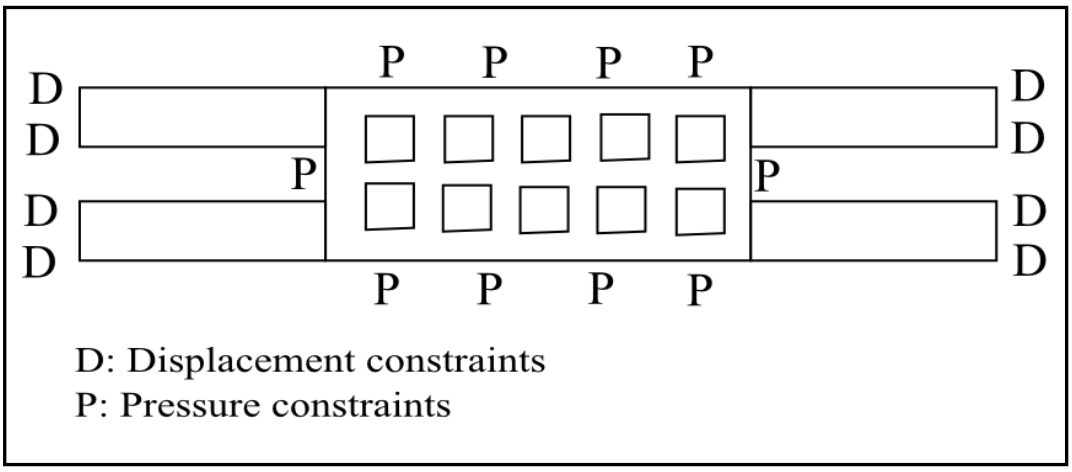

Figure 4.4: Boundary conditions on typical finite element model.

4.4 Material Properties

For all analysis, material properties specified to be linear since there is no thermal effect included. In addition, displacement of the plate is assumed to be small enough that even for a membrane model to be used in the analysis, the linear material model still applies. The material properties that have been assigned to both the structure and surrounding fluid is shown in Table 4.5 and Table 4.6 respectively.

Table 4.5: MEMS structure material properties.

Properties	Values
Young's modulus	98.5e3 kg/μm/s^2
Density	19.32e-15 kg/μm^3
Poisson ratio	0.42
Thermal expansion coefficient	14.0 (10^{-6}/ ^{o}C) @ 20 ^{o}C

Table 4.6: Properties of air.

Properties	Values
Viscosity	18.5e-12 kg/µm/s
Ambient pressure	0.1 kg/µm/s^2
Reference pressure for free path	0.1 kg/µm/s^2
Mean free path at reference pressure	65e-9 µm

4.5 The Finite Elements

In this analysis, there are two different domains involved which are structural and fluidic domains. The structural domain is the MEMS structure while the fluidic domain is the air surrounding the structure. Both domains are required to be coupled at their interface since one domain influences the other and no vacuum should exist between the interfaces.

4.5.1 The Structural Domain

As the main objective of this work is to study the applicability of two-dimensional (2D) plane structure in the modelling of the complex three-dimensional (3D) perforated MEMS structure, two different finite elements are used to model the structural domain for comparison. In order to simulate the full three-dimensional structural analysis, 20-node three-dimensional hexahedral element that exhibits quadratic approximation of displacement is preferred. This element type is labelled SOLID186 in ANSYS, and hereafter is referred to as 3D solid model in this thesis.

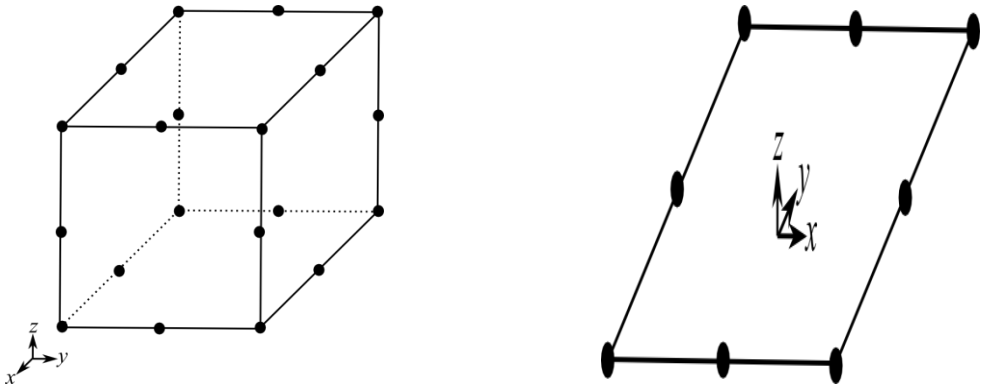

(a) (b)

Figure 4.5: Geometries and node locations of standard (a) 20-node hexahedral elements (SOLID186) and (b) 8-node shell elements (SHELL281).

For two-dimensional model, the 8-node shell element is used. It consists of eight nodes with six degrees of freedom per node: translations in the *x*, *y*, and *z*-axis and rotations about the *x*, *y*, and *z*-axis. This element is labelled SHELL281 in ANSYS, and will be referred to as 2D shell element model. Alternatively, this element can be defined as a membrane element that allows only translational DOF (i.e., zero rotations). This element type will be referred to as 2D membrane model. The thickness of shell element implicitly defines the structure thickness as mentioned in Section 3.1.2. The geometry and node location for both elements are shown in Figure 4.5.

4.5.2 The Fluidic Domain

The fluidic domain is characterized by two different behaviours of the fluid flow due to the geometry of the perforated plate. The first fluid flow behaviour is in the gap between the moving plate and the fixed base substrate. An

8-node quadrilateral element type with pressure degrees of freedom is used (cf. Section 3.2). The element is known as FLUID136 in ANSYS. The fluid in the gap is modelled by overlaying this element on the below the solid element mentioned above. The element behaviour is based on the Reynolds squeeze film theory as discussed in Section 3.2. In addition it also includes rarefied gases theory. However there are some assumptions to be considered:

1. Isothermal viscous gas flow condition is assumed.
2. Lateral dimension of the structure is much larger than the gap size.
3. Pressure change is small relative to the ambient pressure.
4. Knudsen number is less than 880.

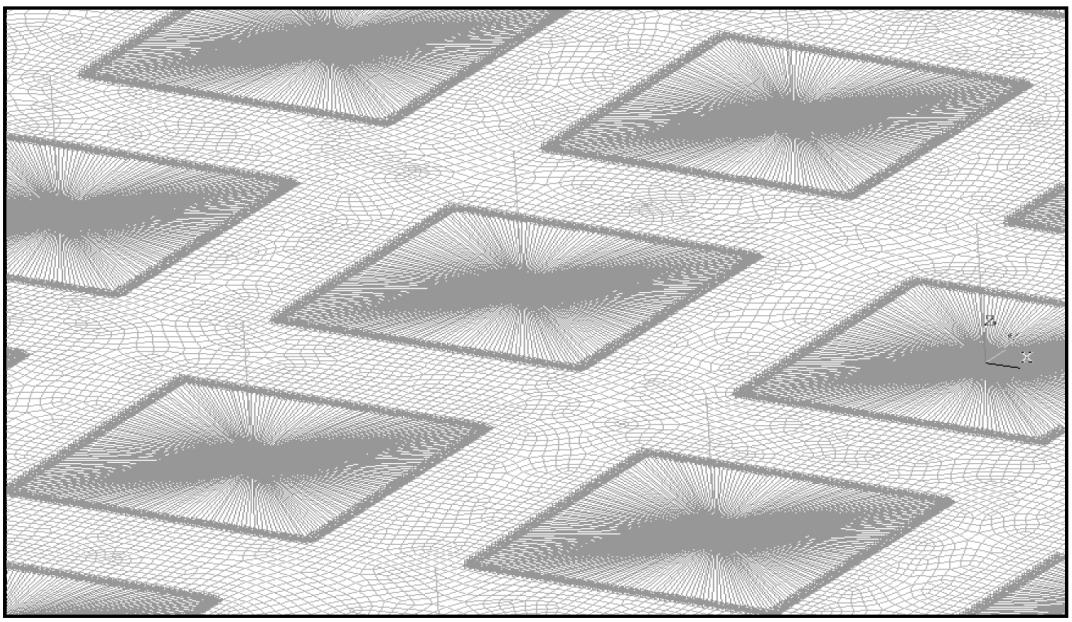

Figure 4.6: Fluid domain mesh in perforated plate.

The second fluid flow behaviour is for the flow through the hole defined by two nodes. This element type is labelled FLUID138 in ANSYS. The first node is pointed at the centre of the cross section of the holes region on the same plane as the squeeze film element is located. The position of second node is at the opposite face of the structure through the hole depth. This element preserve the pressure drop through the hole by coupling the pressure DOF for the nodes of the squeeze film elements at the periphery of the hole to the pressure DOF for first node of this element while the pressure DOF for second node should be set to the surrounding pressure as shown in Figure 4.6. A sample of the APDL command for model the FLUID138 element is included in Appendix B. This element accounts the gas rarefaction effect and fringe effects due to the short channel length. Table 4.7 shows a summary of the characteristics for all the elements involved in the analysis.

4.6 Mesh Generation

Meshing generation is one of the most critical steps since it will determine the accuracy of solution and the computational cost. In general, a fine mesh may result in better approximation of the solution with a costly computation cost and vice versa. Thus, seeking a mesh with optimal size on shapes of elements is a main objective to meet in the meshing procedure.

Table 4.7: Summary of the elements characteristics.

Element type	ANSYS label	Degree of freedom	Dimension	Characteristics
20-nodes hexahedral	SOLID 186	Translation	3D	Twenty nodes hexahedral-shaped element that exhibits quadratic approximation displacement.
8-nodes quadrilateral shell	SHELL 281	Translation and rotational (zero rotation may be assumed)	2D	Eight nodes quadrilateral-shaped element that exhibits quadratic approximation displacement.
8-nodes quadrilateral	FLUID 136	Pressure	2D	The element should be oriented such that the element normal is pointing toward the fluid domain.
2-nodes	FLUID 138	Pressure	1D	The first node is positioned at the centre of the cross section of the holes region on the same plane as the elements used to model the squeeze film fluid region. The second node is positioned at the opposite face of the structure through the hole length.

As the model involves the fluid-structure interaction, these two different physics must be meshed properly. First, the structural geometries were meshed with quadrilateral shape element with free type meshing. In this analysis, meshing around to 50 000 elements is considered. Test with 100 000 elements and more only change the results by about 2%. The meshed geometry of both 3D solid and 2D shell elements are shown in Figures 4.7 and 4.8.

Then, the fluid gap elements were overlaid on the surface of an existing structural mesh to define the behaviour of fluid domain in the gap while ensuring element compatibility at the interface. In order to preserve the pressure drop through the perforated holes, single fluid hole element is defined at the each hole.

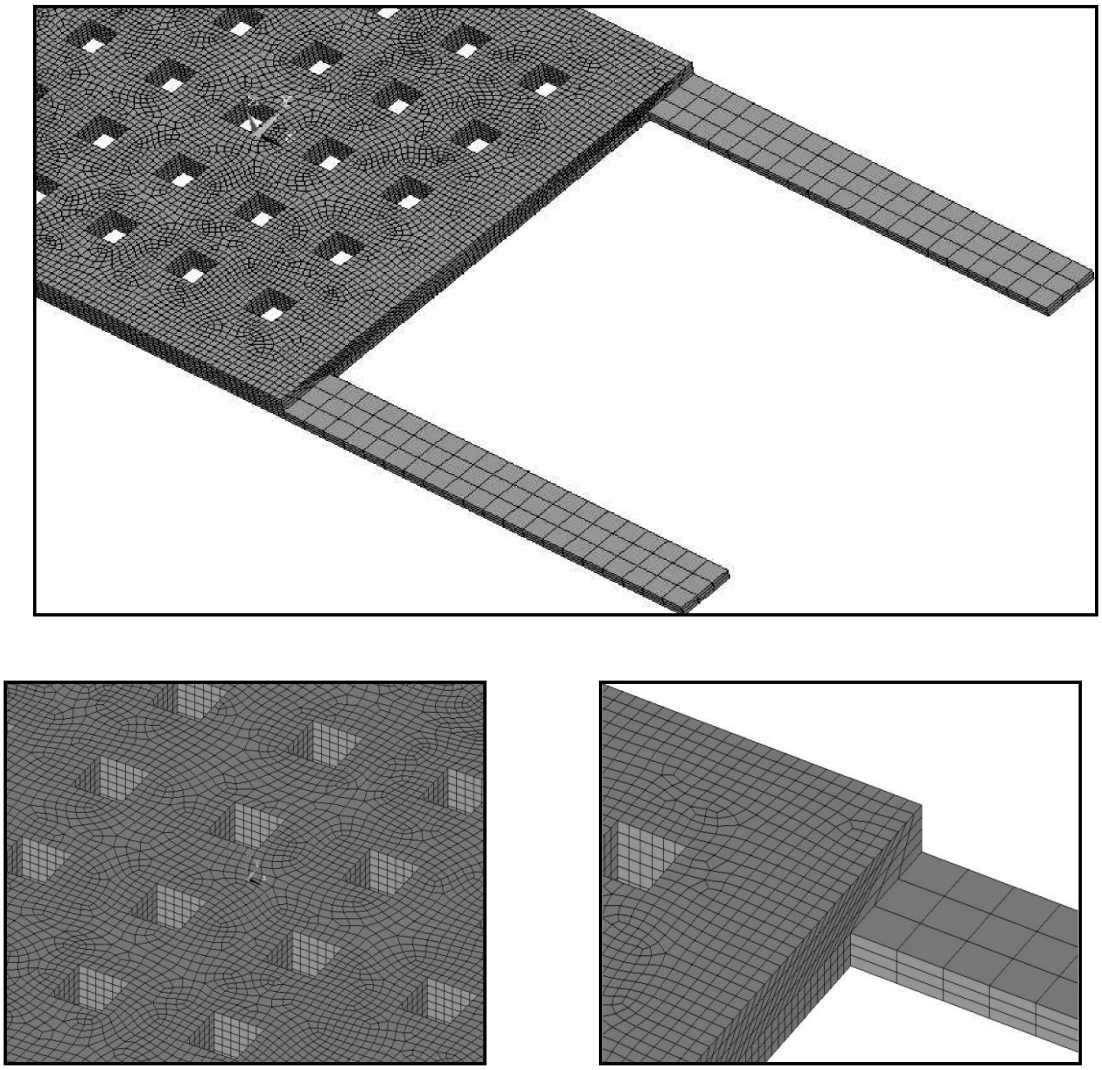

Figure 4.7: Meshing of 3D solid element for structural model.

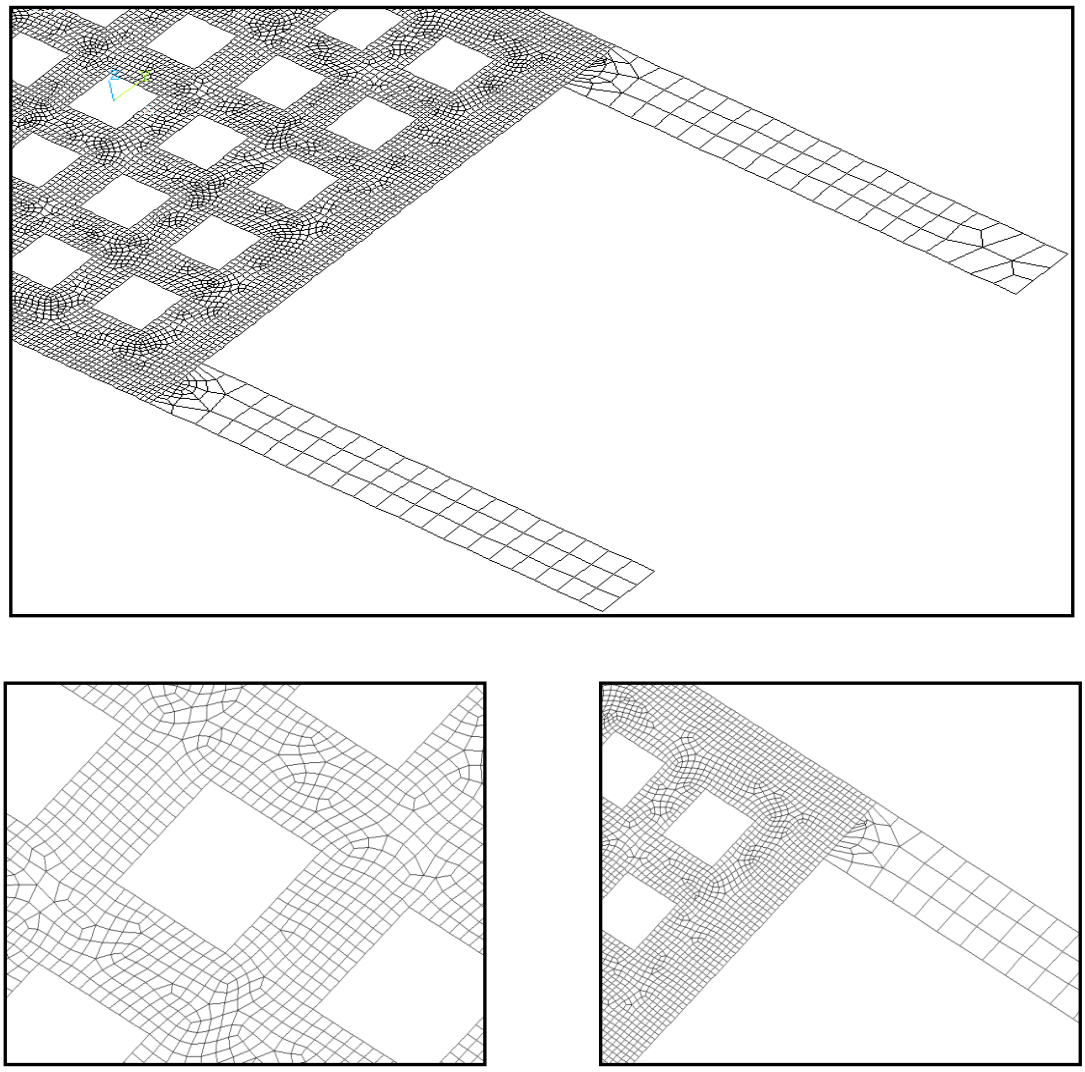

Figure 4.8: Meshing of 2D shell element for structural model.

4.7 Solution and Postprocessing

There are three types of analysis available in the squeeze film behaviour studies using ANSYS that are the static, harmonic, and modal analysis. In general, static analysis is used to determine the damping effects at low operating frequencies while the harmonic response analysis can be used to compute damping and stiffness parameters at higher frequencies. Modal analysis is used to determine the natural frequencies and mode shapes of the structure.

In this work, Modal Projection Method is use for the extraction of damping and stiffness coefficients of the fluid. This technique provides an efficient method for analysis of flexible oscillating structures. Damping and stiffness coefficients extraction is based on the structure velocity profile determination through a series of harmonic analysis. The flows of the steps in performing the analysis via this method are shown in Figure 4.9.

Pre-stress effect is subjected to the 2D shell element model to compensate the variations of stress state produced by the assumptions appeared in shell element theory. This stiffening effect normally needs to be considered for thin structure with bending stiffness very small compared to axial stiffness. The effect of stress stiffening is accounted for by generating and the using an additional stiffness matrix, hereinafter called the ‘stress stiffness matrix’. This matrix is added to the regular stiffness matrix in order to give the total stiffness.

Once the ANSYS solution phase has ended, that is when the damping and stiffness parameters is compute, results can be now be accessed through postprocessing phase in ANSYS.

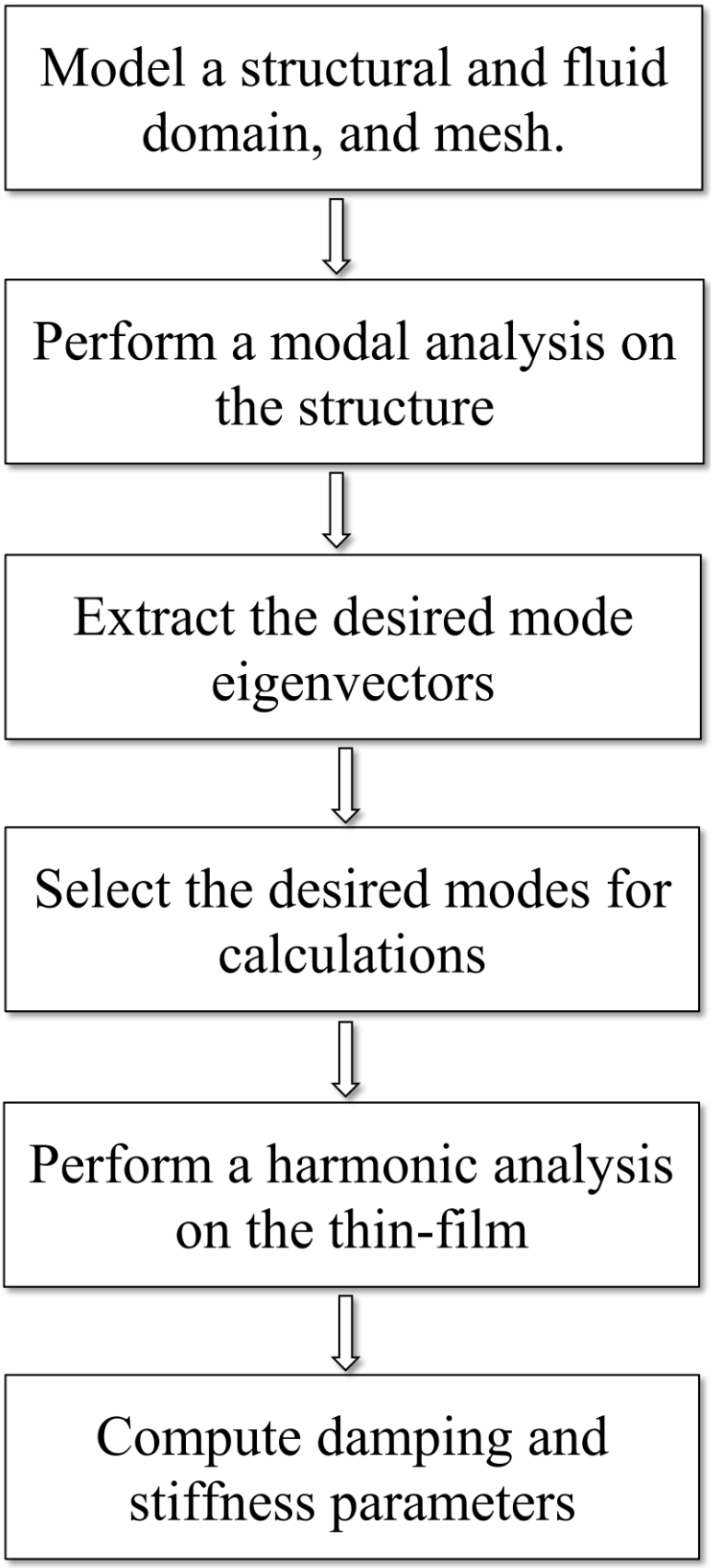

Figure 4.9: Flows of the steps in modal projection method.

CHAPTER FIVE

RESULTS AND DISCUSSIONS

The results obtained from the analysis will be discussed in details in this chapter. It consists of three sections. In the first section, the preliminary modal analysis is done to validate the accuracy of numerical models with respect to the relevant theories for plate vibrations. In the subsequent section, the modal analysis of perforated MEMS structures is performed to verify the accuracy of numerical models as described in Chapter 3 in terms of computations for natural frequencies. The mode shapes of the structures are also presented. The analysis of squeeze film damping will be demonstrated in the next section. In the last section, the computational cost of such numerical models will be analyzed.

5.1 Preliminary Modal Analysis

In this preliminary study, the modal analysis of a simple perforated plate will be presented. The analysis uses different finite element types to evaluate their accuracies with established closed-form solution.

A square plate with a centrally located circular hole is modelled. The dimensions of square plates are 10 000 μm × 10 000 μm × 100 μm and the following gold material properties are given: Young Modulus $E = 98.5 \times 10^3$ kg / μm s^2, density $\rho = 19.32 \times 10^{-15}$ kg / μm^3, Poisson ratio $\upsilon = 0.30$, and thermal

expansion coefficient $\alpha = 14 \times 10^{-6}\ ^{o}C^{-1}$ at 20 ^{o}C. Diameter of circular hole is 200 μm. The model is as shown in the Figure 5.1.

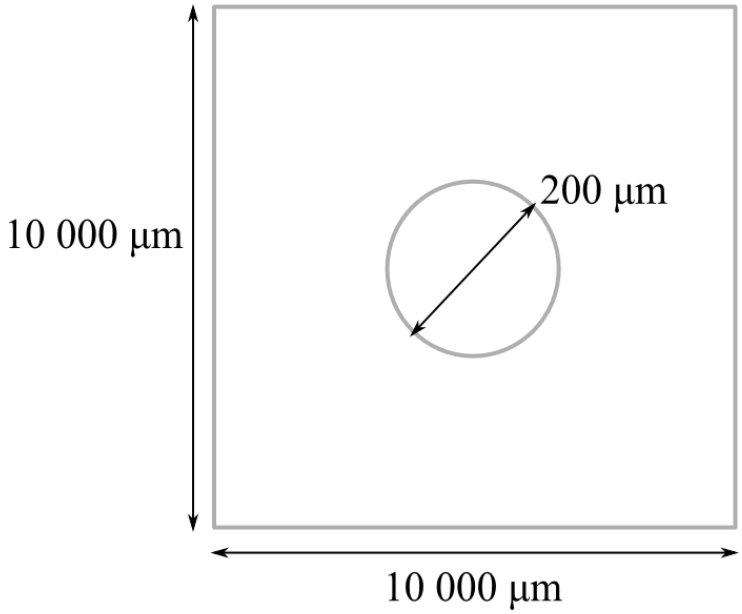

Figure 5.1: A square plate with a circular hole.

For boundary condition, square plate four sides are clamped so that the degrees of freedom of all four edges are made zero. Meshing the perforated plate models was done using two different structural element types: 3D solid elements and 2D shell elements. Such numerical results were validated with the theoretical study done by Takahashi (1958) as mentioned in Section 2.4. The resulting frequencies values were shown in Table 5.1.

Table 5.1: Natural frequencies and relative errors for different element types.

Element type	No. of nodes	Natural frequency of first mode (Hz)	Relative errors
3-D solid	81198	4229	-0.40
2-D shell	83304	4062	3.56
Theory	–	4212	–

As can be seen from the table above, the relative error of the 2D elements with respect to the theoretical study is below 5% which is generally acceptable. The results prove the applicability of the 2D shell elements that are based on thin plate Reissner-Mindlin theory for use in modal analysis of a plate with a hole. This preliminary study was set out with the aim of assessing the applicability of such element types against classical plate theory in solving the perforated structure.

5.2 Modal Analysis of Perforated MEMS Structures

In this section, the perforated structure model is validated for the solution of natural frequencies. The structures as summarized in Table 5.2 are used in this analysis. The natural frequency evaluation by the numerical approach was carried out using three different structural element types: 3D solid model, 2D shell model, and 2D membrane model. The approximation number of elements used for meshing 3D and 2D models are 50 000.

Table 5.2: Plate dimensions for modal analysis (cf. Figure 4.2).

Plate	Plate length, L (μm)	Plate width, W (μm)	Holes side, S_0 (μm)	No. of holes, $M \times N$
1	376	99	7.20	18 × 4
2			9.30	
3			10.70	
4			12.60	
5		158	7.20	18 × 7
6		277	7.20	18 × 13

The FE computations were compared with the experimental data acquired from the previous work made by De Pasquale *et al*. (2009). The natural frequency of the first mode is assessed. Table 5.3 lists the differences between the natural frequencies from the FE computations and the experiment.

Table 5.3: Resonance frequency values obtained from the experimental work De Pasquale *et al*. (2009) and through FEA simulations for each plate structure.

Plate	Resonance frequency, f_n (kHz)			
	Experimental	Numerical approaches		
		3D solid model	2D shell model	2D membrane model
1	20.25	19.90	20.88	16.73
2	20.70	20.18	21.52	17.30
3	20.98	20.46	22.11	17.81
4	21.92	21.04	23.15	18.74
5	17.00	16.94	17.13	13.44
6	13.61	13.55	13.20	10.21

As shown, the natural frequency of the structures increased through the increase of the holes size, which can be seen in Figure 5.2. However, as expected, the data also show that the resonance frequency decreased with the decrease of the plate aspect ratio, *L/W*. Figure 5.3 shows that the resonance frequency decreased with the increase plate width.

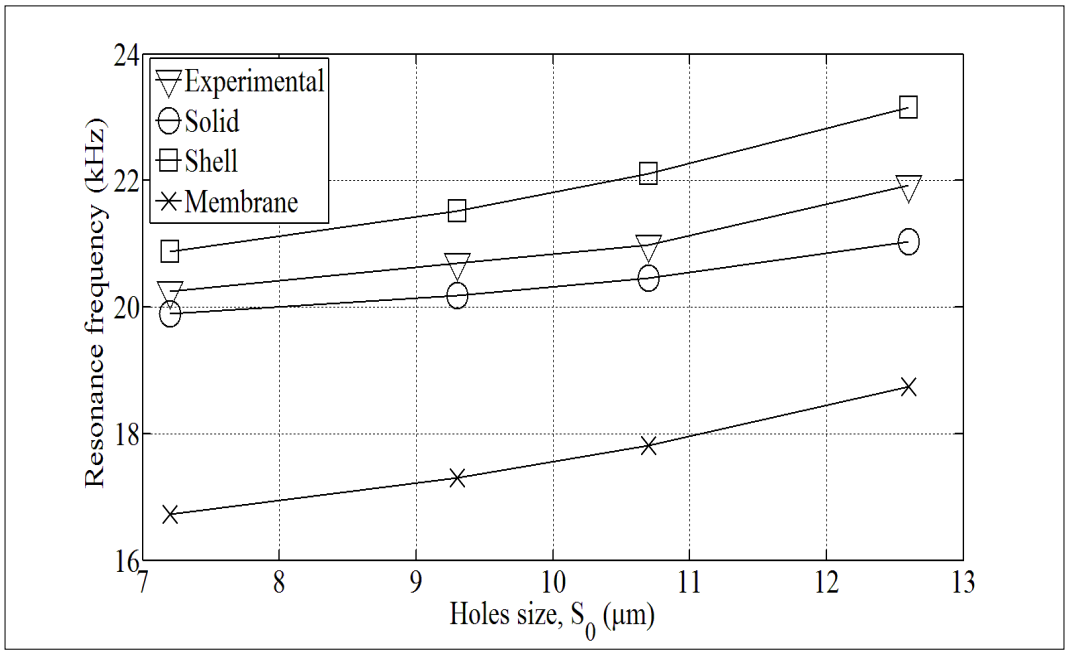

Figure 5.2: Resonance frequency results for increasing holes size (18 × 4 holes).

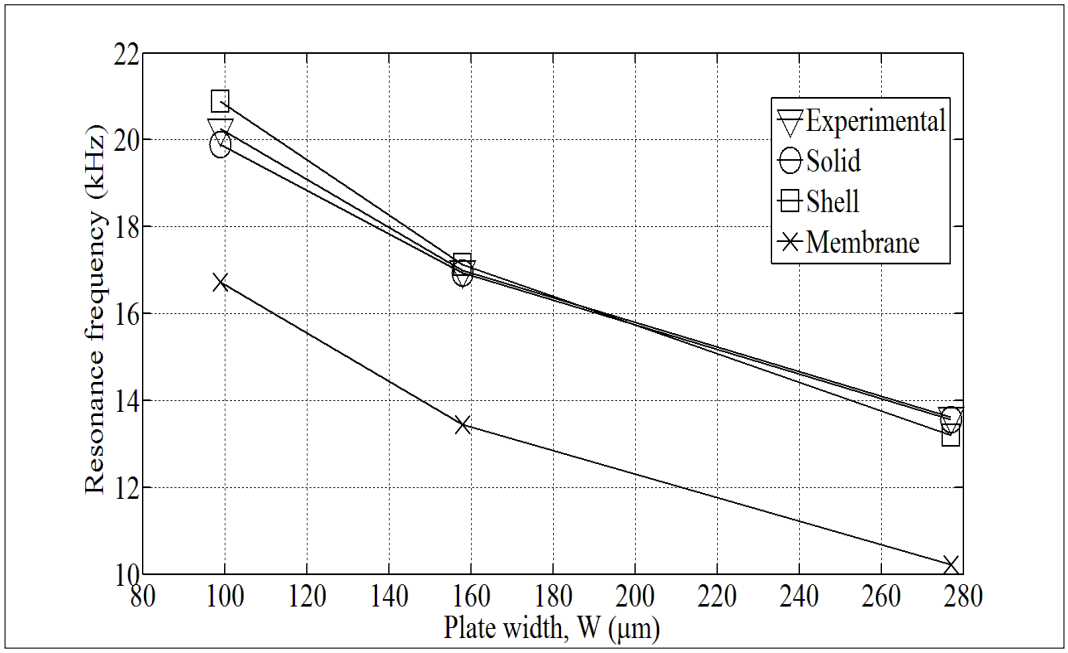

Figure 5.3: Resonance frequency results for increasing plate width (S_0 = 7.20 μm).

In terms of relative errors with respect to the experimental data, Table 5.4 lists the percentage differences of the results data in Table 5.3.

Table 5.4: Percentage differences results for numerical models with respect to the experimental values.

Plate	Percentage differences with respect to experimental values, ε (%)		
	3D solid model	2D shell model	2D membrane model
1	1.73	-3.11	17.38
2	2.51	-3.96	16.43
3	2.48	-5.39	15.11
4	4.01	-5.61	14.51
5	0.35	-0.76	20.94
6	0.44	3.01	24.98

The comparison of the relative errors as a function of perforated holes size S_0 is shown in Figure 5.4. As indicated, the 2D membrane model has the lowest accuracy. From the mathematical model, the only difference between the shell and membrane models is the absence of rotation. It can be concluded that neglecting rotation causes over-prediction of the first natural frequency of the perforated structure. 3D solid model shows the most accurate results.

Observing the data for 2D shell model, it suggests that 2D shell model tends to under-predict the natural frequency. It is suspected that although both bending and shear deformations are allowed similar to 3D model, the rank-2 elasticity tensors are not sufficient to capture the true deformation of the plate since it only allows first order estimate of shear deformations. Nevertheless, within the generally accepted 5% error, application of 2D shell model can acceptably valid.

In Figure 5.5, it shows the comparison of the accuracy of numerical models with respect to the plate width. The models exhibit similar trends as described before. 3D membrane model gives the lowest accuracy compared to the other models. While the solid model provides the best accuracy, the shell model is still with the acceptable range of accuracy. However, the solid model results were consistent with the experimental data.

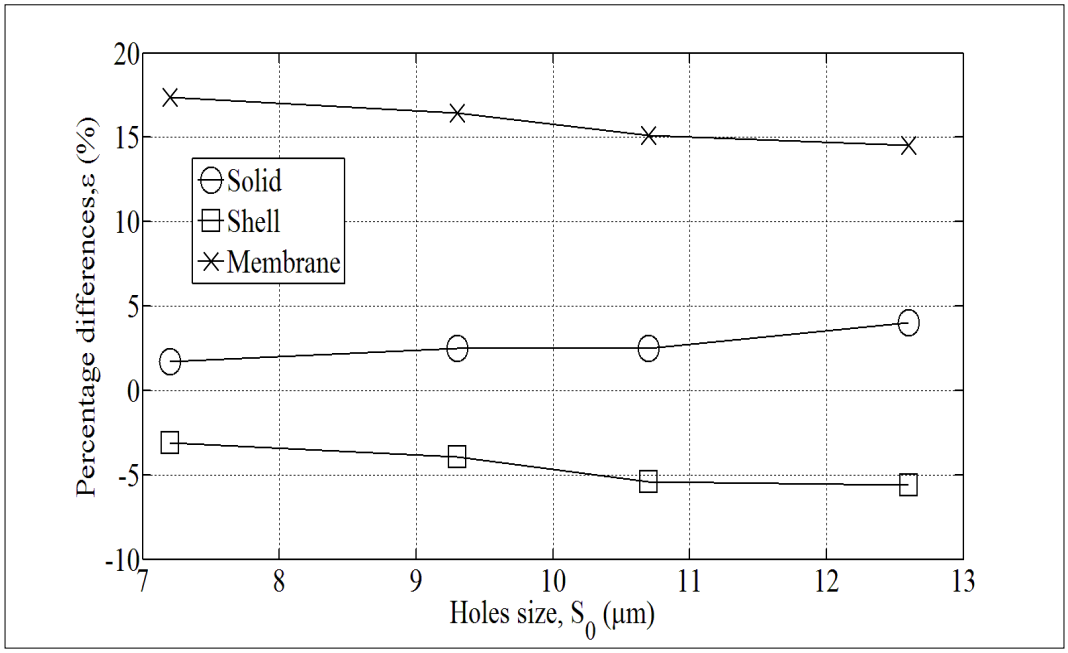

Figure 5.4: Influences of holes size on the numerical models accuracy (18 × 4 holes).

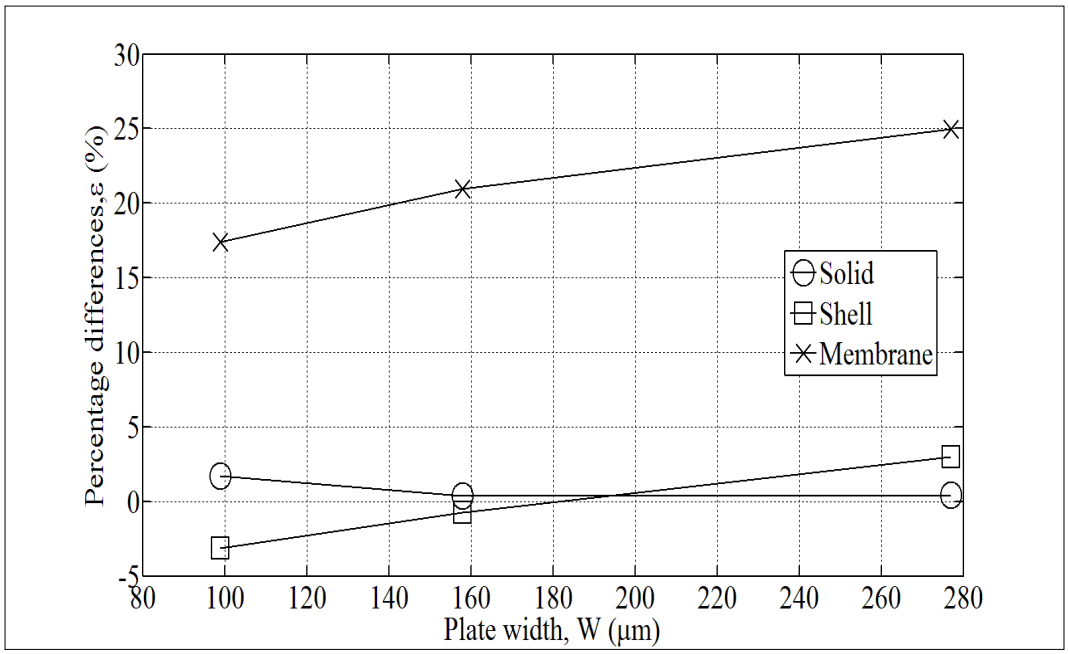

Figure 5.5: Influences of plate width on the numerical models accuracy (S_0 = 7.20 μm).

There are several factors that can explain the small discrepancies found between the simulated models and experimental results. One source of error is the material properties defined in ANSYS simulation and those of the experimental structure can vary. The two significant properties that would affect the difference between the experimental and simulated models are Young's modulus and density. The values of the properties are dependent on the fabrication process involved. Another possible reason for the discrepancy is the residual stress that likely to be present within the structure after the fabrication process.

The corresponding mode shape of the structures was also determined in the numerical approaches. The mode shape plots for Plate 1 are selected here as representative of the other plate. The mode shapes of the first natural frequency of such plates for different numerical models are shown in the Figure 5.6. The mode shapes of all plates for different numerical models are attached in Appendix A.

Colouring was used as an indicator for the out-of-plane *z*-direction displacement, where a dark red indicates large displacements from the equilibrium position and dark blue indicates negligible displacement. As shown, the deformed shape characteristics of all plate structures corresponding to this mode are represented by out of plane bending and the vertical translation in the *z*-axis direction.

As seen in the solid model, there are variations of mode shape colouring when decreasing the aspect ratio of plate dimension while for both 2D models, there are not too many variations especially in the membrane model.

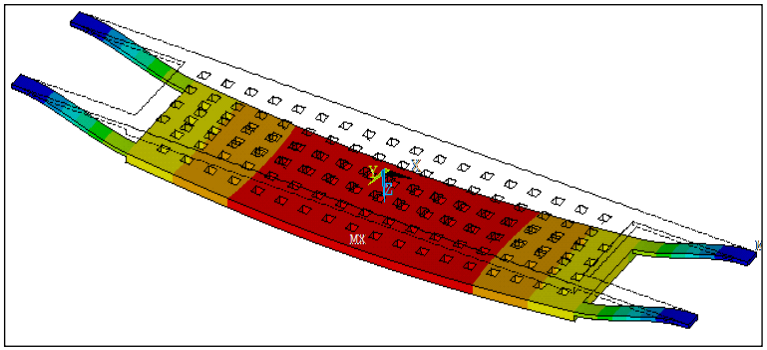

(a)

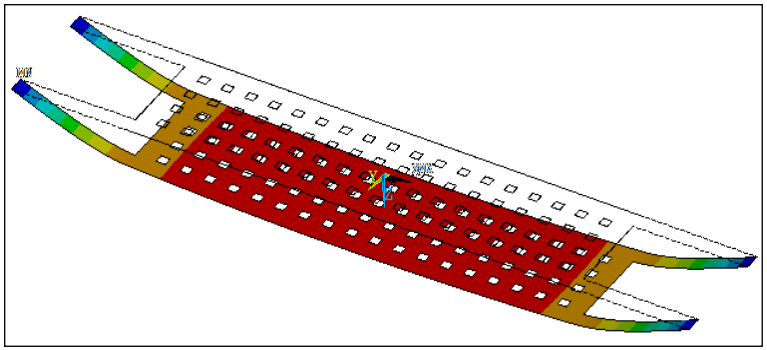

(b)

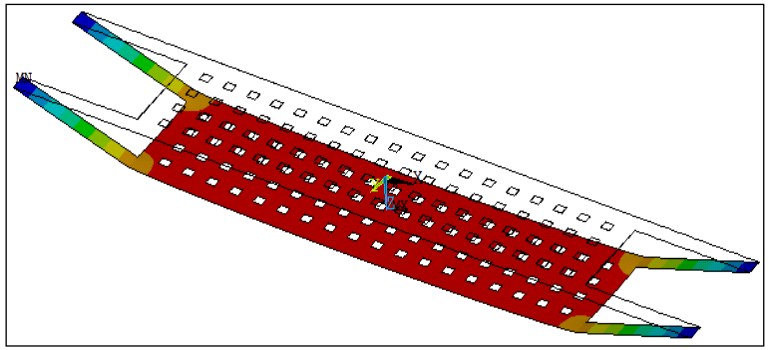

(c)

Figure 5.6: The simulated mode shapes of Plate 1 at first mode of vibration for (a) 3D solid model (b) 2D shell model and (c) 2D membrane model.

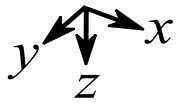

Based on the modal analysis results, we can conclude that even though complex 3D solid model result is considered the most accurate, however, the 2D shell model results are also very close. Thus, it is indicating that the validity of a simpler 2D shell model element in determination of natural frequency of MEMS perforated structure. The next section will discuss the validation of such numerical models in analyzing the squeeze film damping behaviour.

5.3 Analysis of Squeeze Film Damping

A parameter of interest in the analysis of squeeze film behaviour in MEMS structures is the damping coefficient. This is because the damping is directly related to the dynamic response of the system. The accuracy of the numerical models is studied in terms of solving squeeze film damping problem in perforated MEMS structure.

In this study, evaluations of the squeeze film damping coefficients were performed for a variety of cases that correspond to the experimental works investigated in the past. The experimental data is needed as the benchmark to evaluate the model effectiveness. In particular, the experimental data on damping coefficients by De Pasquale *et al*. (2009) is considered.

De Pasquale *et al*. (2009) reported the damping coefficient for twenty-eight square gold perforated plates. There are four plates for each number of holes, which differ in terms of holes size. All the characteristic dimensions of such cases are collected in Table 5.5.

Table 5.5: Geometrical characteristics of gold plates reported by De Pasquale *et al*. (2009) (cf. Figure 4.3).

Plate	Plate side, L (μm)	Holes side, S_0 (μm)	No of holes, $M \times M$
7	55	7.20	2 × 2
8		9.30	
9		10.70	
10		12.60	
11	76	7.20	3 × 3
12		9.30	
13		10.70	
14		12.60	
15	96	7.20	4 × 4
16		9.30	
17		10.70	
18		12.60	
19	115	7.20	5 × 5
20		9.30	
21		10.70	
22		12.60	
23	137	7.20	6 × 6
24		9.30	
25		10.70	
26		12.60	
27	157	7.20	7 × 7
28		9.30	
29		10.70	
30		12.60	
31	185	7.20	8 × 8
32		9.30	
33		10.70	
34		12.60	

Table 5.6: Damping coefficient values obtained from the experimental work De Pasquale *et al*. (2009) and through FEA simulations for each plate structure.

Plate	Damping coefficient ($\times 10^{-6}$ Ns/m)			
	Experimental	Numerical approaches		
		3D solid model	2D shell model	2D membrane model
7	2.341	2.746	2.720	3.341
8	2.124	1.944	1.951	2.292
9	1.492	1.604	1.627	1.846
10	1.168	1.305	1.342	1.446
11	3.143	3.554	3.556	5.976
12	2.970	2.148	2.196	3.517
13	2.483	1.639	1.687	2.593
14	1.702	1.223	1.267	1.824
15	6.218	4.059	4.145	8.180
16	4.588	2.239	2.324	4.399
17	3.542	1.613	1.698	3.092
18	3.374	1.124	1.194	2.033
19	9.030	4.326	4.502	9.635
20	6.043	2.198	2.366	4.889
21	5.155	1.546	1.660	3.309
22	4.606	1.026	1.111	2.076
23	10.796	4.758	5.069	11.433
24	7.478	2.309	2.558	5.615
25	6.433	1.554	1.743	3.723
26	6.087	1.011	1.118	2.260
27	15.966	4.763	5.323	12.323
28	10.450	2.365	2.599	5.880
29	9.292	1.516	1.736	3.838
30	8.108	0.933	1.078	2.267
31	19.334	5.682	6.216	14.705
32	13.611	2.652	3.017	7.021
33	12.163	1.765	2.002	4.583
34	10.843	1.044	1.226	2.712

In this analysis, the damping coefficient of squeeze film is evaluated by numerical FEM simulations using three different structural models: 3D solid model, 2D shell model, and 2D membrane model. Table 5.6 presents the values of damping coefficients determined by experimental data and numerically evaluated by the different FEM models.

Figure 5.7 presents the comparison between three different models in the FEA simulation in terms of the percentage differences with respect to the experimental data. Firstly, what is interesting in this data is that the results provided by the 2D shell model are very closer to the results of 3D solid model for the whole plates. The shell model gives a slightly better accuracy rather than the solid model. The average differences between both models are about 2% only. The results of this study indicate that the rotational DOF introduced in the shell element can cause the characteristic of the shell element to behave like a solid element in damping analysis of squeeze film.

However, both models are surprisingly providing a good accuracy for a small number of holes cases only. As the number of holes increases, the 2D membrane element clearly provides the better agreement. These phenomena related to the equivalent theory that relevant to each classification of plate types as described in the Chapter 3.

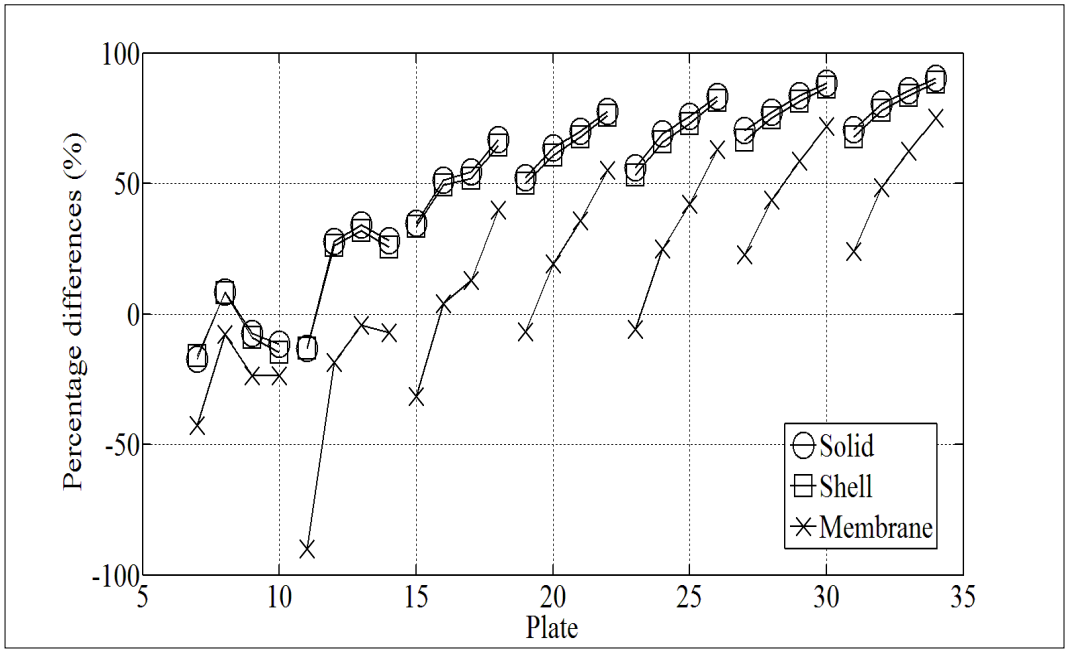

Figure 5.7: Percentage errors of damping coefficients returned by different FEM models.

As mentioned before, 3D elasticity theory can be used to describe the behaviour of the plate that had ratio l/T_p less than 10 while the classical plate theory that implemented two-dimensional form analysis can be used to describe the behaviour of the plate that had ratio l/T_p more than 10. Refer to the Table 5.7 that shows the ratio of the lateral dimension of a plate, l to the plate thickness, T_p, only plates 7 - 10 have the ratio less than 10. It is evident that the 3D solid element model is only applicable for such plates.

In the Figure 5.7, it also noted that the percentage differences values were increasing when the number of holes increases. Furthermore, the differences values also increasing when the size of holes becomes larger in most plates. The possible reason for this discrepancy is due to increasing singularity points when

more holes are introduced into the plate and the hole sizes also becomes larger, thus degenerate the accuracy of finite element solution.

Table 5.7: Ratio between the lateral dimension of a plate, l to the plate thickness, T_p for each plate.

Plate	l/T_p		Plate	l/T_p
7	8.73		21	18.25
8			22	
9			23	21.75
10			24	
11	12.06		25	
12			26	
13			27	24.92
14			28	
15	15.24		29	
16			30	
17			31	29.37
18			32	
19	18.25		33	
20			34	

Next, the accuracy of numerical approaches is compared with the results given by related analytical models. In this work, the analytical models that proposed by Veijola (2006) and De Pasquale *et al*. (2010) have been referred. We considered Veijola's model since he reported their model effectiveness by validated with the same study cases as experimental work done by De Pasquale *et al*. (2009). But, that model was assumed the plates are uniformly perforated. However, in this work study cases, the distance between outmost holes and the

edge of the plate, S_2 is not same as the distance between the holes, S_1. According to that, De Pasquale *et al*. model was used to overcome the error when they introduced the pressure frame model due to that non-uniformly perforation. Besides, the contribution of supporting beams to the damping force also has been recommended to improve the original Veijola's model. Table 5.8 provides the results obtained from both analytical models of calculated damping coefficients.

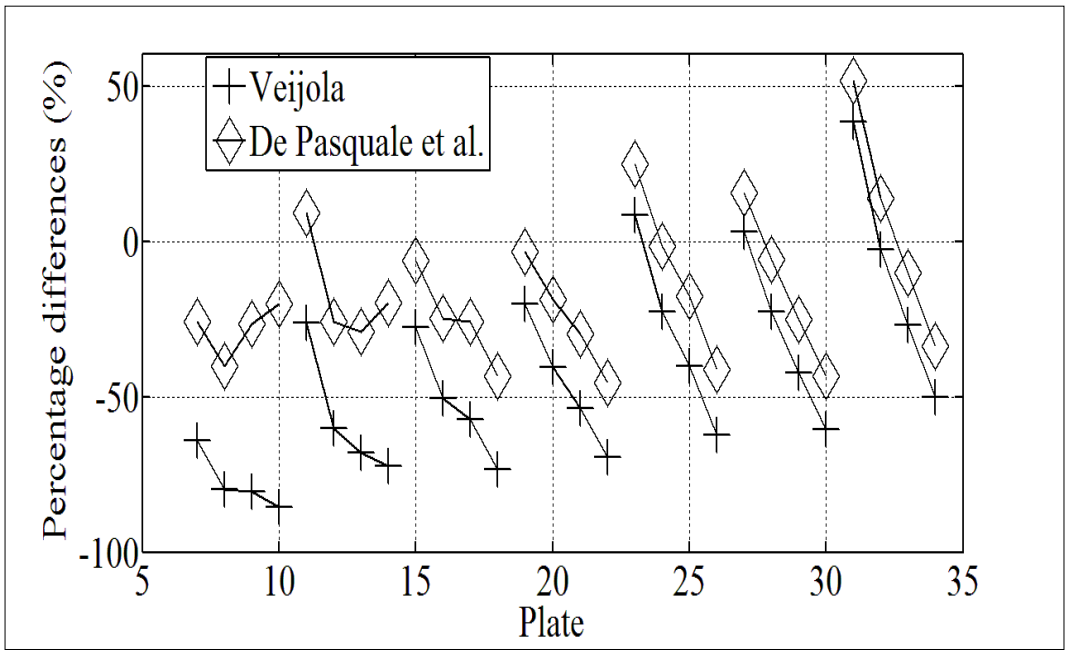

Figure 5.8: Comparison of two analytical models for percentage differences of damping coefficients with respect to the experimental values.

The comparison of results obtained through these analytical models in terms of their percentage differences to the experimental data is plotted in Figure 5.8. As shown, it is apparent that the corrections made by De Pasquale *et al*. model has much improved the results of Veijola's model, especially for the small number of holes cases. As the number of holes becomes larger, it seems that the differences between both models become less significant.

Table 5.8: Damping coefficients values analytically calculated.

Plate	Damping coefficients ($\times 10^{-6}$ Ns/m)	
	Veijola (2006) model	De Pasquale *et al*. (2010) model
7	0.838	1.732
8	0.432	1.271
9	0.288	1.093
10	0.169	0.933
11	2.314	3.433
12	1.182	2.206
13	0.791	1.758
14	0.469	1.365
15	4.500	5.822
16	2.264	3.455
17	1.511	2.622
18	0.896	1.911
19	7.221	8.713
20	3.583	4.911
21	2.380	3.609
22	1.406	2.516
23	11.691	13.469
24	5.783	7.349
25	3.851	5.290
26	2.290	3.573
27	16.443	18.432
28	8.082	9.821
29	5.373	6.962
30	3.193	4.599
31	26.727	29.296
32	13.257	15.489
33	8.902	10.932
34	5.386	7.168

Figure 5.9 plotted the comparison between 2D membrane model of numerical approach and De Pasquale *et al*. analytical model in terms of their percentage differences in damping coefficient with respect to the experimental data. The surprising correlation between these models is they produces a mirror trend in *x*-axis. Overall, the finite element of the 2D membrane model gives a good agreement result in a small number of holes cases. As the number of holes increases, the analytical model given by De Pasquale *et al*. provides better accuracy. This discrepancy is due to the error present in the finite element approaches become larger when increasing the number of holes in the structure.

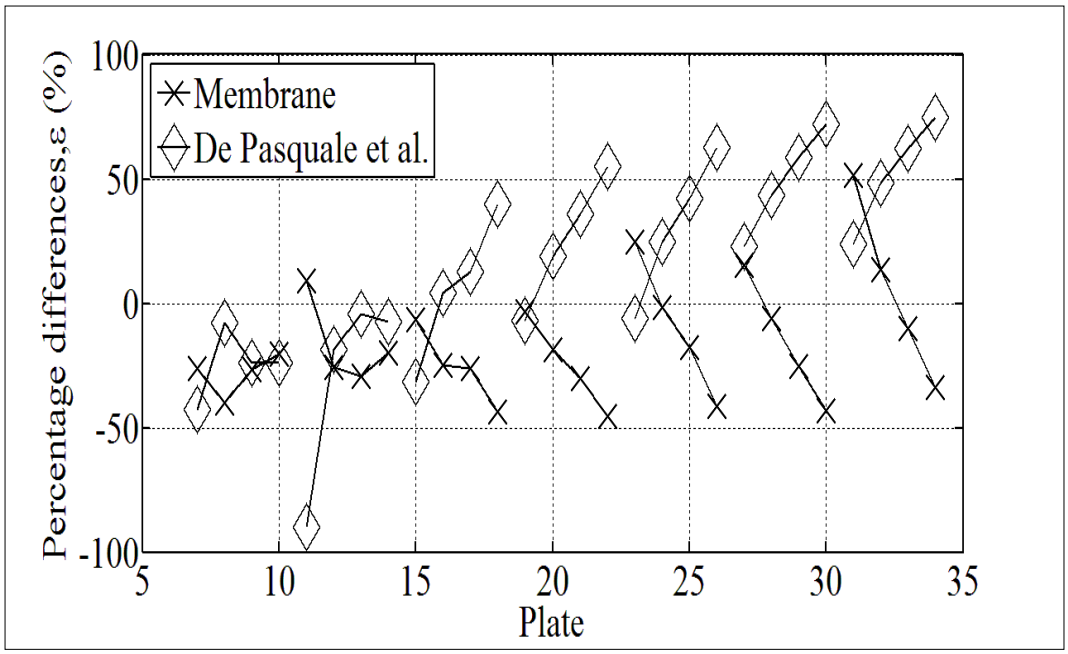

Figure 5.9: Comparison between FEM 2D membrane model and De Pasquale *et al*. analytical model for percentage differences of damping coefficients with respect to the experimental data.

As the conclusion to the squeeze film damping analysis, the results indicate that the 2D membrane model gave the best accuracy in a larger number of perforated holes cases. The 2D shell model only shows the better agreement with experimental data in a small number of holes cases. Meanwhile, the 3D solid model results only lies 2% lower than the shell model in terms of accuracy with respect to the experimental data. In the next section, the computational cost of such numerical models in doing the squeeze film analysis will be studied.

5.4 Computational Effort of Numerical Models

As another validation of the effectiveness finite element models, the computational costs of such numerical models as described before were measured and the results were compared. In the simulation analysis, the key is to achieve reliable and accurate results quickly and robustly. Here, there are two important criteria are considered in delivering the performance of the numerical model: the overall computation time and amount of memory required to store computation data.

The most typical problem that is related to the analysis performance is the density of finite element model mesh. This parameter is directly related to the modelling precision and computational resources. Usually, a denser mesh is preferable in the finite element analysis, since it will lead to smaller errors of modelling results. However, decrease in finite element size leads to increase of simulation time. Therefore, a large amount of computational power may be required in such case.

In study the performance of such numerical models, twelve plates with the different number of holes and holes size from the previous section is chosen as the study cases to be evaluated. Table 5.9 below summarizes the geometrical characteristics of the plate structure.

Table 5.9: Geometrical characteristics of plate for computational requirements study.

Plate	Plate side, L (μm)	Holes side, S_0 (μm)	No of holes, $M \times M$
7	55	7.20	2 × 2
8		9.30	
9		10.70	
10		12.60	
19	115	7.20	5 × 5
20		9.30	
21		10.70	
22		12.60	
31	185	7.20	8 × 8
32		9.30	
33		10.70	
34		12.60	

5.4.1 Computation Time

As engineering simulations become more sophisticated, designers are looking forward to reducing overall simulation processing time in order to save the cost. For the analysis of simulation time of such numerical models, the time taken to solve the squeeze film damping analysis is extracted at a variable number

of degrees of freedom (DOF). The number of DOF can vary depending on the change in the mesh size of the element.

In Figure 5.10, the computation time in solving such analysis of the 2×2 number of holes case given by different holes sizes were plotted for 3D solid, 2D shell, and 2D membrane numerical models. Figures 5.11 and 5.12 presents the same results obtained from the 5×5 number of holes and 8×8 number of holes cases, respectively.

From all this data, we can see that in a small number of holes plates, increases the holes size did not give any significant effect to the computational time for all the numerical models. However, when the number of holes becomes larger, increases the size of holes will results significant differences in computational time, especially for 3D solid element.

The clear observation for performance of such numerical models in simulation time study can be seen in the Figures 5.13, 5.14, and 5.15. The results of these plotted shows that the two-dimensional models give faster solution time than the complex three-dimensional model. This is expected, as the two-dimensional element models involved the area meshed only rather than three-dimensional element that meshed the whole volume of structure.

The most interesting finding is that the 2D membrane model produces slightly faster than the 2D shell model. This result may be explained by the fact that the membrane element only consists of translational DOF rather than shell

model that also involved rotational DOF. The neglected of the rotational DOF in membrane element generates the solution time become slightly faster.

In general, therefore, it can conclude that the 3D solid model gave a long computational time compare than the 2D shell model. However, the 2D membrane model will offer the less computational time rather than the 2D shell model in squeeze film damping. The differences between these models seem to become significant when the number of DOF involved is increases.

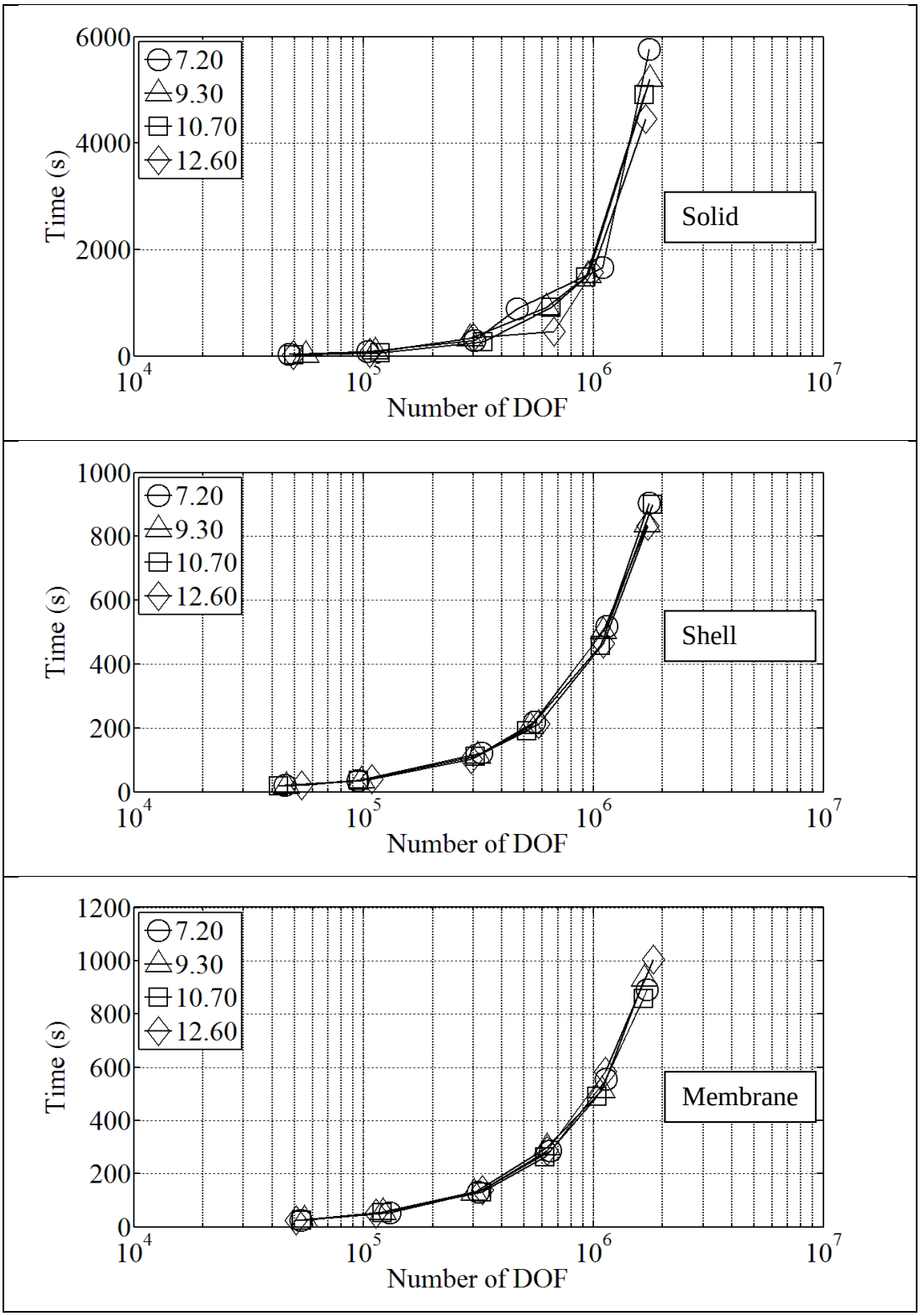

Figure 5.10: Comparison of the time duration to solve squeeze film damping given by different holes sizes and numerical models for 2 × 2 number of holes plates.

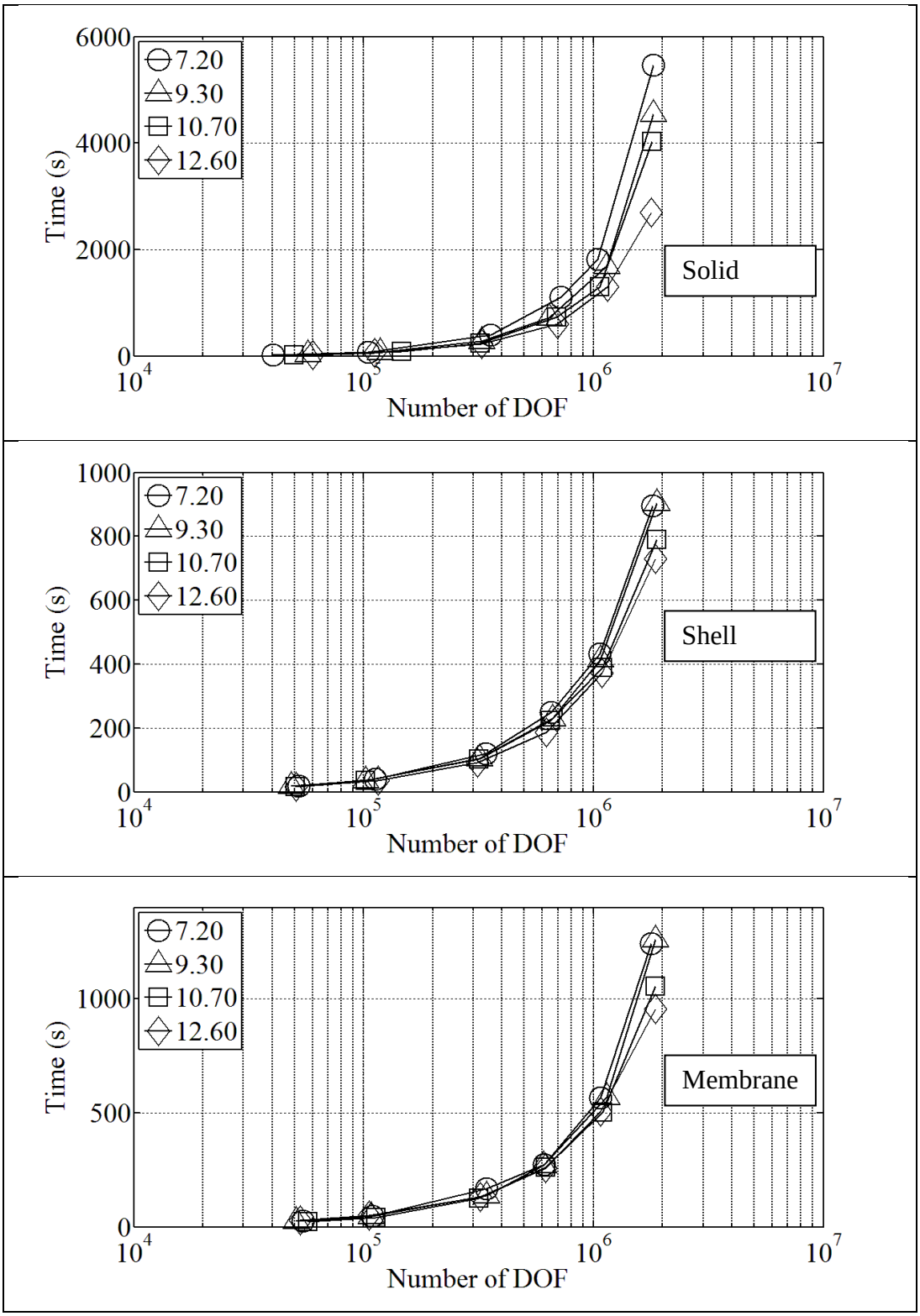

Figure 5.11: Comparison of the time duration to solve squeeze film damping given by different holes sizes and numerical models for 5 × 5 number of holes plates.

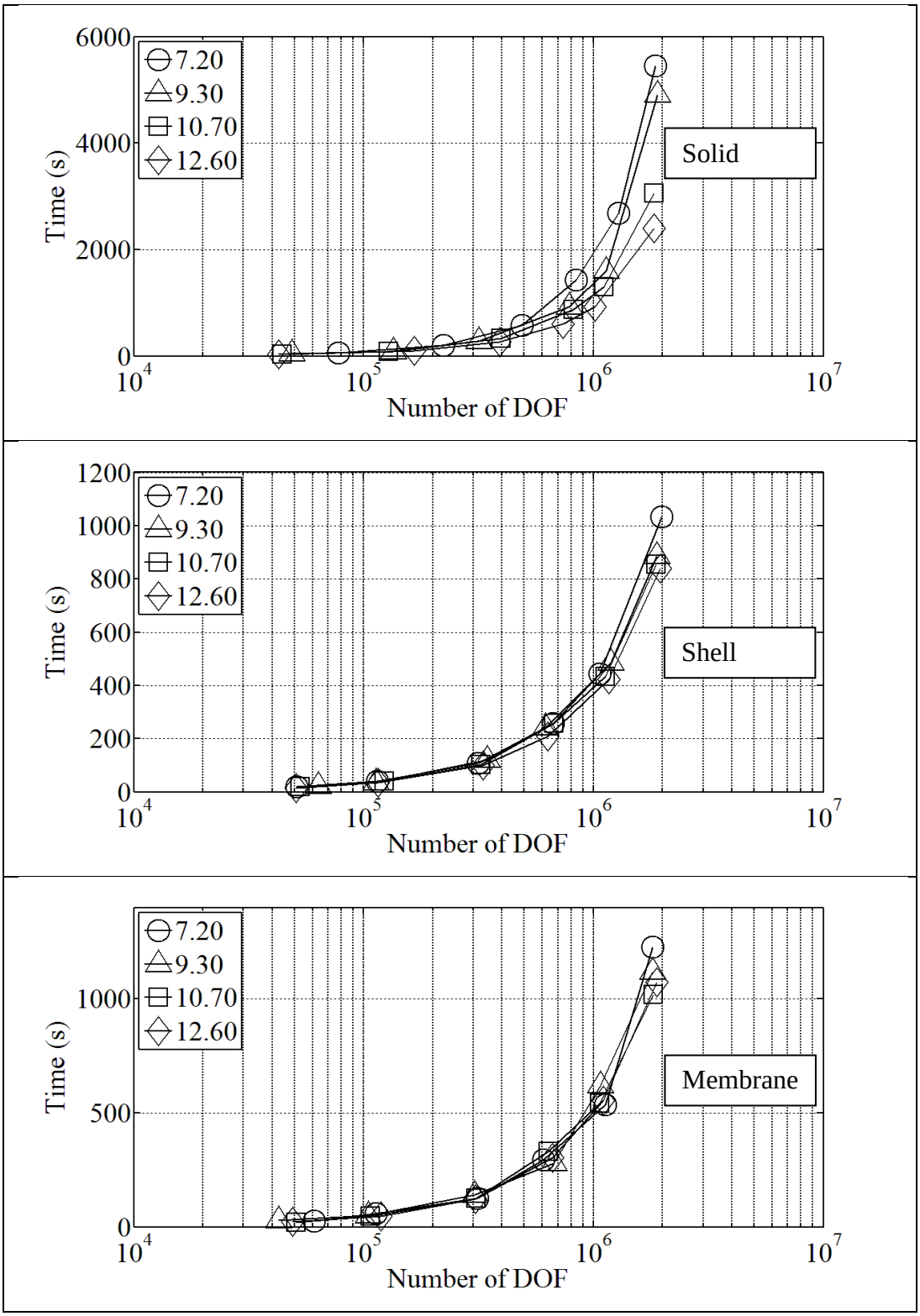

Figure 5.12: Comparison of the time duration to solve squeeze film damping given by different holes sizes and numerical models for 8 × 8 number of holes plates.

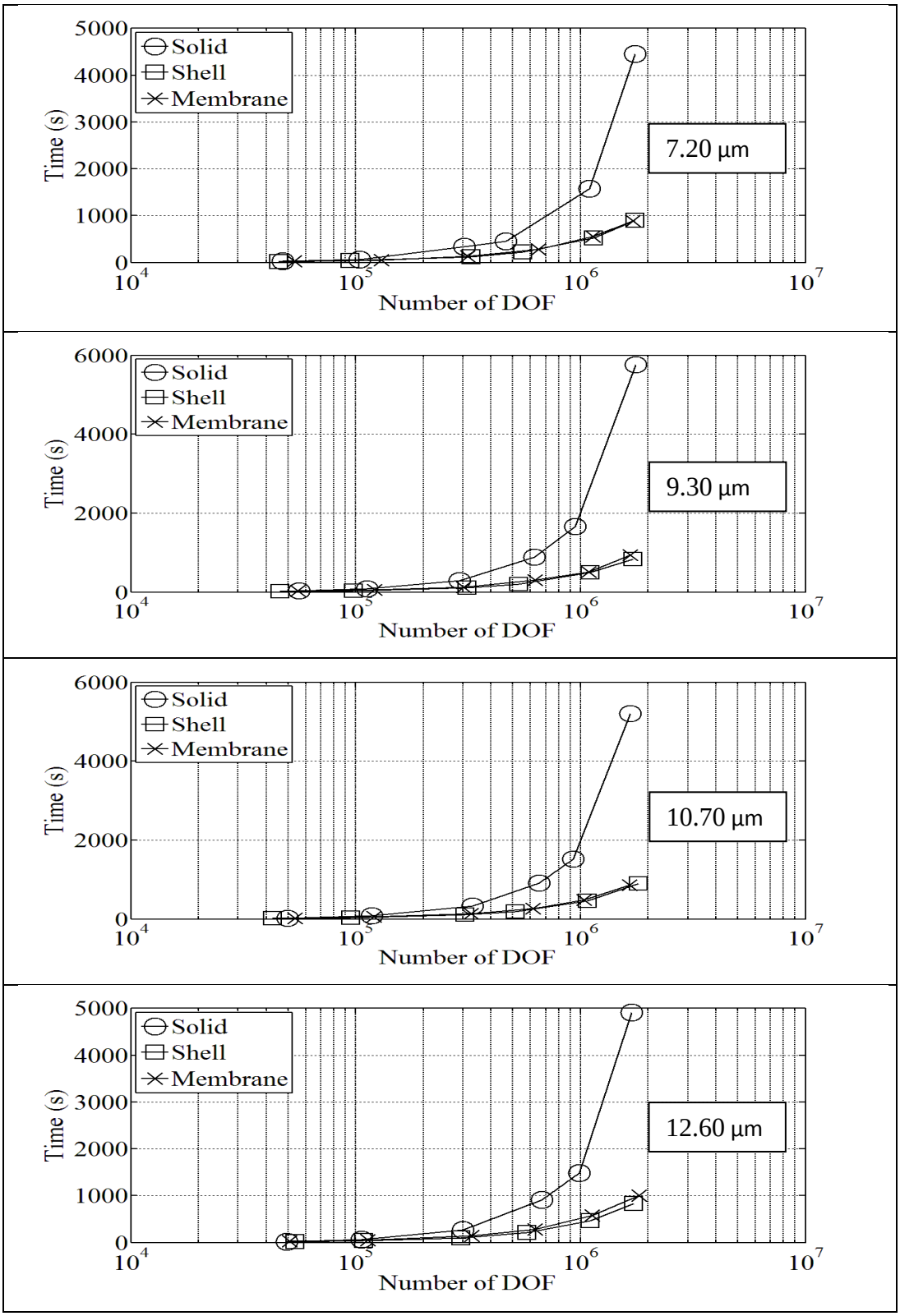

Figure 5.13: Comparison of the time duration to solve squeeze film damping given by different numerical models for different perforated holes sizes for 2 × 2 number of holes plates.

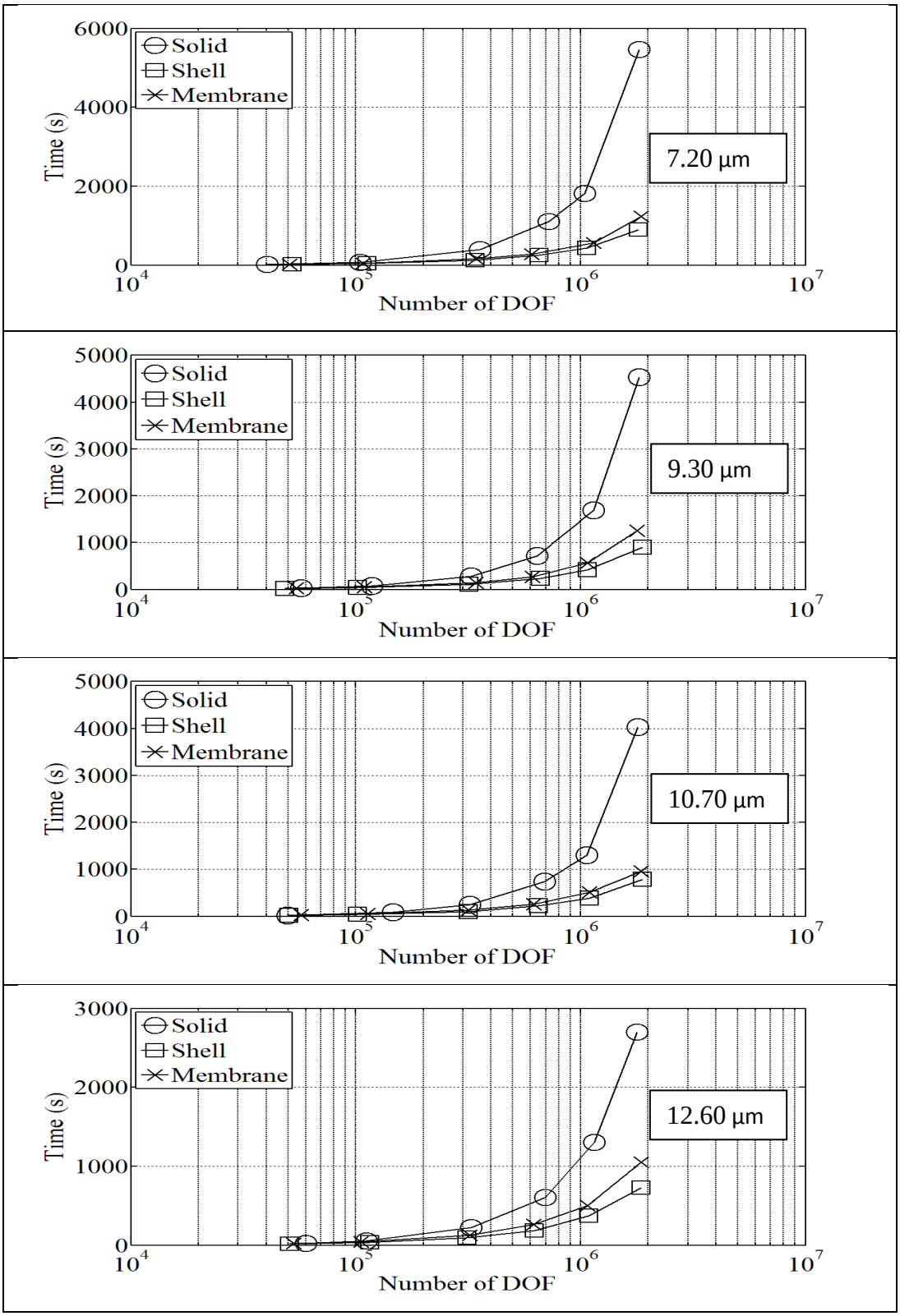

Figure 5.14: Comparison of the time duration to solve squeeze film damping given by different numerical models for different perforated holes sizes for 5 × 5 number of holes plates.

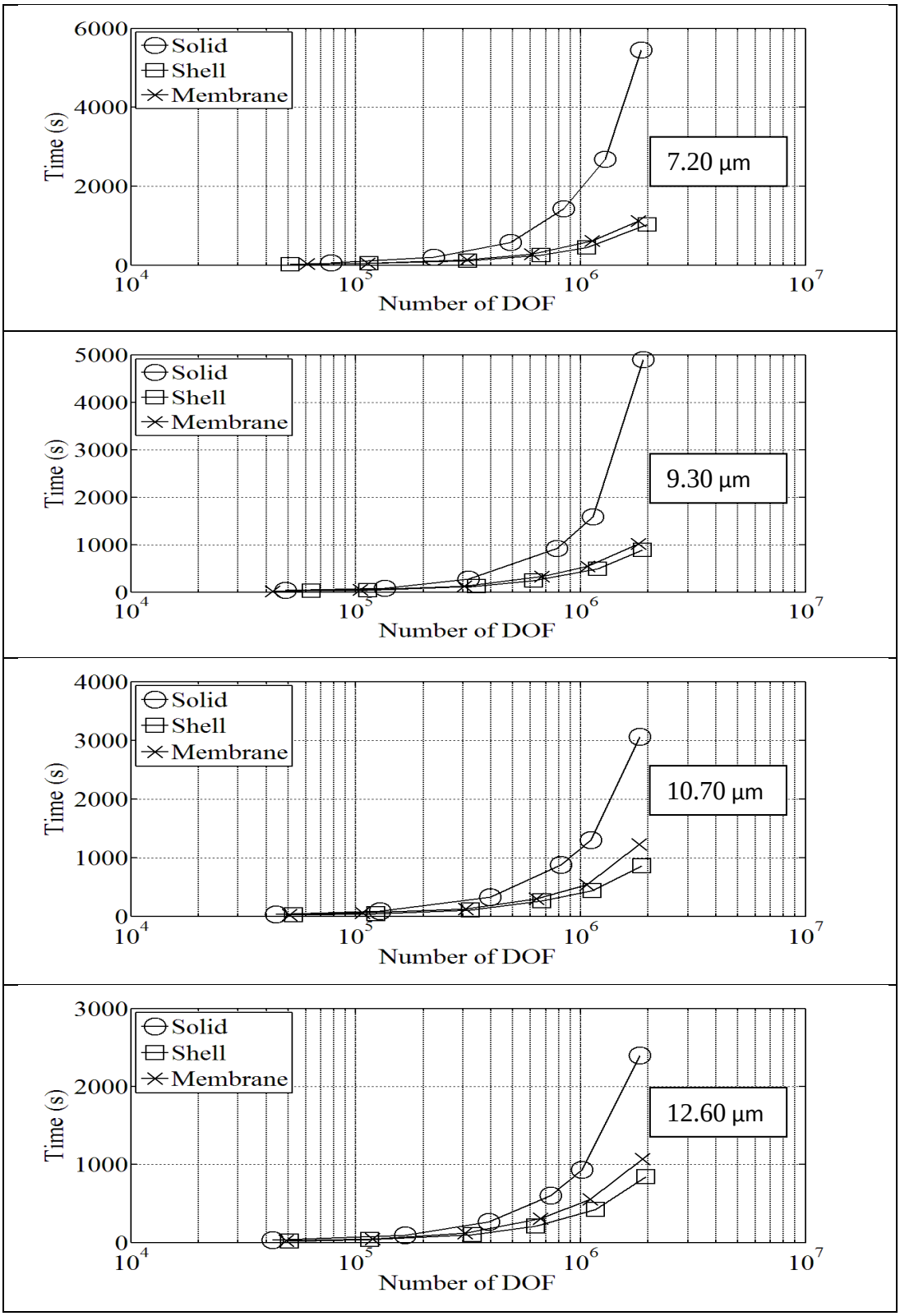

Figure 5.15: Comparison of the time duration to solve squeeze film damping given by different numerical models for different perforated holes sizes for 8 × 8 number of holes plates.

5.4.2 Storage Memory Requirements

To yield reliable results in the finite element analysis, the model simulation must be sufficiently detailed. As the level of detail is increase, computer memory requirements also increase. This will lead to the increasing of overall costs.

Figure 5.16 obtained the storage memory required in solving squeeze film damping analysis of the 2×2 number of holes case given by different holes sizes for 3D solid, 2D shell, and 2D membrane numerical models. Figures 5.17 and 5.18 shows the same results obtained from the 5×5 number of holes and 8×8 number of holes cases, respectively.

Based on the observation from this plotted data, increases the sizes of hole did not give any significant effect to the amount of storage memory required in the analysis applies for the any number of holes cases tested. This trend is consistent for the 3D solid, 2D shell, and 2D membrane models.

The amount of computational storage required of such numerical models for different holes sizes are plotted in the Figures 5.19, 5.20, and 5.21 regarding the different number of holes involved. These results demonstrate that the three-dimensional model required large computational storage than the simple two-dimensional models. This is also expected, as the three-dimensional element model involves the complex volume meshed rather than two-dimensional element that involves area meshed only.

As the 2D membrane model is based on the neglected the rotational DOF of the 2D shell model, it is clearly expected that the membrane model will require fewer amounts of memory storage than the shell model.

It is to be noted that 2D membrane model required smaller amount of memory storage rather than the 2D shell model. However, 3D solid model will need at least twice the computational memory storage than both models in the squeeze film damping analysis. The differences between these models seem to become more significant when the number of DOF involved is increases.

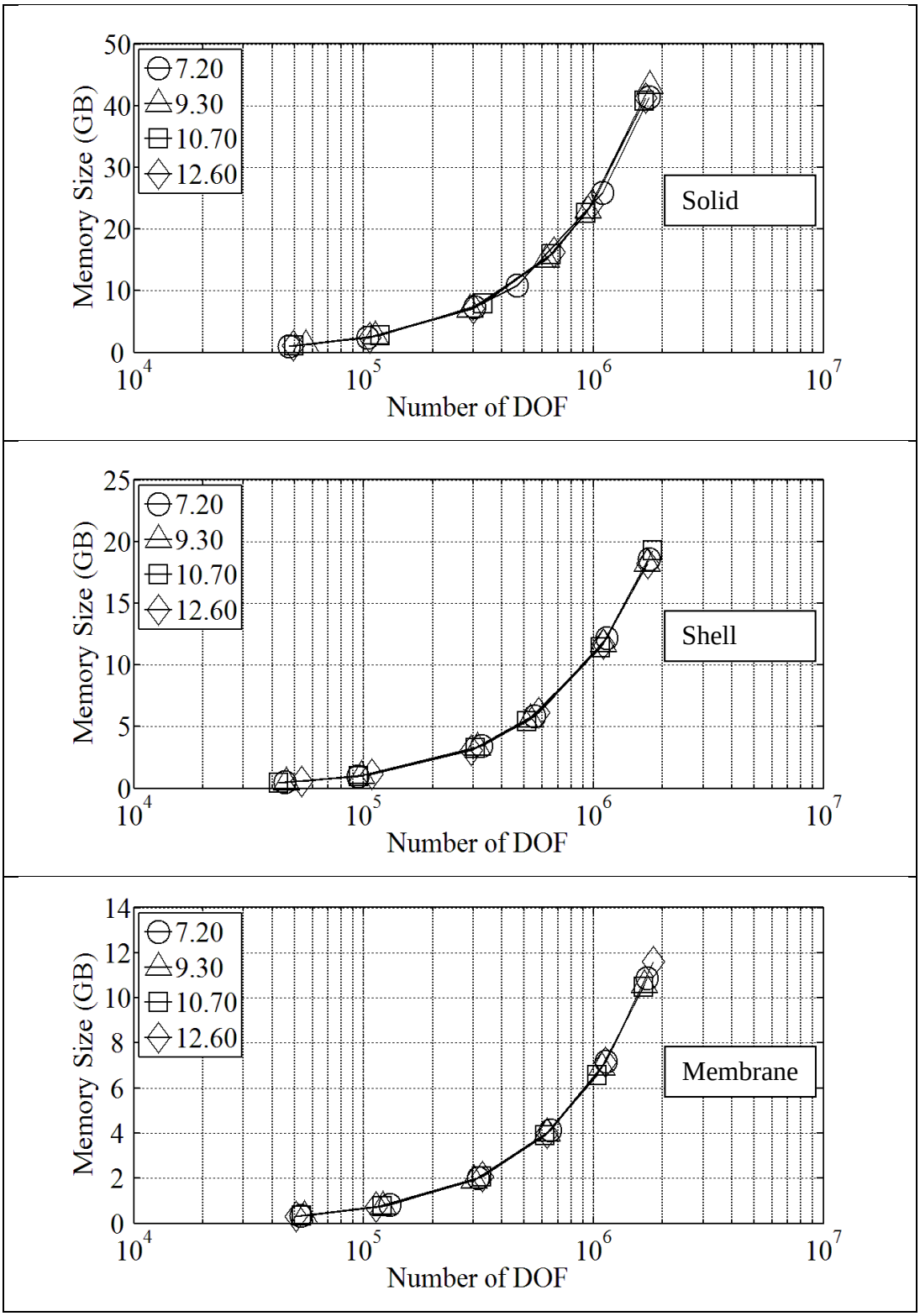

Figure 5.16: Comparison of the memory requirement to solve squeeze film damping given by different holes sizes and numerical models for 2 × 2 number of holes plates.

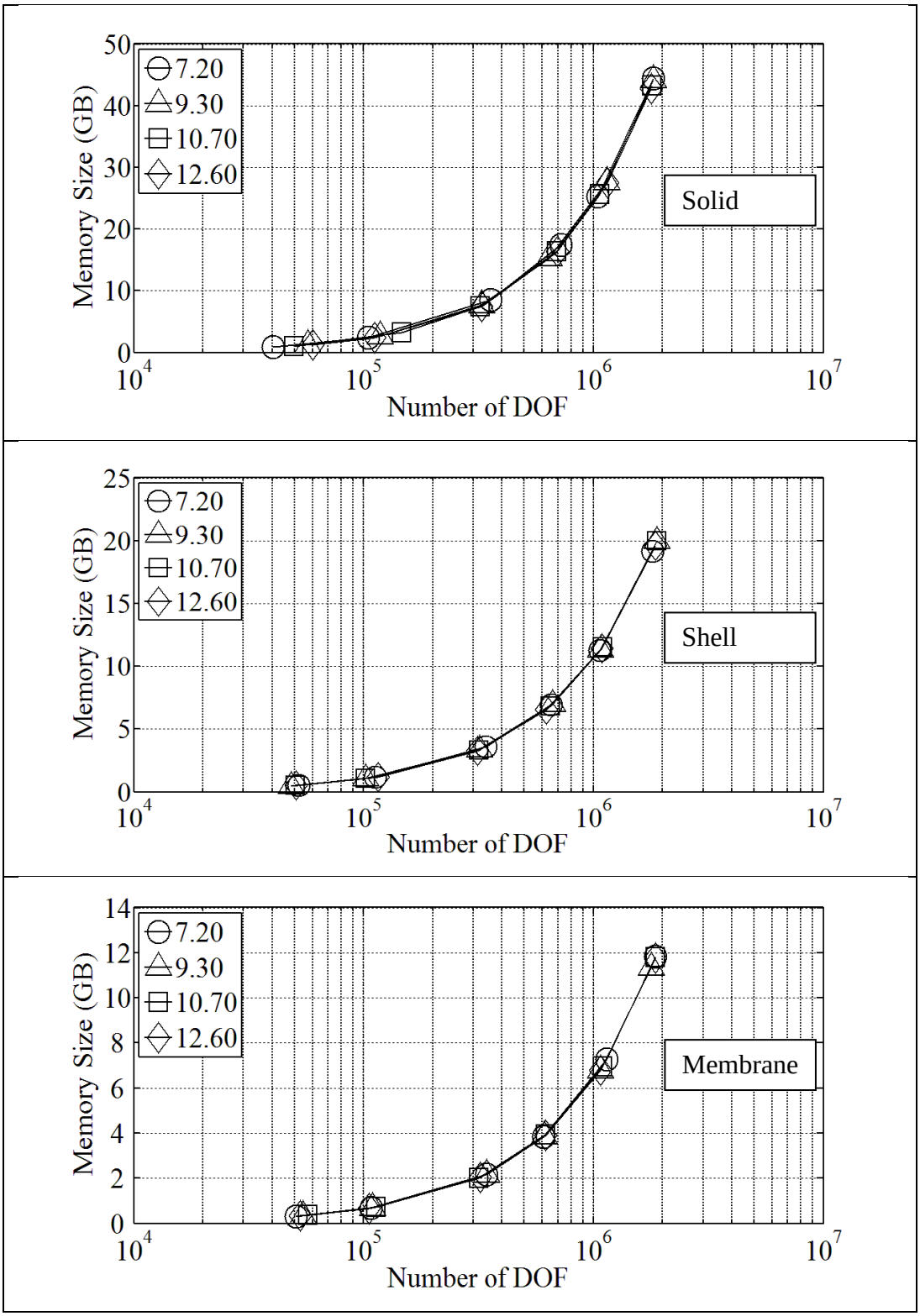

Figure 5.17: Comparison of the memory requirement to solve squeeze film damping given by different holes sizes and numerical models for 5 × 5 number of holes plates.

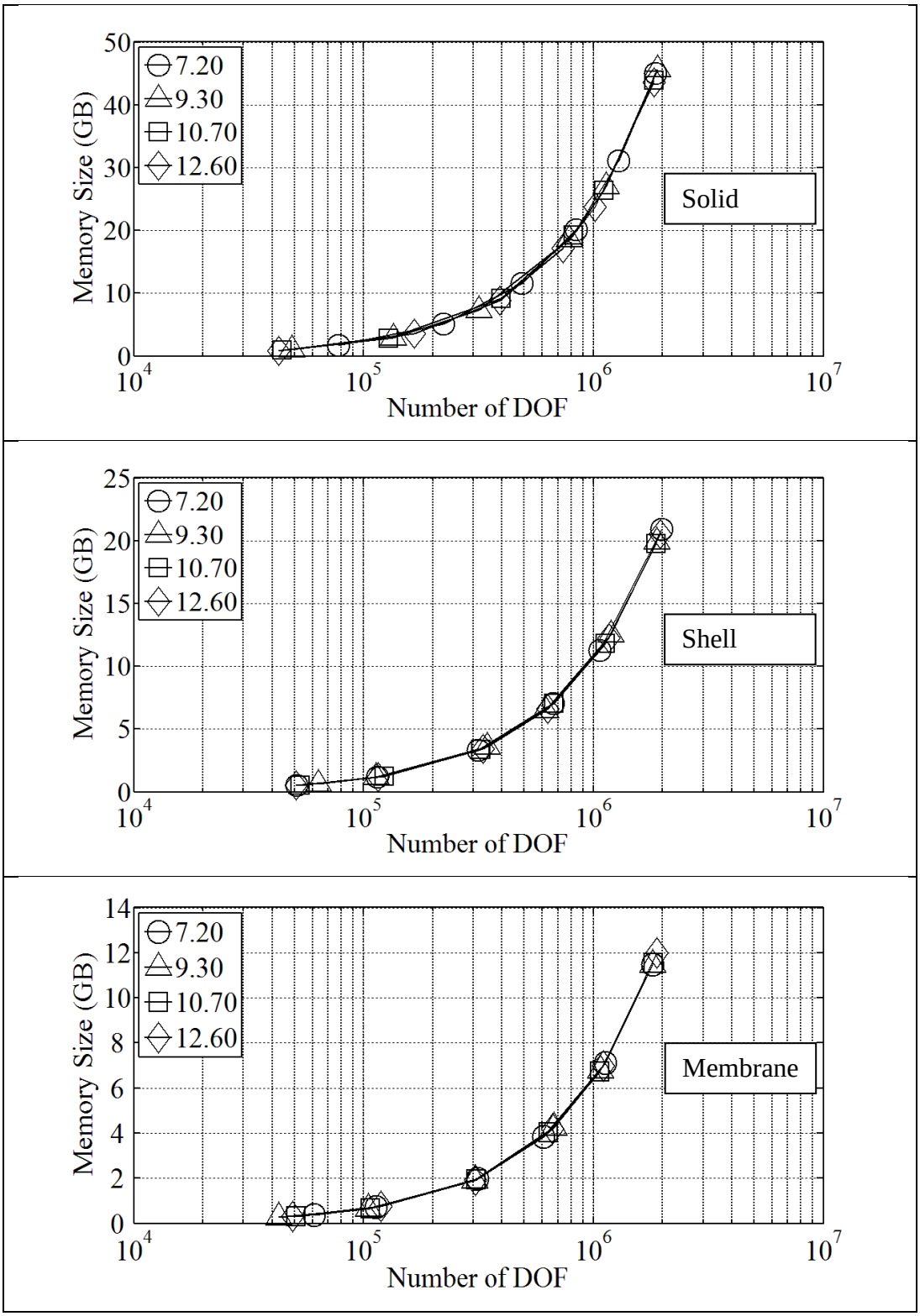

Figure 5.18: Comparison of the memory requirement to solve squeeze film damping given by different holes sizes and numerical models for 8 × 8 number of holes plates.

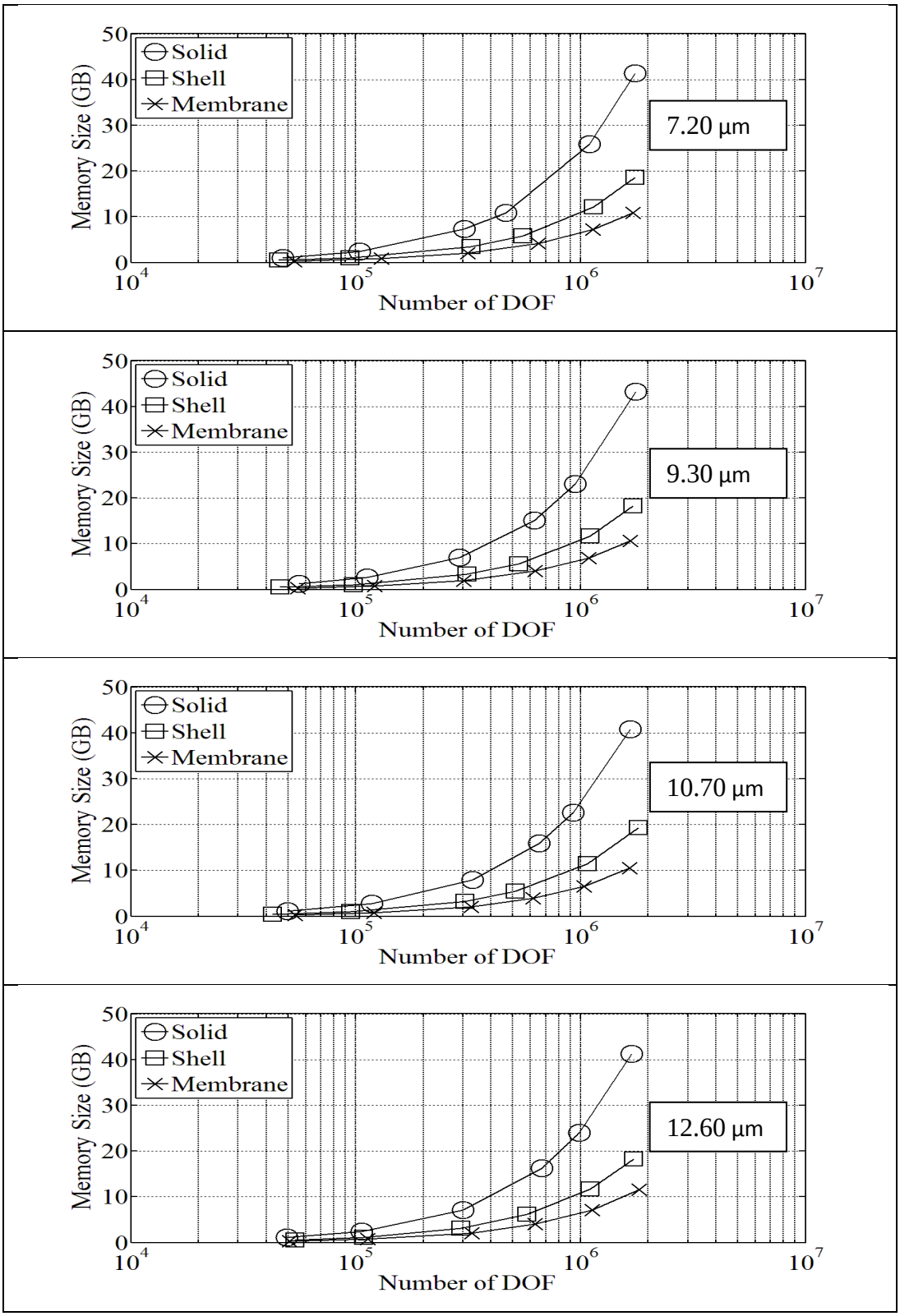

Figure 5.19: Comparison of the memory requirement to solve squeeze film damping given by different numerical models for different perforated holes sizes for 2 × 2 number of holes plates.

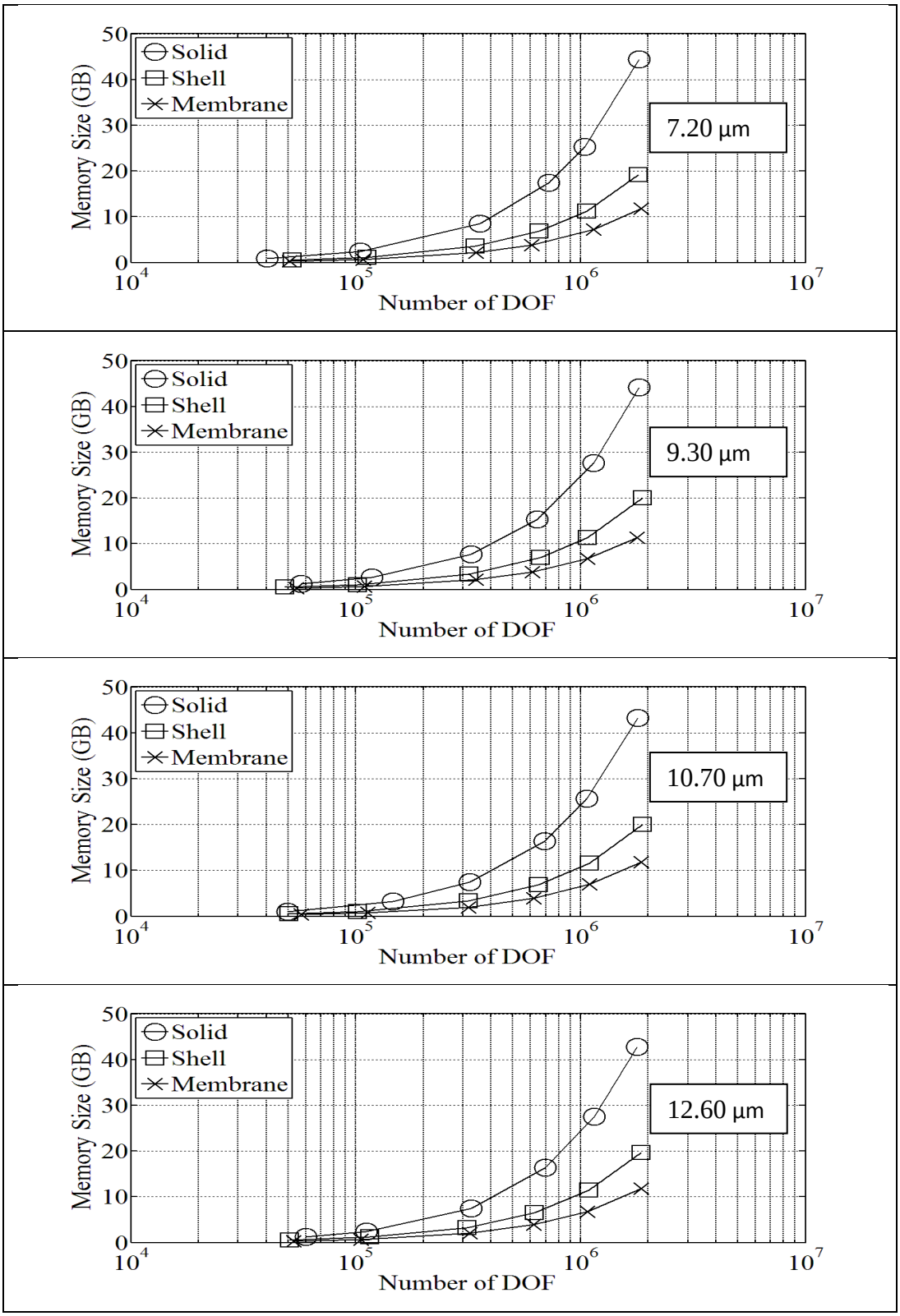

Figure 5.20: Comparison of the memory requirement to solve squeeze film damping given by different numerical models for different perforated holes sizes for 5 × 5 number of holes plates.

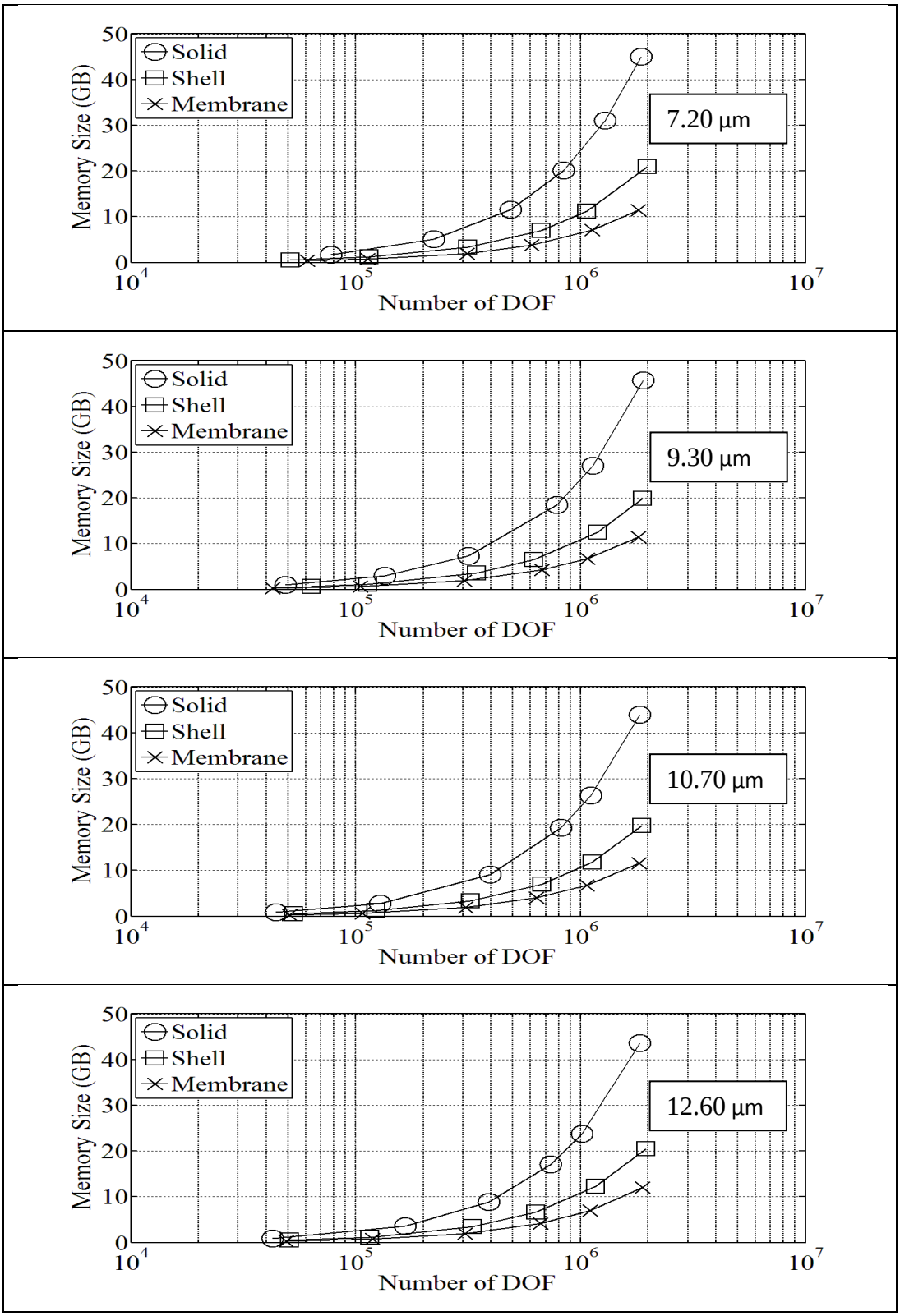

Figure 5.21: Comparison of the memory requirement to solve squeeze film damping given by different numerical models for different perforated holes sizes for 8 × 8 number of holes plates.

CHAPTER SIX

CONCLUSION AND FUTURE WORKS

6.1 Executive Summary

This thesis mainly focuses in development of two-dimensional finite element model that is based on the established structural and fluidic theoretical frameworks in the dynamic analysis of MEMS perforated structure. In the preliminary studies, the modal analysis of simple perforated plate was performed to evaluate the applicability of such proposed model. A general 3D solid model and proposed 2D shell model results were compared with the related theoretical work with good agreement of results.

For the modal analysis of perforated MEMS structure, it was found that 3D solid model gave a better agreement with the experimental data. However, the 2D shell model produces a result slightly close to the solid model. Meanwhile, the 2D membrane model result showed that it is not applicable in such analysis. In the squeeze film damping analysis, 2D shell element model provided the better accuracy results in modelling the small number of holes cases. When the number of holes becomes larger, the 2D membrane element model indicates the better agreement with the experimental data. The 3D solid model yields the results accuracy slightly lower than the shell element model.

The study of performance of such numerical models presents that the 2D membrane model consumed low computational time and memory storage for the analysis of squeeze film damping. 2D shell model utilized slightly higher computational time and memory whereas the 3D solid model taken long computational time and large memory storage in similar mesh density. When the mesh density becomes denser, the differences between these models become more significant.

In short, the goal for modelling the squeeze film damping analysis of perforated MEMS structures on two-dimensional model that on Reissner-Mindlin theory has successfully achieved.

6.2 Recommendations for Future Work

In squeeze film damping analysis, a proposed two-dimensional model that derived under the Reissner-Mindlin theory is not adequate to produce very good agreements results with respect to the experimental data. This may due to the some assumptions presented in this theory formulation. Nowadays, a lot of shell element formulations has been introduced in the literatures as mentioned in Section 2.4. A more sophisticated approach to shell elements to capture nonlinear shear should be pursued in the analysis.

For most MEMS devices, air gap height is large enough to neglect the effect of surface roughness on squeeze film damping. However, when the size of the device reduces to nano scale, it eventually affect the behaviour of squeeze film. This implementation will provide good prospect in increases the modelling accuracy. However, the measurement of surface roughness profile of two surfaces facing each other in the air gap in MEMS structure is most challenging part.

REFERENCES

ANSYS 12.0, *Verification Manual*, ANSYS Inc.

Bao, M. (2005). *Analysis and Design Principles of MEMS Devices*: Elsevier B.V.

Bao, M., & Yang, H. (2007). Squeeze film air damping in MEMS. *Sensors and Actuators, A: Physical, 136*(1), 3-27.

Bao, M., Yang, H., Sun, Y., & French, P. J. (2003). Modified Reynolds' equation and analytical analysis of squeeze-film air damping of perforated structures. *Journal of Micromechanics and Microengineering, 13*(6), 795-800.

Bao, M., Yang, H., Yin, H., & Sun, Y. (2002). Energy transfer model for squeeze-film air damping in low vacuum. *Journal of Micromechanics and Microengineering, 12*(3), 341-346.

Bathe, K. J. (1996). *Finite Element Procedures*: Prentice Hall.

Beltman, W. M., Van Der Hoogt, P. J. M., Spiering, R. M. E. J., & Tijdeman, H. (1997). Air loads on a rigid plate oscillating normal to a fixed surface. *Journal of Sound and Vibration, 206*(2), 217-241.

Bryzek, J., Petersen, K., & McCulley, W. (1994). Micromachines on the march. *IEEE Spectrum, 31*(5), 20-31.

Chaterjee, S., & Pohit, G. (2010). Squeeze-film damping characteristics of cantilever microresonators for higher modes of flexural vibration. *International Journal of Engineering, Science and Technology, 2*, 187-199.

Cho, Y.-H., Pisano, A. P., & Howe, R. T. (1994). Viscous damping model laterally oscillating microstructures. *Journal of Microelectromechanical Systems, 3*(2), 81-87.

Christian, R. (1966). The theory of oscillating-vane vacuum gauges. *Vacuum, 16*(4), 175-178.

Clark, J. V., Bindel, D., Kao, W., Zhu, E., Kuo, A., Zhou, N., et al. (2002). Addressing the needs of complex MEMS design. *In: Micro Electro Mechanical Systems, 2002. The Fifteenth IEEE International Conference on, 2002.* 204-209.

De Pasquale, G., & Somà, A. (2009). Numerical and experimental validation of out-of-plane resonance closed formulas for MEMS suspended plates with square holes. *Microsystem Technologies, 15*(3), 391-400.

De Pasquale, G., & Veijola, T. (2008). Comparative numerical study of FEM methods solving gas damping in perforated MEMS devices. *Microfluidics and Nanofluidics, 5*(4), 517-528.

De Pasquale, G., Veijola, T., & Somá, A. (2010). Modelling and validation of air damping in perforated gold and silicon MEMS plates. *Journal of Micromechanics and Microengineering, 20*(1).

De Pasquale, G., Veijola, T., & Somà, A. (2009). Gas damping effect on thin vibrating gold plates: Experiments and modeling. *In: Design, Test, Integration & Packaging of MEMS/MOEMS, 2009. MEMS/MOEMS '09. Symposium on, 1-3 April 2009,* 23-28.

Feng, C., Zhao, Y.-P., & Liu, D. Q. (2007). Squeeze-film effects in MEMS devices with perforated plates for small amplitude vibration. *Microsystem Technologies, 13*(7), 625-633.

Guo, Z. J., McGruer, N. E., & Adams, G. G. (2007). Modeling, simulation and measurement of the dynamic performance of an ohmic contact, electrostatically actuated RF MEMS switch. *Journal of Micromechanics and Microengineering, 17*(9), 1899-1909.

Hannot, S., & Rixen, D. J. (2009). A Fully Coupled FEM Model of Electromechanically Actuated MEMS with Squeeze Film Damping. *In: Proceedings of the ASME 2009 International Design Engineering Technical Conferences & Computers and Information in Engineering Conference IDETC/CIE*.

Hauptmann, R., & Schweizerhof, K. (1998). A systematic development of 'solid-shell' element formulations for linear and non-linear analyses employing only displacement degrees of freedom. *International Journal for Numerical Methods in Engineering, 42*(1), 49-69.

Hegarty, R. F., & Ariman, T. (1975). Elasto-dynamic analysis of rectangular plates with circular holes. *International Journal of Solids and Structures, 11*(7-8), 895-906.

Homentcovschi, D., & Miles, R. N. (2005). Viscous damping of perforated planar micromechanical structures. *Sensors and Actuators, A: Physical, 119*(2), 544-552.

Homentcovschi, D., & Miles, R. N. (2010). Viscous damping and spring force in periodic perforated planar microstructures when the Reynolds' equation cannot be applied. *Journal of the Acoustical Society of America, 127*(3), 1288-1299.

Hosaka, H., Itao, K., & Kuroda, S. (1995). Damping characteristics of beam-shaped micro-oscillators. *Sensors and Actuators: A. Physical, 49*(1-2), 87-95.

Huang, M., & Sakiyama, T. (1999). Free vibration analysis of rectangular plates with variously-shaped holes. *Journal of Sound and Vibration, 226*(4), 769-786.

Hutcherson, S., & Ye, W. (2004). On the squeeze-film damping of micro-resonators in the free-molecule regime. *Journal of Micromechanics and Microengineering, 14*(12), 1726-1733.

Kádár, Z., Kindt, W., Bossche, A., & Mollinger, J. (1996). Quality factor of torsional resonators in the low-pressure region. *Sensors and Actuators, A: Physical, 53*(1-3), 299-303.

Karniadakis, G., Beskok, A., & Aluru, N. (2005). *Microflows and Nanoflows: Fundamentals and Simulation*: Springer.

Kim, E.-S., Cho, Y.-H., & Kim, M.-U. (1999). Effect of holes and edges on the squeeze film damping of perforated micromechanical structures. *In: Micro Electro Mechanical Systems, 1999. MEMS '99. Twelfth IEEE International Conference on, 17-21 Jan 1999*. 296-301.

Kwok, P. Y., Weinberg, M. S., & Breuer, K. S. (2005). Fluid effects in vibrating micromachined structures. *Journal of Microelectromechanical Systems, 14*(4), 770-781.

Lee, H. P., Lim, S. P., & Chow, S. T. (1990). Prediction of natural frequencies of rectangular plates with rectangular cutouts. *Computers and Structures, 36*(5), 861-869.

Langlois, W. E. (1961). *Isothermal squeeze films*: Defense Technical Information Center.

Leissa, A. W. (1969). *Vibration of plates*: Scientific and Technical Information Division, National Aeronautics and Space Administration.

Li, B., Wu, H., Zhu, C., & Liu, J. (1999). Theoretical analysis on damping characteristics of resonant microbeam in vacuum. *Sensors and Actuators, A: Physical, 77*(3), 191-194.

Li, W. L. (2004). Modeling of head/disk interface - An average flow model. *Tribology Letters, 17*(3), 669-676.

Lifshitz, R., & Roukes, M. L. (2000). Thermoelastic damping in micro- and nanomechanical systems. *Physical Review B - Condensed Matter and Materials Physics, 61*(8), 5600-5609.

Mehner, J. E., Doetzel, W., Schauwecker, B., & Ostergaard, D. (2003). Reduced order modeling of fluid structural interactions in MEMS based on model projection techniques. *In: TRANSDUCERS, Solid-State Sensors, Actuators and Microsystems, 12th International Conference on, 2003*, 2, 1840-1843

Mihailovich, R. E., & MacDonald, N. C. (1995). Dissipation measurements of vacuum-operated single-crystal silicon microresonators. *Sensors and Actuators: A. Physical, 50*(3), 199-207.

Mohite, S. S., Kesari, H., Sonti, V. R., & Pratap, R. (2005). Analytical solutions for the stiffness and damping coefficients of squeeze films in MEMS devices with perforated back plates. *Journal of Micromechanics and Microengineering, 15*(11), 2083-2092.

Nayfeh, A. H., & Younis, M.I. (2004). A new approach to the modelling and simulation of flexible microstructures under the effect of squeeze-film damping. *Journal of Micromechanics and Microengineering, 14*(2), 170-181.

Pandey, A. K., & Pratap, R. (2007). Effect of flexural modes on squeeze film damping in MEMS cantilever resonators. *Journal of Micromechanics and Microengineering, 17*(12), 2475-2484.

Pandey, A. K., & Pratap, R. (2008). A comparative study of analytical squeeze film damping models in rigid rectangular perforated MEMS structures with experimental results. *Microfluidics and Nanofluidics, 4*(3), 205-218.

Pandey, A. K., Pratap, R., & Chau, F. S. (2008). Effect of pressure on fluid damping in MEMS torsional resonators with flow ranging from continuum to molecular regime. *Experimental Mechanics, 48*(1), 91-106.

Pratap, R., Mohite, S., & Pandey, A. K. (2007). Squeeze film effects in MEMS devices. *Journal of the Indian Institute of Science, 87*(1), 75-94.

Rao, S. S. (2007). *Vibration of Continuous Systems*: Wiley.

Schoop, H. (1989). A simple nonlinear flat element for large displacement structures. *Computers and Structures, 32*(2), 379-385.

Somà, A., & De Pasquale, G. (2007). Identification of test structures for reduced order modeling of the squeeze fim damping in MEMS. *In: DTIP of MEMS and MOEMS - Symposium on Design, Test, Integration and Packaging of MEMS/MOEMS.*

Somà, A., & De Pasquale, G. (2008). Numerical and experimental comparison of MEMS suspended plates dynamic behaviour under squeeze film damping effect. *Analog Integrated Circuits and Signal Processing*, 1-12.

Starr, J. B. (1990, June). Squeeze-film damping in solid-state accelerometers. In: *Solid-State Sensor and Actuator Workshop, 1990. 4th Technical Digest.*, 44-47.

Sumali, H. (2007). Squeeze-film damping in the free molecular regime: Model validation and measurement on a MEMS. *Journal of Micromechanics and Microengineering, 17*(11), 2231-2240.

Takahashi, S. (1958). Vibration of rectangular plates with circular holes. *Bulletin of JSME, 1*(4), 380-385.

Tilmans, H. A. C., Elwenspoek, M., & Fluitman, J. H. J. (1992). Micro resonant force gauges. *Sensors and Actuators: A. Physical, 30*(1-2), 35-53.

Veijola, T. (2006). Analytic damping model for an MEM perforation cell. *Microfluidics and Nanofluidics, 2*(3), 249-260.

Veijola, T., De Pasquale, G., & Somà, A. (2009). Experimental validation of compact damping models of perforated MEMS devices. *Microsystem Technologies, 15*(8), 1121-1128.

Veijola, T., Kuisma, H., Lahdenperä, J., & Ryhänen, T. (1995). Equivalent-circuit model of the squeezed gas film in a silicon accelerometer. *Sensors and Actuators: A. Physical, 48*(3), 239-248.

Veijola, T., & Råback, P. (2007). Methods for solving gas damping problems in perforated microstructures using a 2D finite-element solver. *Sensors, 7*(7), 1069-1090.

Ventsel, E., & Krauthammer, T. (2001). *Thin Plates and Shells: Theory: Analysis, and Applications*: Taylor & Francis.

Wriggers, P., Eberlein, R., & Gruttmann, F. (1995). An axisymmetrical quasi-Kirchhoff-type shell element for large plastic deformations. *Archive of Applied Mechanics, 65*(7), 465-477.

Yasumura, K. Y., Stowe, T. D., Chow, E. M., Pfafman, T., Kenny, T. W., Stipe, B. C., et al. (2000). Quality factors in micron- and submicron-thick cantilevers. *Journal of Microelectromechanical Systems, 9*(1), 117-125.

Ye, W., Wang, X., Hemmert, W., Freeman, D., & White, J. (2003). Air damping in laterally oscillating microresonators: A numerical and experimental study. *Journal of Microelectromechanical Systems, 12*(5), 557-566.

Zienkiewicz, O. C., & Taylor, R. L. (2005). *The Finite Element Method for Solid and Structural Mechanics*: Elsevier Butterworth-Heinemann.

Zook, J. D., Burns, D. W., Guckel, H., Sniegowski, J. J., Engelstad, R. L., & Feng, Z. (1992). Characteristics of polysilicon resonant microbeams. *Sensors and Actuators: A. Physical, 35*(1), 51-59.

APPENDICES

APPENDIX A

Mode Shapes at First Mode of Vibration

A.1 Mode Shapes at First Mode of Vibration for Plate 1

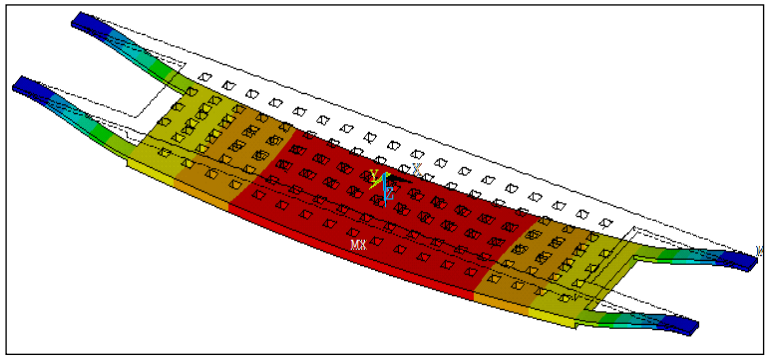

(a) 3D Solid Model

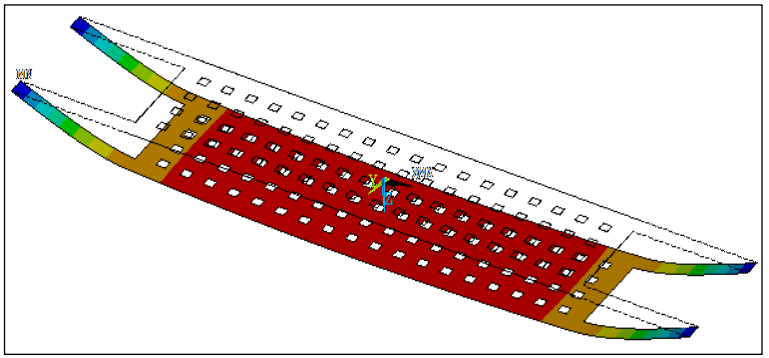

(b) 2D Shell Model

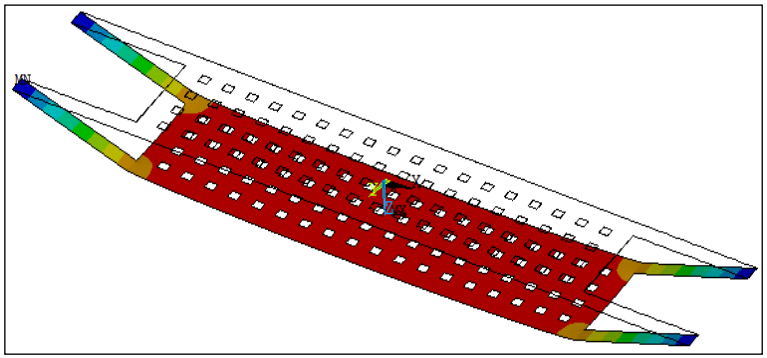

(c) 2D Membrane Model

A.2 Mode Shapes at First Mode of Vibration for Plate 2

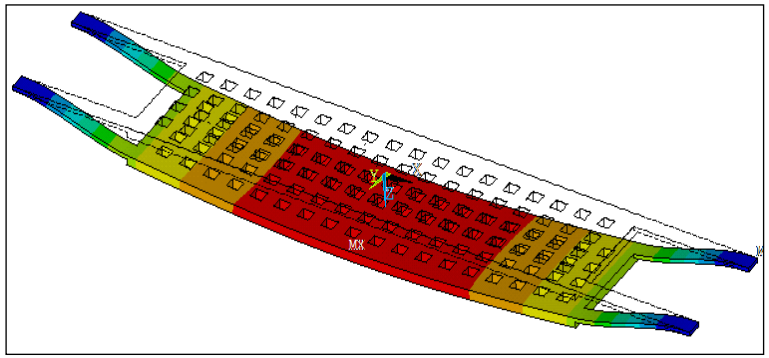

(a) 3D Solid Model

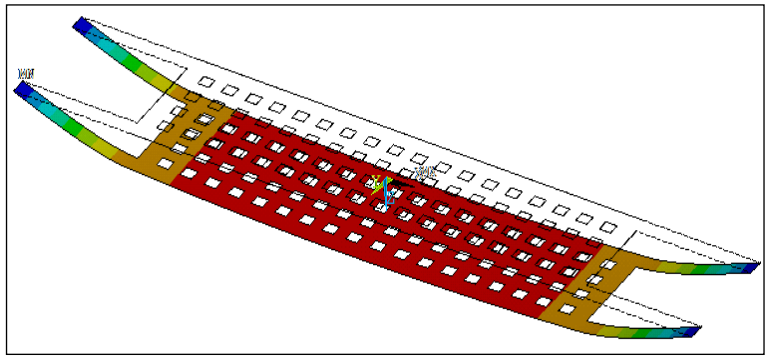

(b) 2D Shell Model

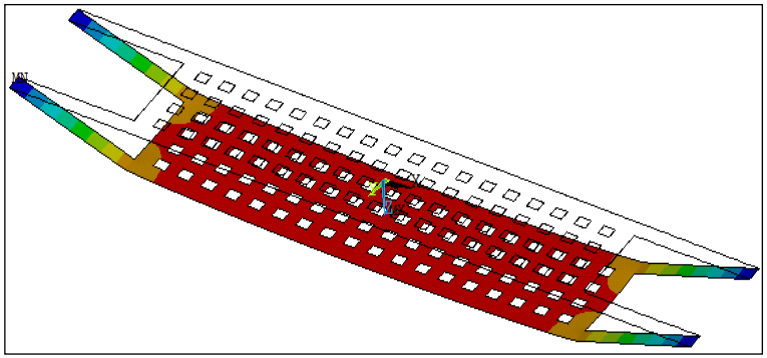

(c) 2D Membrane Model

A.3 Mode Shapes at First Mode of Vibration for Plate 3

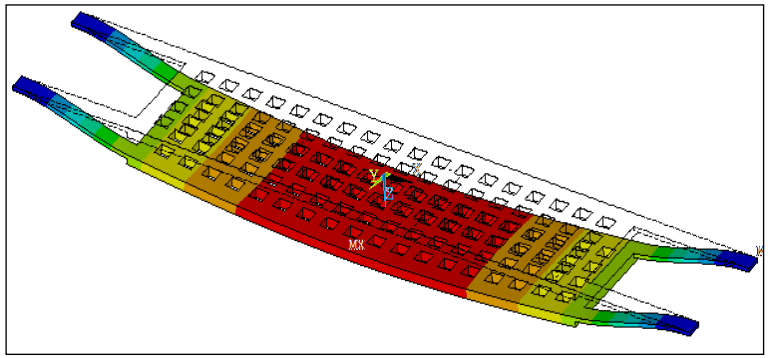

(a) 3D Solid Model

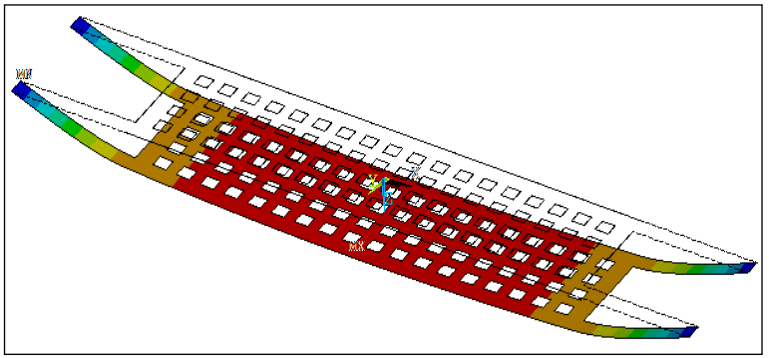

(b) 2D Shell Model

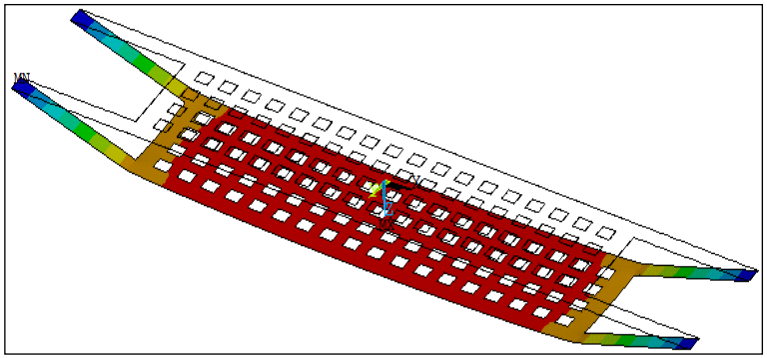

(c) 2D Membrane Model

A.4 Mode Shapes at First Mode of Vibration for Plate 4

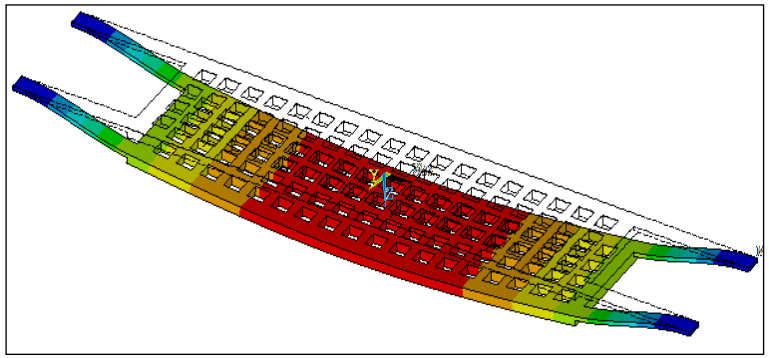

(a) 3D Solid Model

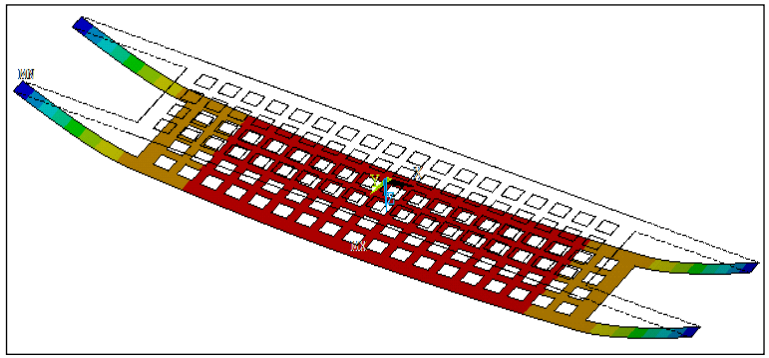

(b) 2D Shell Model

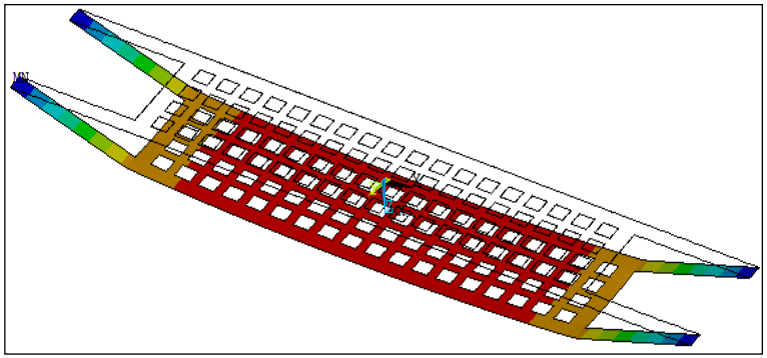

(c) 2D Membrane Model

A.5 Mode Shapes at First Mode of Vibration for Plate 5

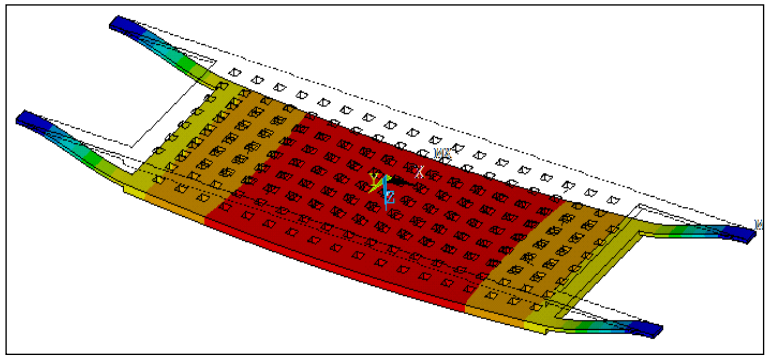

(a) 3D Solid Model

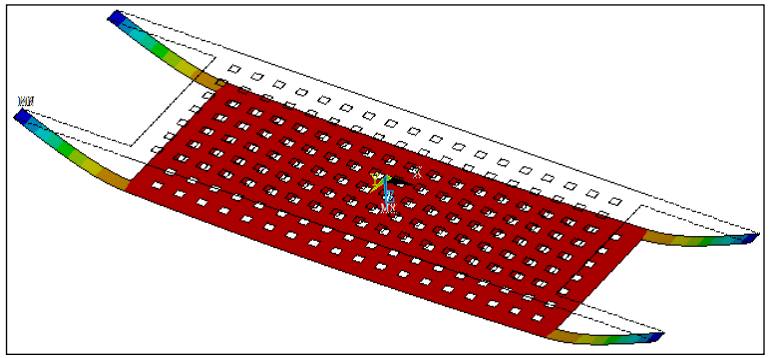

(b) 2D Shell Model

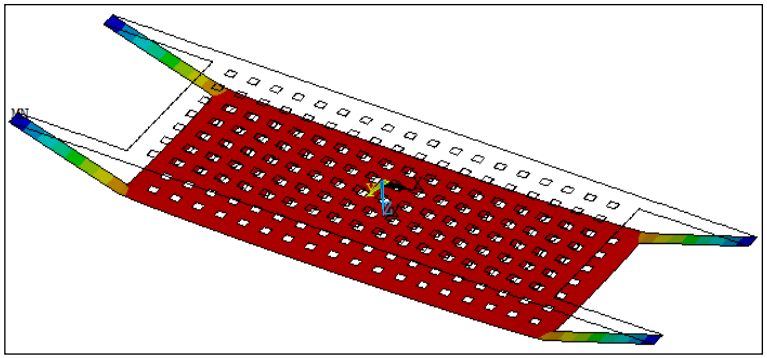

(c) 2D Membrane Model

A.6 Mode Shapes at First Mode of Vibration for Plate 6

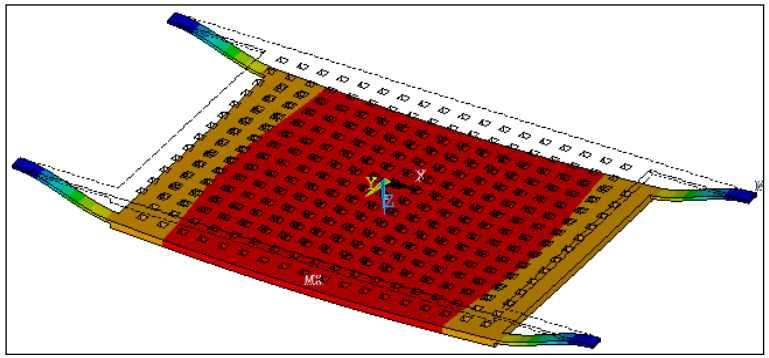

(a) 3D Solid Model

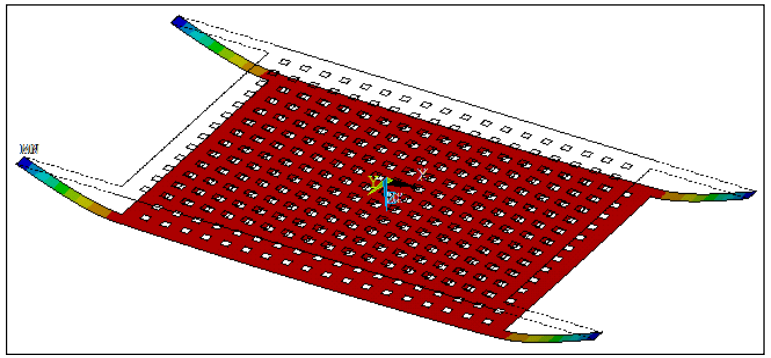

(b) 2D Shell Model

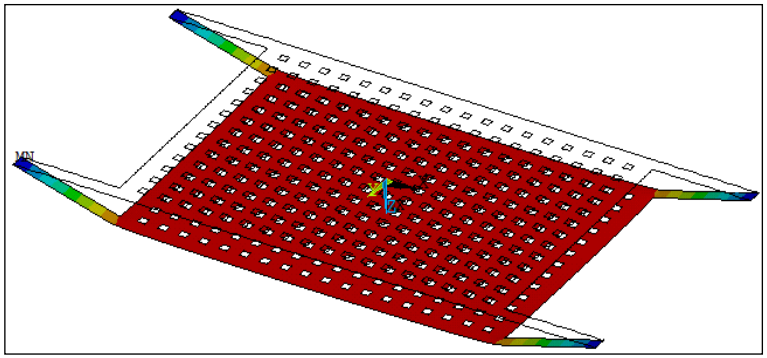

(c) 2D Membrane Model

APPENDIX B: Sample APDL Command for Model FLUID138 Element

Plate 1 structure (2 × 2 no. of holes)

```
/prep7

s_ll=27.5              : Half plate length
s_t=6.3                : Plate thickness

c_1=55/6               : Hole center
c_2=c_1+c_1

s_d=7.2                : Hole size

!holes generation for 1st row

*do,i,1,2
nsel,all
*get,numb,node,,num,max
n,numb+1,-s_ll+i*c_2,c_1,0      ! Location for first node of
                                FLUID138 element
n,numb+2,-s_ll+i*c_2,c_1,s_t    ! Location for second node of
                                FLUID138 element
type,2
mat,2
real,2
e,numb+1,numb+2                 ! Define element

esel,s,type,,1
nsle,s,1
local,11,0,-s_ll+i*c_2,c_1
csys,11
nsel,r,loc,x,s_d/2,-s_d/2       ! Select all nodes on the hole
nsel,r,loc,y,s_d/2,-s_d/2       circumference
nsel,a,node,,numb+1
*get,next,node,,num,min
cp,i,pres,numb+1,next
nsel,u,node,,numb+1
nsel,u,node,,next
cp,i,pres,all                   ! Coupled DOF set for pressure
                                constant
csys,0
allsel
*enddo
```

```
!holes generation for 2nd row

*do,i,1,2
nsel,all
*get,numb,node,,num,max
n,numb+1,-s_ll+i*c_2,-c_1,0        ! Location for first node of
                                   FLUID138 element
n,numb+2,-s_ll+i*c_2,-c_1,s_t      ! Location for second node of
                                   FLUID138 element
type,2
mat,2
real,2
e,numb+1,numb+2                    ! Define element

esel,s,type,,1
nsle,s,1
local,11,0,-s_ll+i*c_2,-c_1
csys,11
nsel,r,loc,x,s_d/2,-s_d/2          ! Select all nodes on the hole
nsel,r,loc,y,s_d/2,-s_d/2          circumference
nsel,a,node,,numb+1
*get,next,node,,num,min
cp,i+2,pres,numb+1,next
nsel,u,node,,numb+1
nsel,u,node,,next
cp,i+2,pres,all                    ! Coupled DOF set for pressure
                                   constant
csys,0
allsel
*enddo
```